Quaternary Science Reviews 245 (2020) 106528

Contents lists available at ScienceDirect

Quaternary Science Reviews

journal homepage: www.elsevier.com/locate/quascirev

Late Pleistocene glaciers in Greece: A new ^{36}Cl chronology

James L. Allard [a, *], Philip D. Hughes [a], Jamie C. Woodward [a], David Fink [b], Krista Simon [b], Klaus M. Wilcken [b]

[a] Department of Geography, The University of Manchester, Manchester, M13 9PL, UK
[b] Australian Nuclear Science and Technology Organisation, PMB1, Menai, NSW, 2234, Australia

ARTICLE INFO

Article history:
Received 22 June 2020
Received in revised form
28 July 2020
Accepted 3 August 2020
Available online 19 August 2020

Keywords:
Quaternary
Glaciation
Glacial geochronology
Cosmogenic surface exposure dating
Geomorphology
Moraine
Pindus mountains
Greece
Mediterranean

ABSTRACT

Glaciers formed in the highest mountains of Greece during the Late Pleistocene, but the timing of glacier maxima is poorly understood. This paper presents 27 ^{36}Cl terrestrial cosmogenic nuclide exposure ages from glacial boulders on Mount Tymphi (2497 m a.s.l., 40°N) in Epirus, northwest Greece. These ages address both a significant geographical gap in Mediterranean glacial chronologies and a temporal gap in the glacial history of this region by targeting the previously undated Late Pleistocene record. Late Pleistocene glaciers were restricted to the cirques and upper valleys of Mount Tymphi. Terminal and lateral moraines between 1700 m and 2050 m a.s.l. mark the extent of Late Pleistocene glaciers on the southern side of Mount Tymphi. Moraines marking the maximum extent of Late Pleistocene glaciation date to 29.0 ± 3.0 ka and 25.7 ± 2.6 ka, taking the oldest ages as most representative of moraine emplacement. Glaciers had retreated to the high cirques by 24.5 ± 2.4 ka during Heinrich Stadial 2. Rock glaciers formed under cold and drier conditions during this period of glacier retreat. This ^{36}Cl dataset complements published U-series ages from secondary calcites in glacial sediments below 1700 m elevation, which demonstrate more extensive Middle Pleistocene glaciations in MIS 6 and MIS 12. A Late Pleistocene glacier maxima on Mount Tymphi at 25.7–29 ka is in good agreement with well-preserved outwash sediments dating to 24–28 ka in the Voidomatis River record downstream and is consistent with the Ioaninna basin pollen record indicating cool and wet conditions, most favourable for glacier growth, at 25–30 ka.

1. Introduction

Terrestrial cosmogenic nuclide (TCN) dating has been employed by geomorphologists to build chronologies for landscape change over both short and long timescales (100–1,000,000 years) (Gosse and Phillips, 2001; Ivy-Ochs and Kober, 2008; Darvill, 2013; Granger et al., 2013). This method has proved especially valuable in glaciated areas for dating moraine formation and the deposition of glacially-transported boulders as well as for establishing the exposure age of bedrock surfaces. These applications have enabled the development of robust chronologies for reconstructions of glacial maxima and rates of glacier recession in a range of geomorphological settings.

The glacial history of the Balkan Peninsula has been the subject of research since the late 19th century (Brückner, 1890; Cvijić, 1889). Developments in geochronology during the last two decades have established a dating framework for the Pleistocene glacial history of Greece. Uranium-series dating of secondary calcites within moraines has identified extensive glaciation during Marine Isotope Stage (MIS) 12 and MIS 6 from the two stratigraphically oldest sets of deposits on Mount Tymphi, North-west Greece (Fig. 1, location E) (Woodward et al., 2004; Hughes et al., 2006a). This is consistent with evidence from elsewhere on the Balkan peninsula (Marjanac and Marjanac, 2004; Marjanac et al., 2008; Hughes et al., 2010, 2011; Marjanac, 2012; Adamson et al., 2014, 2016; Marjanac and Marjanac, 2016; Leontaritis et al., 2020), with, for example, large ice caps on Durmitor, Montenegro, covering ~1500 km^2 and 720 km^2 during MIS 12 and MIS 6 respectively (Hughes et al., 2011). At Mount Chelmos, in the Peloponnesus (Fig. 1, location P), three phases of Late Pleistocene glaciation have been identified using ^{36}Cl TCN dating on limestone moraine boulders (Pope et al., 2017). Glaciers advanced and stabilised between 40 and 30 ka, before retreating at 23–21 ka soon after the global Last Glacial Maximum (LGM; 27.5–23.3 ka).

* Corresponding author.
E-mail address: james.allard@manchester.ac.uk (J.L. Allard).

https://doi.org/10.1016/j.quascirev.2020.106528
0277-3791/

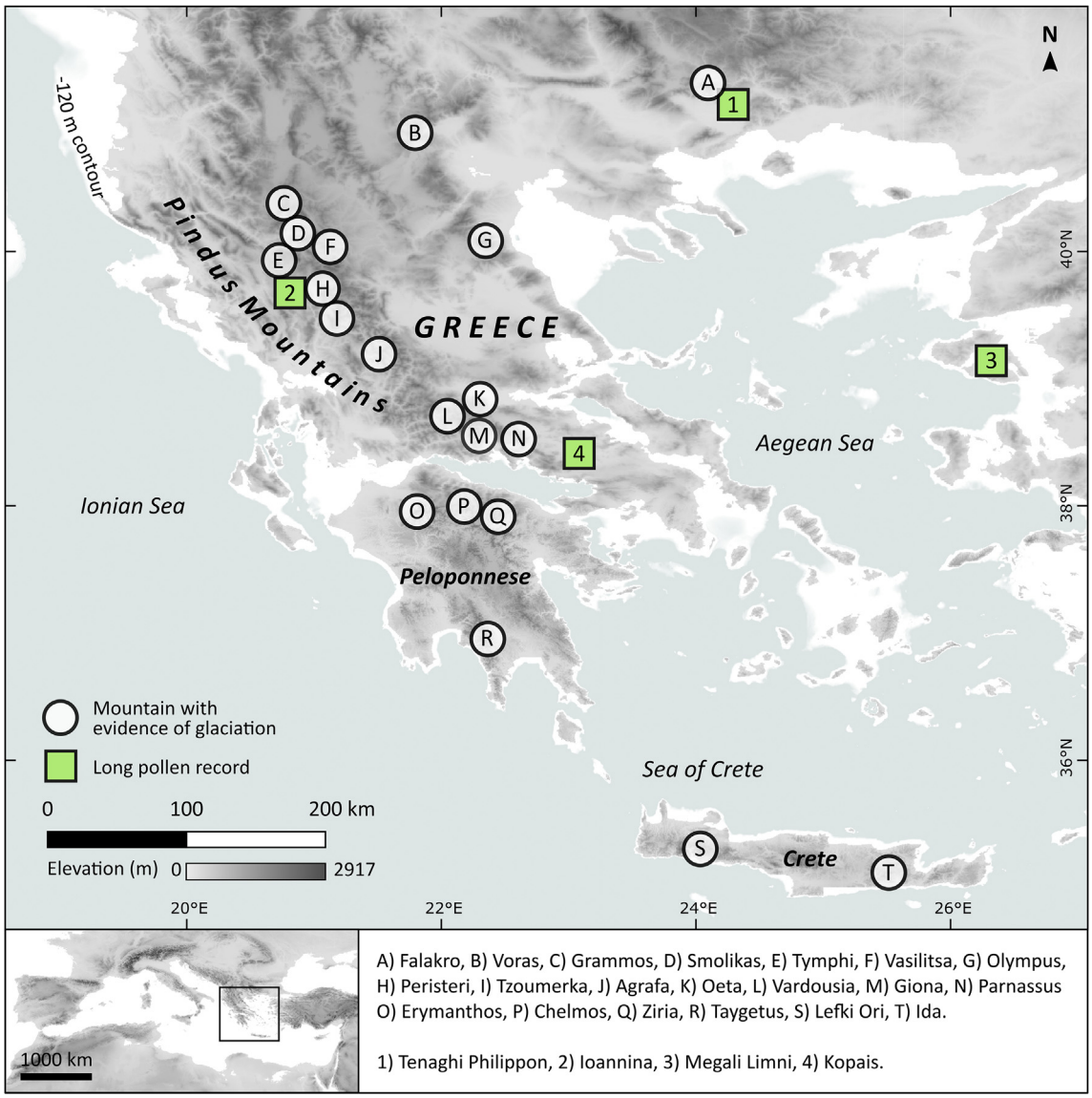

Fig. 1. Mountains in Greece where evidence of glaciation has been identified (A–T) and the location of long pollen records discussed in the text (1–4). The focus of this study is the glacial landforms of Mount Tymphi in the Pindus Mountains (location E).

Glaciers then stabilised at 13–10 ka in the Late-glacial, and possibly during the Younger Dryas. Terminal moraines on Mount Chelmos that lie further downvalley remain undated and are hypothesised to be of Middle Pleistocene age (Pope et al., 2017; Leontaritis et al., 2020). Optically-stimulated luminescence (OSL) dating in the Spanolakos valley of Mount Chelmos may also indicate an earlier phase of Late Pleistocene glacier activity early in the last glacial cycle at c. 89–86 ka (Pavlopoulos et al., 2018).

At least 3 sets of glacial deposits have also been recorded in the Mount Olympus glacial sequence (Fig. 1, location G) (Smith et al., 1997), which provides an important comparison to the record on Mount Tymphi (Woodward et al., 2004). Pioneering ^{36}Cl TCN dating was conducted here by Manz (1998). Since then, 20 ^{36}Cl exposure dates have been published from moraine boulders and ice-moulded bedrock in the high cirques of Mount Olympus (Styllas et al., 2018). Moraine stabilisation during the Late-glacial at c. 15.5 ± 2.0 ka preceded retreat at c. 14–13.5 ± 2.0 ka that separated a later stabilisation at 12.5 ± 1.5 ka. Cirque glaciation persisted during the Holocene at 9.6 ± 1.1 ka, 2.5 ± 0.3 ka, and 0.64 ± 0.08 ka in the Megala Kazania cirque (Styllas et al., 2018).

Elsewhere in the Mediterranean mountains, robust glacial chronologies have been developed in Iberia (Rodríguez-Rodríguez et al., 2015; Andrés et al., 2018; Oliva et al., 2019) and Turkey (Akçar et al., 2017; Sarıkaya and Çiner, 2017). The recent success of ^{36}Cl TCN dating in the Balkans (e.g. Pope et al., 2017; Gromig et al., 2018) and the wider Mediterranean offers the potential for dating glacial surfaces more widely in the limestone mountains of the Balkan peninsula - and in doing so addressing an important geographical gap in the Mediterranean glacial record and a temporal gap in the glacial record of Greece (Hughes and Woodward, 2017). In some parts of the Mediterranean glaciers were larger during MIS 5, 4, and 3 than during the global LGM of MIS 2 (e.g. Lewis et al., 2009; Pallàs et al., 2010; Delmas et al., 2011; Reber et al., 2014; Pope et al., 2017; Hughes et al., 2018). Understanding where, when and why Mediterranean glaciers reached their maxima during the last glacial cycle is not only important for understanding the dynamics of the glacial climate in this region, but also for the better understanding of sediment and meltwater delivery to river

systems, the dynamics of Mediterranean refugia, and has implications for understanding the environmental context of Middle and Upper Palaeolithic archaeological records (Hughes and Woodward, 2008, 2017). This paper has three principal aims: *(1) to date the Late Pleistocene record on Mount Tymphi, (2) to correlate this glacial record with existing records of landscape change and human activity in NW Greece,* and *(3) to explore the problems of ^{36}Cl TCN dating on old moraines with existing age control.*

Here we present the results from ^{36}Cl exposure dating of limestone boulders and glaciated bedrock in the uppermost valleys and cirques of Mount Tymphi (2497 m), in northwest Greece. We address both a significant geographical gap in Mediterranean glacial chronologies and the temporal gap in the glacial history of this region by targeting the previously undated Late Pleistocene glacial record. Coupled with published Uranium-series ages from older, lower elevation moraines (Woodward et al., 2004; Hughes et al., 2006a), this is the first glacial chronology in the east-central Mediterranean based on multiple dating methods.

2. Study area

Mount Tymphi is located in the Pindus Mountains, northwest Greece (Fig. 1). Multiple summits exceeding 2000 m a.s.l. form a massif c. 200 km^2 that trends from southeast to northwest, culminating at Gamila (2497 m a.s.l.), the highest summit of Mount Tymphi (Fig. 2). Palaeocene to Eocene crystalline limestones dominate the upper slopes and contain bands of chert (IGME, 1970; Woodward et al., 1992; Bailey et al., 1997). Senonian-Jurassic dolomites and limestones are also exposed on the cliffs of the highest summits (IGME, 1970; 1983). In contrast, the lower slopes are dominated by late Eocene to Miocene flysch, including thin beds of graded sandstones intercalated with softer fissile siltstones (Lewin et al., 1991; Woodward et al., 1992; Hughes et al., 2006a). The highest summits form a drainage divide separating the Aoös River to the north and the Voidomatis River to the south (Woodward et al., 1994). The Voidomatis catchment drains an area of 384 km^2 to the south of the drainage divide, including the high relief glaciated terrain to the northeast of Tsepelovo village (Fig. 2) (Lewin et al., 1991; Woodward et al., 1992). Glaciofluvial sediments and Palaeolithic rockshelters flank the Voidomatis River within the Vikos canyon and on the Konitsa basin to the west (Lewin et al., 1991). Northwest Greece is located in a transition between Mediterranean and central European climates (Hughes, 2004). In July, a mean temperature of c. 15 °C is typical at high elevations, with 20 °C on the lower slopes (Furlan, 1977; Woodward et al., 1994). Mean annual precipitation at Skamnelli Meteorological Station (1180 m a.s.l) on the southeast slopes of Mount Tymphi is 1721 mm (Fotiadi et al., 1999). At higher elevations, annual precipitation very likely exceeds 2000 mm (Furlan, 1977; Hughes, 2004, p. 276). Winter precipitation falls as snow at high elevations and snow patches typically survive into the summer months.

Many of the moraines between c. 900–2100 m a.s.l. are well preserved partly due to karstic drainage and cementation of moraines (Woodward et al., 2004; Hughes et al., 2006a). Three distinct sets of glacial deposits have been identified on the Tymphi massif (Fig. 3) (Hughes, 2004). This is a classic example of a Mediterranean glacio-karst landscape (Hughes et al., 2006a; Woodward et al., 2008; Lewin and Woodward, 2009; Woodward and Hughes, 2019). Lateral and terminal moraines, glacially-transported limestone boulders, ice-moulded bedrock pavements, kame terraces and tills are present in the glacially-eroded U-shaped valleys that emanate from the south-facing cirques (Fig. 3) (Lewin et al., 1991). Exposed sections in lateral moraines contain unweathered diamictons of sub-rounded and striated boulders and gravel-sized

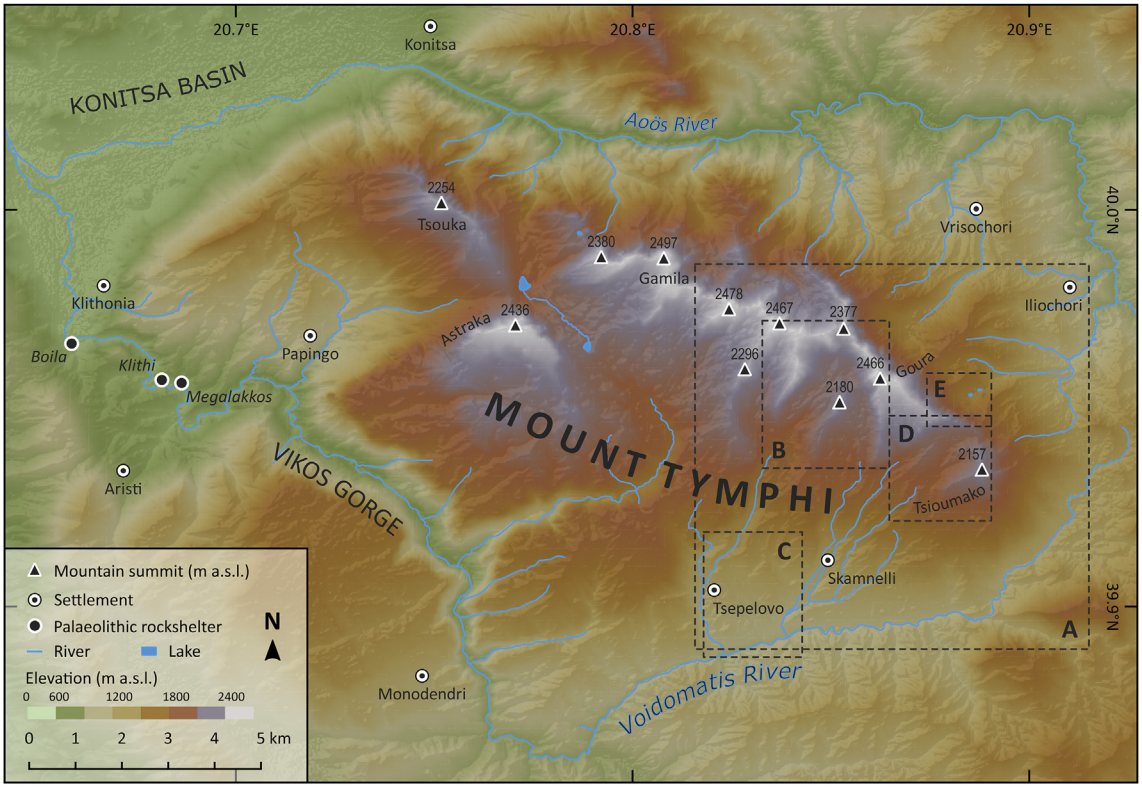

Fig. 2. DEM of the Mount Tymphi study area showing major peaks and dashed boxes A–E, where limestone boulders were sampled for ^{36}Cl exposure ages. Details of the glacial geomorphology and ^{36}Cl ages for each of the sites A to E are given in Figs. 3, 6 and 8a, 8b and 9 respectively.

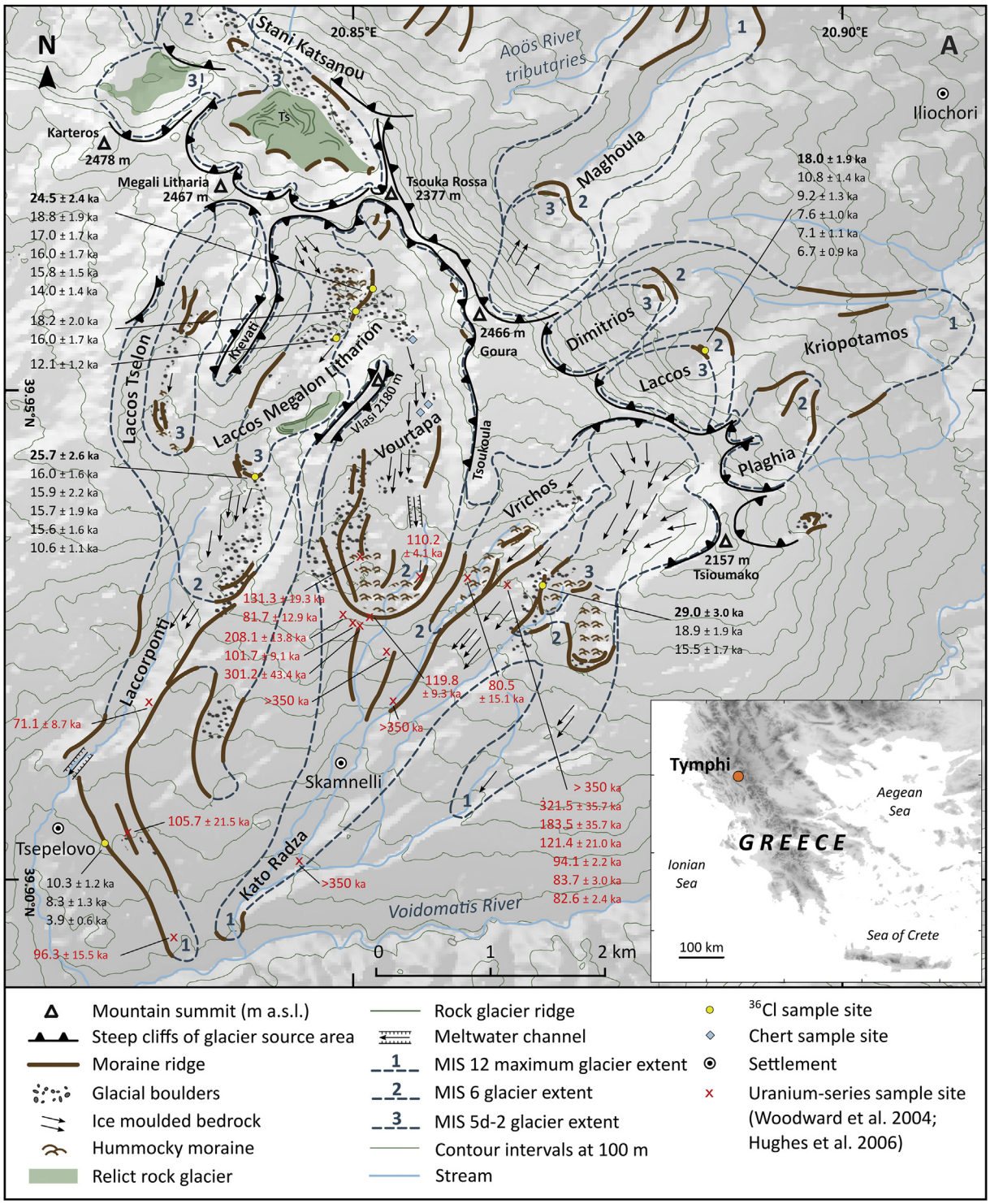

Fig. 3. Glacial geomorphology of the Mount Tymphi massif, Epirus, northwest Greece. The location and ^{36}Cl ages of moraine boulders are identified along with Uranium-series sample sites and ages from secondary carbonates within glacial deposits (Woodward et al., 2004; Hughes et al., 2006a). The maximum extent of glaciation during MIS 12 (Skamnellian Stage), MIS 6 (Vlasian Stage) and MIS 5d–2 (Tymphian Stage) is denoted by stratigraphical units 1, 2 and 3 respectively. A more detailed reconstruction of Late Pleistocene glacier ice thickness and extent is shown in Fig. 10. Adapted from data in Woodward et al. (2004) and Hughes et al. (2006). This is map tile A in Fig. 2.

clasts in a calcium carbonate-rich rock flour matrix (Woodward et al., 1992). Periglacial features have been recorded in the highest parts of the massif. Frost-shattered bedrock and patterned ground are evident on the mountain summits (Hagedorn, 1969; Hughes, 2004) and in the north, relict rock glaciers occupy the high cirques (Hughes et al., 2003). Thick screes also mantle the high slopes beneath arêtes and steep valley walls. Karst features including dolines, stepped limestone pavements, solution channels, vertical shafts and cave systems are also well developed (Waltham, 1978; Lewin et al., 1991; Hughes et al., 2006a; Lewin and Woodward, 2009). Dolines are particularly common along former glacial margins where they have been enlarged by sinking points of

glacial meltwater (Veress et al., 2019). The Pindus Mountains are seismically active. Uplift in the Epirus region is estimated to be between 40 and 80 m in the last 100 ka (King and Bailey, 1985).

Evidence of multiple glacial periods is echoed by the presence of glacial outwash in the sedimentary record of the Voidomatis River (Woodward et al., 1994, 2008). Welldated fluvial units downstream of the glaciated upper catchment in the Vikos canyon, the lower Vikos gorge, and on the Konitsa basin, represent periods of peak glacial sediment input during the Middle and Late Pleistocene (Lewin et al., 1991; Woodward et al., 1992, 1994). The rapid response of regional tree populations recorded in the Ioannina pollen record (Tzedakis et al., 2002) c. 30 km to the south of Mount Tymphi provides a record of moisture supply and climatic change that helps to frame our understanding of long-term changes in glacier mass balance.

3. Methods

3.1. Geomorphological mapping

Building on previous work (Hughes, 2004; Woodward et al., 2004; Hughes et al., 2006a), geomorphological mapping of glacial depositional and erosional features was conducted using high resolution satellite imagery (Bing Maps and Google Earth), 1:50,000 topographic maps (Anavasi, 2018) and during fieldwork in summer 2018. Geomorphological mapping followed the principles of morphostratigraphy outlined in Hughes (2013). Detailed geomorphological maps were produced using SRTM digital elevation model (DEM) data, available from https://earthexplorer.usgs.gov/ at a resolution of 1 arc-second (30 m) (USGS, 2019). The WGS 84 coordinate reference system was selected and a hillshade model was derived from the DEM to help visualise the topography.

3.2. ^{36}Cl cosmogenic nuclide exposure dating

Terrestrial cosmogenic nuclide (TCN) dating works on the basis that a rock or sediment surface accumulates cosmogenic nuclides as it is exposed to cosmic rays (Phillips et al., 1986; Ivy-Ochs and Kober, 2008). The concentration of cosmogenic nuclides within a surface is determined by the length of time it has been exposed to cosmic rays, the local production rate of the target nuclide (Lal, 1991) and the surface erosion rate. Cosmogenic isotopes are produced in commonly occurring minerals and can therefore be analysed on various lithologies. The mountains of Greece and the western Balkans are dominated by crystalline limestones, the surfaces of which accumulate ^{36}Cl isotopes when exposed to cosmic rays. A total of 82 ^{36}Cl cosmogenic nuclide exposure ages have been published from this region (e.g. Manz, 1998; Pope et al., 2017; Gromig et al., 2017; Styllas et al., 2018; Žebre et al., 2019; Çiner et al., 2019; Sarıkaya et al., 2020), with encouraging results in a range of contexts.

3.2.1. Sample collection

Sampling was focussed in the upper valleys and cirques of the Tymphi massif, to the northeast of Tsepelovo and Skamnelli villages (Fig. 2, box A; detailed in Fig. 3). To obtain an accurate landform age it is recommended to collect at least 3 samples per landform; and 6–7 boulders from older and tall moraines (50–100 m height and 40–100 ka old) (Putkonen and Swanson, 2003). We sampled 27 glacial boulders for ^{36}Cl TCN dating, from 5 sets of moraines (Table 1). We selected 3–6 large (1–5 m diameter) and partly embedded boulders on the crest of each moraine to minimise the processes and effects of incomplete exposure and inheritance (Hallet and Putkonen, 1994; Zreda et al., 1994; Putkonen and Swanson, 2003; Balco, 2011; Heyman et al., 2011; Applegate et al.,

Table 1
^{36}Cl sample locations and attributes of glacial boulders.

Sample ID	Latitude	Longitude	Elevation	Sample thickness	Density	Topographic shielding	Boulder dimensions
	°N	°E	m (a.s.l)	cm	g/cm^3		m (L x W x H)
Laccos Megalon Litharion							
MLL-01	39.94115	20.83997	1714	3.5	2.7	0.9720	2.2 × 2.1 x 1.7
MLL-02	39.94115	20.83996	1712	2	2.6	0.9720	1.7 × 1.3 x 0.95
MLL-03	39.94114	20.83988	1710	2.5	2.7	0.9720	1.85 × 1.5 x 1.25
MLL-04	39.94255	20.83931	1705	3.5	2.7	0.9798	1.1 × 1.0 x 0.6
MLL-05	39.94267	20.83923	1706	1.5	2.7	0.9798	2.7 × 1.9 x 1.7
MLL-06	39.94281	20.83828	1744	1.5	2.6	0.9796	2.9 × 2.6 x 2.0
MLL-07	39.96107	20.85183	2033	2.5	2.6	0.9781	1.7 × 1.4 x 0.8
MLL-08	39.96045	20.85197	2034	2.5	2.6	0.9781	1.3 × 1.0 x 0.9
MLL-09	39.96038	20.85202	2035	2	2.5	0.9781	2.2 × 1.3 x 1.3
MLL-10	39.96019	20.85166	2029	4.5	2.5	0.9781	2.5 × 1.7 x 1.5
MLL-11	39.96015	20.85179	2031	2	2.7	0.9781	1.6 × 1.5 x 0.6
MLL-12	39.95971	20.85174	2030	2.5	2.5	0.9781	2.2 × 1.9 x 1.4
MLL-13	39.95806	20.85028	2001	2	2.6	0.9828	2.3 × 1.9 x 1.9
MLL-14	39.95783	20.85019	2001	2.5	2.6	0.9828	5.2 × 2.3 x 2.3
MLL-15	39.95531	20.84828	1996	3	2.6	0.9828	3.9 × 3.3 x 2.8
Tsioumako							
TMK-01	39.93113	20.86956	1766	2.5	2.6	0.9980	2.8 × 2.6 x 1.8
TMK-02	39.93005	20.86937	1773	2.5	2.7	0.9980	3.1 × 1.9 x 1.3
TMK-03	39.92993	20.86934	1771	2.5	2.6	0.9980	2.2 × 1.4 x 1.3
Laccorponti							
TS-01	39.904166	20.824381	1121	3	2.6	0.9976	3.7 × 3.05 x 1.9
TS-02	39.90371	20.82462	1113	2.5	2.8	0.9976	2.95 × 2.1 x 1.25
TS-03	39.90363	20.82472	1110	2.5	2.7	0.9976	2.95 × 2.7 x 1.25
Laccos							
LAC-01	39.95384	20.88566	1428	2.5	2.3	0.9461	1.8 × 1.65 x 1.4
LAC-02	39.95384	20.88575	1430	2.5	2.6	0.9461	1.3 × 1.3 x 1.0
LAC-03	39.9544	20.88562	1426	2.5	2.7	0.9461	1.7 × 1.5 x 1.35
LAC-04	39.95409	20.88546	1430	2.5	2.8	0.9461	1.6 × 1.1 x 1.1
LAC-05	39.95406	20.88598	1423	2.5	2.7	0.9461	0.8 × 0.7 x 0.5
LAC-06	39.95392	20.88549	1433	2.5	2.7	0.9461	5.0 × 5.0 x 5.0

2010; et al., 2012). We used a hammer and chisel to obtain samples (~500 g) from the upper 3–5 cm on the top and centre of each boulder. Care was taken to avoid surface irregularities and karst weathering features such as dissolution hollows and rillenkarren channels which complicate the interpretation of nuclide concentrations. Topographic shielding was measured in the field using a hand-held abney level and compass (Gosse and Phillips, 2001) and calculated using the online Topographic Shielding Calculator v2.0 http://stoneage.ice-d.org/math/skyline/skyline_in.html (Balco, 2018). Sample elevation, GPS location data, and boulder dimensions were all measured in the field.

3.2.2. Sample preparation

Limestone rock samples were processed at The University of Manchester and at the Australian Nuclear Science and Technology Organisation (ANSTO). Rock samples were crushed and sieved into grain sizes (0–250 μm, 250–500 μm and >500 μm) following Stone et al. (1996). 50 g of the 250–500 μm was sub-sampled, washed with de-ionised water and then leached in 1.5 M HNO_3 to remove atmospheric ^{36}Cl, secondary carbonates and organic particles. About 20 g of the leached sample was then dissolved in 2 M HNO_3 and a^{37}Cl enriched spike was added with known ratios of ^{35}Cl:^{37}Cl. Three chemistry blanks were prepared alongside the 27 samples. $AgNO_3$ was added to the solution to recover the chloride and produce a AgCl precipitate. This AgCl was then dissolved in NH_3 and with the addition of a saturated $Ba(NO_3)_2$ solution, $BaSO_4$ was precipitated in order to remove ^{36}S. Final AgCl precipitation was achieved with the addition of HNO_3. The AgCl targets were pressed into an AgBr bed within Cu target holders. ^{36}Cl events and stable Cl isotopes ^{35}Cl and ^{37}Cl were measured by Accelerator Mass Spectrometry (AMS) at ANSTO, Sydney, Australia (Table 2) (Wilcken et al., 2019). Major element concentrations (Table 3) were determined using inductively coupled plasma optical emission spectrometry (ICP-OES) at The University of Manchester. Trace elements and rare earths (Table 3) were measured with inductively coupled plasma mass spectrometry (ICP-MS) at The University of Manchester. CO_2 content was determined using loss on ignition. Rock density was calculated using a water displacement method.

3.2.3. ^{36}Cl exposure age calculations

Exposure ages were calculated using the CRONUS ^{36}Cl Exposure Age Calculator v2.0 http://cronus.cosmogenicnuclides.rocks/2.0/html/cl/ (Table 4 and Fig. 4) (Marrero et al., 2016a). Cosmogenic ^{36}Cl production rates for Ca spallation (56.0 ± 4.1 atoms ^{36}Cl (g Ca)$^{-1}$ yr^{-1}), K spallation (155 ± 11 atoms ^{36}Cl (g K)$^{-1}$ yr^{-1}), and thermal neutron production (759 ± 180 neutrons (g air)$^{-1}$ yr^{-1}) were used (Marrero et al., 2016b) with the time dependent LSDn (Sa) scaling scheme (Lifton et al., 2014). Lower Ca production rates of Stone et al. (1996) and Schimmelpfennig et al. (2011) produce ages up to 24% older (Table 5). We correct ^{36}Cl exposure ages using an independent and minimum estimate of limestone erosion (see section 3.2.4) and hence, for our choice in production rate used in Table 4, ages reported here provide minimum limiting ages.

Spallation and muon interactions on Ca account for 54–96% of ^{36}Cl produced in these samples, whilst low energy thermal neutron absorption by ^{35}Cl accounts for the remaining 46–4% of total ^{36}Cl produced. The low K_2O content (<0.03%) of the samples means that K spallation accounts for <0.2% of total ^{36}Cl production and thus differences in K spallation production rates are negligible for these samples. Spallation from Fe and Ti contribute to <0.01% of total ^{36}Cl production. The LSDn (Sa) scaling framework includes separate scaling factors for spallation reactions with Ca, K, Fe and Ti, and also

Table 2
Analytical data for ^{36}Cl samples on Mount Tymphi.

Sample ID	Sample mass (g)	Mass of Cl spike solution (mg)[a]	Analytical stable isotope ratio ($^{37}Cl/^{35}Cl$)[b]	Analytical $^{36}Cl/Cl$ ratio ($^{36}Cl/10^{15}$ Cl)[c]	^{36}Cl measured (10^4 atoms g^{-1} rock)
MLL-01	20.211	1.051	0.963 ± 0.033	759.046 ± 38.837	111.55 ± 12.10
MLL-02	20.210	1.086	1.060 ± 0.042	732.334 ± 37.146	101.30 ± 11.14
MLL-03	20.410	1.088	1.162 ± 0.028	643.759 ± 27.321	81.40 ± 8.46
MLL-04	20.250	1.102	1.172 ± 0.030	700.755 ± 28.805	89.82 ± 9.32
MLL-05	20.350	1.148	1.163 ± 0.049	664.394 ± 65.985	88.81 ± 12.52
MLL-06	20.260	1.103	0.994 ± 0.029	566.214 ± 49.190	84.19 ± 10.81
MLL-07	20.350	1.104	1.060 ± 0.027	752.143 ± 29.471	105.07 ± 10.63
MLL-08	20.320	1.145	1.344 ± 0.036	922.776 ± 39.884	110.21 ± 11.95
MLL-09	20.280	1.102	1.222 ± 0.031	938.613 ± 39.547	116.28 ± 12.21
MLL-10	20.500	1.004	0.826 ± 0.022	727.688 ± 35.776	119.16 ± 12.65
MLL-11	20.530	1.093	0.813 ± 0.018	648.441 ± 27.019	117.51 ± 11.94
MLL-12	20.360	1.095	1.164 ± 0.035	744.825 ± 35.460	94.93 ± 10.17
MLL-13	20.180	1.041	0.925 ± 0.032	796.772 ± 52.703	121.22 ± 14.12
MLL-14	20.210	1.096	1.125 ± 0.035	779.019 ± 45.445	103.18 ± 11.56
MLL-15	20.450	1.107	1.179 ± 0.041	677.821 ± 28.103	86.04 ± 9.12
TMK-01	20.150	1.124	1.357 ± 0.052	1264.018 ± 53.508	148.52 ± 16.37
TMK-02	20.120	1.100	1.363 ± 0.050	778.909 ± 37.687	89.19 ± 10.05
TMK-03	20.430	1.152	1.357 ± 0.050	671.978 ± 34.961	79.50 ± 9.08
TS-01	20.070	1.106	1.404 ± 0.053	243.975 ± 25.965	27.01 ± 4.12
TS-02	20.450	1.142	1.226 ± 0.033	119.437 ± 13.253	14.49 ± 2.33
TS-03	20.300	1.095	1.288 ± 0.034	280.417 ± 11.682	32.56 ± 3.54
LAC-01	20.320	1.126	0.639 ± 0.012	175.158 ± 11.999	45.72 ± 5.58
LAC-02	20.290	1.103	0.689 ± 0.014	189.410 ± 12.305	43.12 ± 5.12
LAC-03	20.330	1.083	0.642 ± 0.016	138.954 ± 12.001	34.47 ± 4.72
LAC-04	20.750	1.094	0.597 ± 0.010	144.382 ± 13.514	40.14 ± 5.63
LAC-05	20.670	1.106	1.097 ± 0.031	707.171 ± 37.489	94.43 ± 10.23
LAC-06	20.410	1.104	0.617 ± 0.012	139.008 ± 9.683	37.38 ± 4.65

[a] Mass of enriched chlorine spike with a calculated isotopic $^{37}Cl/^{35}Cl$ ratio of 2.0127.
[b] AMS measured $^{37}Cl/^{35}Cl$ ratio in spiked sample with 1 sigma errors.
[c] Background corrected and normalised AMS $^{36}Cl/Cl$ ratio in spiked sample with final total analytical error with reproducibility error derived from spread in standard reference measurements in quadrature.

Table 3
Major and trace element data for the carbonate material of the Mount Tymphi rock samples.

Sample ID	Major elements (wt. %)								Trace elements						
	Al_2O_3	Fe_2O_3	MnO	MgO	CaO	Na_2O	K_2O	CO_2	B	Sm	Gd	U	Th	Li	Cl
	wt. %	wt. %	wt. %	wt. %	wt. %	wt. %	wt. %	wt. %	ppm	ppm	ppm	ppm	ppm	ppm	ppm (a)
MLL-01	0.031	0.009	0.001	0.578	26.093	0.113	0.005	42.843	40.522	0.725	0.964	4.927	<0.001	4.013	37.248
MLL-02	0.032	0.028	0.002	1.639	45.632	0.120	0.013	42.431	20.780	5.741	6.467	10.190	<0.001	7.937	30.557
MLL-03	0.049	0.035	0.004	2.308	56.407	0.144	0.017	42.600	7.911	4.390	5.482	12.026	<0.001	11.465	24.040
MLL-04	0.047	0.022	0.002	0.360	38.060	0.110	0.014	43.084	2.821	2.119	2.768	6.185	<0.001	4.983	23.979
MLL-05	0.030	0.014	0.002	0.402	38.054	0.105	0.007	42.295	<0.001	2.720	3.416	6.371	<0.001	5.714	25.375
MLL-06	0.027	0.015	0.001	0.280	32.806	0.106	0.011	42.228	<0.001	1.572	1.966	4.967	<0.001	4.025	36.191
MLL-07	0.029	0.028	0.003	1.946	30.410	0.102	0.012	42.048	<0.001	3.044	4.434	5.139	<0.001	4.586	30.854
MLL-08	0.027	0.014	0.001	0.376	31.353	0.101	0.006	42.556	<0.001	1.070	1.174	6.107	<0.001	3.284	16.812
MLL-09	0.019	0.011	0.001	0.721	22.214	0.095	0.001	42.882	<0.001	0.972	1.248	3.491	<0.001	0.958	21.377
MLL-10	0.022	0.012	0.003	0.435	47.331	0.138	0.010	42.551	98.486	2.282	2.642	19.176	<0.001	21.778	50.058
MLL-11	0.018	0.011	0.002	0.291	37.042	0.120	0.008	42.682	32.692	1.156	1.486	5.617	<0.001	9.984	56.377
MLL-12	0.035	0.015	0.001	1.770	30.781	0.097	0.010	42.343	13.390	0.933	1.208	6.926	<0.001	4.499	24.109
MLL-13	0.042	0.028	0.002	1.726	33.336	0.103	0.012	42.095	7.891	1.663	2.302	7.249	<0.001	5.905	40.669
MLL-14	0.068	0.035	0.002	1.799	34.536	0.096	0.024	42.283	<0.001	2.272	3.175	10.766	<0.001	7.299	26.593
MLL-15	0.047	0.024	0.003	2.138	40.019	0.100	0.016	42.322	<0.001	2.777	3.985	7.487	<0.001	6.354	23.505
TMK-01	0.036	0.029	0.004	0.367	31.627	0.082	0.011	42.651	<0.001	2.004	2.433	8.306	<0.001	3.562	16.116
TMK-02	0.037	0.027	0.006	0.342	38.196	0.098	0.012	41.857	<0.001	1.539	1.955	10.904	<0.001	8.203	15.598
TMK-03	0.035	0.032	0.001	0.273	25.995	0.077	0.008	42.165	<0.001	1.622	1.935	3.381	<0.001	3.952	16.301
TS-01	0.016	0.023	0.005	0.567	36.510	0.130	0.017	42.710	87.935	1.394	1.868	17.004	<0.001	16.935	14.268
TS-02	0.074	0.036	0.008	0.425	42.419	0.102	0.025	42.695	38.778	2.885	3.934	8.476	<0.001	8.768	21.791
TS-03	0.028	0.032	0.007	0.398	34.608	0.089	0.007	43.008	17.415	2.029	2.571	9.999	<0.001	10.677	18.276
LAC-01	0.037	0.018	0.003	15.005	27.707	0.083	0.009	43.224	<0.001	2.642	3.616	14.469	<0.001	5.098	103.216
LAC-02	0.028	0.022	0.003	12.652	21.810	0.081	0.011	45.173	<0.001	1.607	2.404	3.720	<0.001	7.867	84.352
LAC-03	0.026	0.020	0.002	12.910	21.353	0.081	0.007	44.669	<0.001	3.616	5.276	14.110	<0.001	5.926	98.165
LAC-04	0.025	0.018	0.003	15.688	27.468	0.090	0.006	42.577	<0.001	4.357	6.443	26.434	<0.001	7.408	116.190
LAC-05	0.041	0.038	0.009	5.469	46.786	0.104	0.022	42.796	<0.001	5.934	7.460	7.967	<0.001	12.769	27.981
LAC-06	0.041	0.031	0.003	20.256	34.370	0.113	0.015	43.888	12.661	4.046	5.747	28.428	<0.001	15.439	109.746

[a] Assumed $^{37}Cl/^{35}Cl$ natural ratio in rock of 0.3198.

for low energy reactions (Borchers et al., 2016; Marrero et al., 2016b). All samples were corrected for topographic shielding and sample thickness. No corrections were made for snow shielding as we sampled the tallest available boulders, most representative of the moraine crest and least prone to snow cover. The majority of sample sites were above the treeline and thus exposed to wind, which would inhibit the accumulation of snow (Briner et al., 2005). A fast neutron attenuation length of 177 g/cm^2 was selected (Farber et al., 2008). Sample information and element concentrations are provided in Tables 1–3.

3.2.4. Erosion rate correction

An erosion rate was determined in the field on ice-scoured limestone bedrock at an altitude of 1985 m a.s.l. (39.94826°N, 20.85709°E) in the upper Vourtapa Valley. The maximum observed thickness of up-standing chert veins was used to estimate differential erosion rates (Fig. 5). Chert is much harder than limestone and extremely resistant to weathering (Dirks et al., 2016) with a mohs scale value of 7 compared to 3–4 for limestone. At this site the chert veins stood 8 cm above the limestone clints and highlight more rapid rates of erosion on the limestone (Fig. 5d). This bedrock is within glacier limits ascribed to the Vlasian Stage (MIS 6) based on U-series dating (Woodward et al., 2004; Hughes et al., 2006a). Assuming that glacier erosion is unlikely to have occurred on this bedrock since the end of the Vlasian (~130 ka ago), then this implies an erosion rate of 0.6 mm ka^{-1}. This is a *minimum* erosion rate and therefore these erosion-corrected ages represent minimum exposure ages. Had the upper Vourtapa valley been glaciated again during MIS 2 (for example at 12 ka during the Younger Dryas) then the inferred erosion rate would be only 6.7 mm ka^{-1}. These erosion rate estimates represent the differential erosion rate between chert and limestone. Given that chert is highly resistant and that a recent study (Ben-Israel et al., 2020) suggests that chert erosion rates are very low, we favour ages corrected for 0.6 mm ka^{-1} on the assumption that chert erosion is negligible. Although we suggest it is unlikely that limestone erosion rates were larger than 10 mm ka^{-1}, due to uncertainty in determining an absolute limestone erosion rate for this region we also report ^{36}Cl ages for 0.6, 5, 10 and 20 mm ka^{-1} erosion correction (Table 4). We note that in some cases ^{36}Cl ages decrease when the erosion correction is increased. The thermal neutron flux as a function of depth within a boulder initially increases (to a subsurface peak at ~100 g/cm^2 depth) and attenuates exponentially with depth (Zreda et al., 1994; Gosse and Phillips, 1991). This behaviour is due to diffusion loss of the thermalised neutron flux from shallow depths to the atmosphere. Hence for intermediate erosion rates, depending on the concentration of ^{35}Cl, ^{36}Cl concentrations can increase with depth, resulting in decreasing exposure ages for increasing erosion rates. In this study, samples with >50 ppm Cl result in >25% of ^{36}Cl production via thermal neutrons and exhibit this behaviour as seen in comparing trends for LAC-01–06 to MLL-01–06 in Table 4.

3.3. Glacier reconstructions

Palaeoglacier surfaces and ice volumes were reconstructed using the GlaRe toolbox, a semi-automated GIS tool developed by Pellitero et al. (2016). Glacier reconstructions were produced using SRTM DEM data (USGS, 2019). To take post-glacial landform changes into consideration, the hydrology fill tool was used to smooth the valley floor topography. The DEM resolution was also increased to 5 m by interpolation to smooth the DEM and to avoid spurious surfaces when reconstructing the palaeoglaciers. Geomorphological field evidence including terminal and lateral moraines, glacial boulder limits, trimlines and ice-moulded bedrock were used to establish palaeoglacier dimensions. Where glacial evidence was fragmentary or absent, an outline of the

Table 4
Results of ^{36}Cl analysis and exposure age calculations.

Sample ID	Surface exposure ages				Landform age
	erosion corrected (0.6 mm ka^{-1})	erosion corrected (5 mm ka^{-1})	erosion corrected (10 mm ka^{-1})	erosion corrected (20 mm ka^{-1})	oldest age corrected for 0.6 mm ka^{-1} erosion
	ka	ka	ka	ka	ka
SOUTHERN VALLEYS					
Laccos Megalon Litharion lower valley terminal moraine					
MLL-01	**25.7 ± 2.6**	25.7 ± 2.7	26.7 ± 3.0	32.0 ± 5.2	**25.7 ± 2.6**
MLL-02	15.6 ± 1.6	16.0 ± 1.7	16.4 ± 1.9	18.0 ± 2.4	
MLL-03	10.6 ± 1.1	10.8 ± 1.2	11.1 ± 1.2	11.9 ± 1.4	
MLL-04	16.0 ± 1.6	16.0 ± 1.7	16.8 ± 1.8	18.3 ± 2.2	
MLL-05	15.9 ± 2.2	16.0 ± 2.2	16.3 ± 2.3	17.5 ± 2.8	
MLL-06	15.7 ± 1.9	15.3 ± 1.8	15.2 ± 1.8	15.5 ± 2.1	
Laccos Megalon Litharion cirque terminal moraine					
MLL-07	17.0 ± 1.7	17.0 ± 1.6	16.8 ± 1.7	17.5 ± 1.9	**24.5 ± 2.4**
MLL-08	18.8 ± 1.9	19.0 ± 1.9	19.5 ± 2.0	21.3 ± 2.7	
MLL-09	**24.5 ± 2.4**	23.7 ± 2.3	23.6 ± 2.4	25.0 ± 2.9	
MLL-10	14.0 ± 1.4	14.3 ± 1.5	14.8 ± 1.6	16.3 ± 2.1	
MLL-11	15.8 ± 1.5	15.6 ± 1.5	16.0 ± 1.6	16.7 ± 1.9	
MLL-12	16.0 ± 1.7	16.0 ± 1.7	16.6 ± 1.8	17.7 ± 2.1	
MLL-13	18.2 ± 2.0	17.8 ± 2.0	17.8 ± 2.0	18.8 ± 2.3	
MLL-14	16.0 ± 1.7	16.0 ± 1.7	16.1 ± 1.8	17.1 ± 2.1	
MLL-15	12.1 ± 1.2	12.2 ± 1.3	12.4 ± 1.4	13.1 ± 1.6	
Tsioumako right lateral moraine					
TMK-01	**29.0 ± 3.0**	29.9 ± 3.3	31.9 ± 4.0	40.6 ± 7.4	**29.0 ± 3.0**
TMK-02	15.5 ± 1.7	15.8 ± 1.8	16.4 ± 1.9	18.0 ± 2.4	
TMK-03	18.9 ± 1.9	18.9 ± 2.0	19.2 ± 2.0	20.0 ± 2.5	
Laccorponti lower valley right lateral moraine					
TS-01	8.3 ± 1.3	8.4 ± 1.4	8.7 ± 1.5	9.2 ± 1.6	>**350** *U-series (Woodward et al. 2004; Hughes et al., 2006a)*
TS-02	3.9 ± 0.6	3.9 ± 0.6	3.9 ± 0.6	4.0 ± 0.6	
TS-03	10.3 ± 1.2	10.4 ± 1.2	10.6 ± 1.3	11.2 ± 1.5	
NORTHEASTERN VALLEYS					
Laccos cirque inner terminal moraine					
LAC-01	9.2 ± 1.3	8.6 ± 1.1	8.1 ± 1.0	7.6 ± 0.8	10.8 ± 1.4
LAC-02	10.8 ± 1.4	9.8 ± 1.2	9.1 ± 1.1	8.3 ± 0.9	*Oldest preliminary age*
LAC-04	7.1 ± 1.1	6.6 ± 1.0	6.3 ± 0.9	5.9 ± 0.7	
LAC-06	6.7 ± 0.9	6.4 ± 0.9	6.2 ± 0.8	6.0 ± 0.7	
Laccos cirque outer terminal moraine					
LAC-03	7.6 ± 1.0	7.0 ± 1.0	6.5 ± 0.9	6.0 ± 0.7	18.0 ± 1.9
LAC-05	18.0 ± 1.9	18.4 ± 1.9	19.1 ± 2.0	21.4 ± 2.8	*Oldest preliminary age*

palaeoglacier catchment was created. User defined glacier flowlines were made (from snout to source) and the 'flowline ice thickness' tool was used to calculate palaeo-ice thickness along the flowlines. A default basal shear stress of 100 kPa was used in the flowline thickness construction, representative for both valley and cirque glaciers (Nye, 1952; Weertman, 1971). This gave palaeoglacier extents consistent with the glacial geomorphology. The 'glacier surface interpolation' tool was then applied to reconstruct the surface of the former glacier. The TOPO TO RASTER interpolation method was selected for glacier reconstructions. Palaeoglacier ice thickness was then calculated using the 'raster math' tool. Palaeoglacier area was calculated using the 'map algebra' spatial analyst tool.

3.4. ELA reconstructions

The equilibrium line altitude (ELA) of former glaciers was calculated using the area altitude balance ratio (AABR) method (Osmaston, 1975, 2005; Furbish and Andrews, 1984) in the ELA calculation toolbox developed by Pellitero et al. (2015). A balance ratio (BR) of 1.75 was selected in the AABR calculations, representative of a global average balance ratio (Osmaston, 2005; Rea, 2009). The AABR approach accounts for both glacier hypsometry and mass balance gradients (Osmaston, 2005; Pellitero et al., 2015). ELA calculations were validated using the area altitude (AA) method (Osmaston, 2005).

4. Results

4.1. Glacial geomorphology

Detailed glacial mapping was recorded for all major glaciated valleys of the Mount Tymphi massif as shown in Fig. 3.

4.1.1. Laccos Megalon Litharion

This valley is one of the largest palaeo-glacier source areas on the south-facing slopes of Mount Tymphi (Fig. 6). At its maximum extent, the Laccos Megalon Litharion glacier merged with the Laccos Tselon glacier to form the Laccorponti glacier, which extended approximately 8 km from its source area to c. 850 m a.s.l., where it drained into the Voidomatis River valley (Fig. 3). Three stratigraphic units of glacial deposits have been identified between the Laccos Megalon Litharion cirque and the maximum terminus in the Laccorponti valley (Fig. 3) (Hughes, 2004). They delineate the maximum glacial extents of the Skamnellian (MIS 12), Vlasian (MIS 6) and Tymphian Stages (MIS 5d–2) (Hughes et al., 2006a).

At the head of the valley (1980–2035 m a.s.l), thick glacial deposits on top of a bedrock ridge form a terminal moraine ridge c. 450 m long, that rises between 30 and 50 m above the cirque floor (Fig. 6). These deposits are located 1 km from the cirque headwall. The ridge dissects a large ice-scoured amphitheatre which is littered with large (>1 m diameter) sub-angular and sub-rounded limestone boulders (Fig. 7b). Aside from hummocky moraine

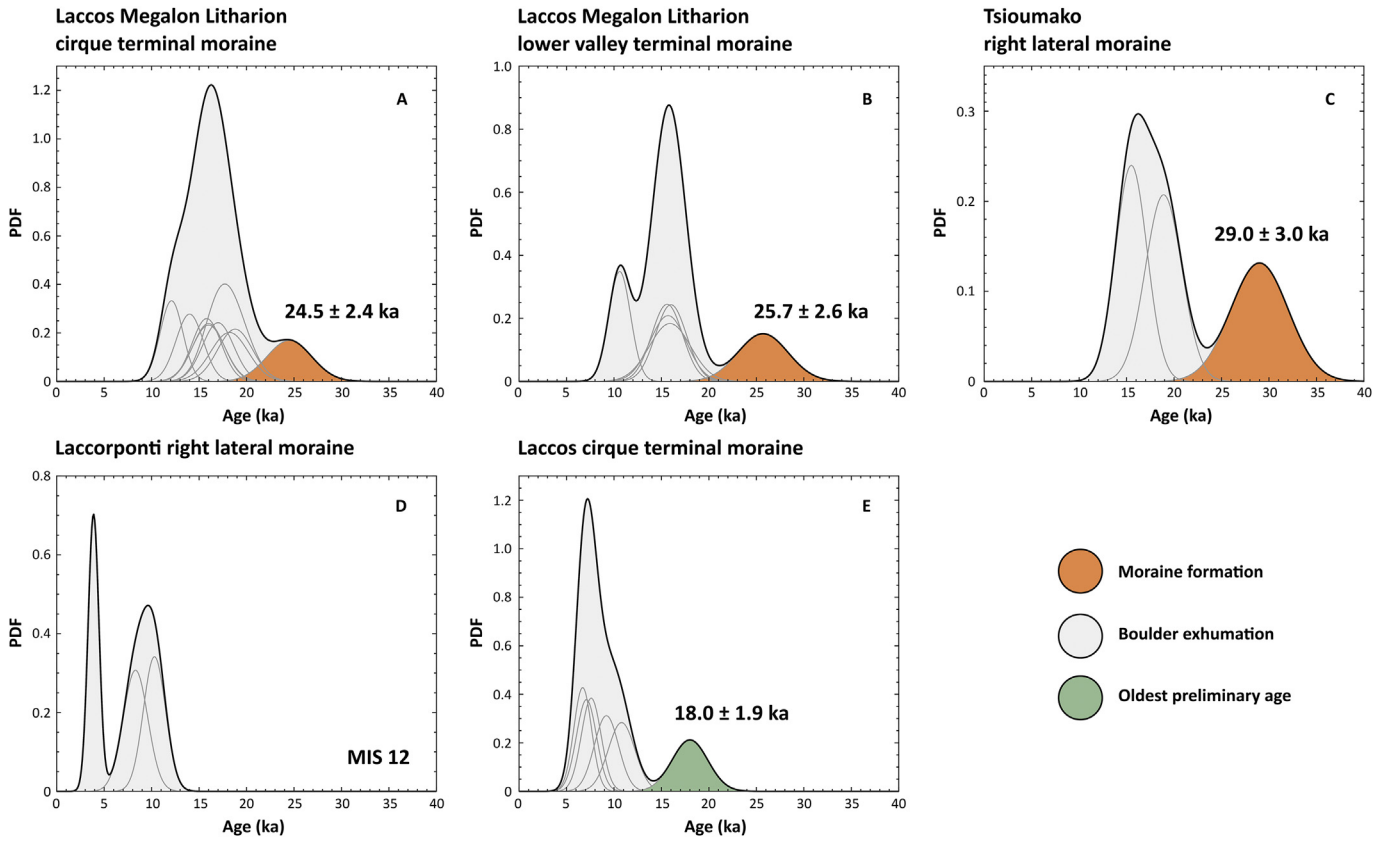

Fig. 4. Probability density function plots of ^{36}Cl exposure ages from Mount Tymphi. a) Laccos Megalon Litharion cirque terminal moraine (MLL-07–MLL-15), b) Laccos Megalon Litharion lower valley terminal moraine (MLL-01–MLL-06), c) Tsioumako right lateral moraine (TMK-01–TMK-03), d) Laccorponti right lateral moraine (TS-01–TS-03), and e) Laccos cirque terminal moraine ridges (LAC-01–LAC-06).

forms within the southeast-facing cirque, this landform marks the upper limit of glacial deposition in the Laccos Megalon Litharion. A lateral moraine ridge (c. 25 m high) extends for 300 m to the southwest from the terminal moraine and through the Laccos Megalon Litharion valley. Large (>2 m diameter) boulders line the moraine crest and are found throughout the valley, often perched on ice-moulded bedrock and roche moutonnées. A boulder ridge interpreted as a lateral moraine extends from 1830 to 1980 m a.s.l. down the western side of the valley, beneath the Krevati arête (Fig. 6). On the eastern side of the valley a talus rock glacier extends down to 1850 m a.s.l., beneath the cliffs of Vlasi (2180 m) (Hughes et al., 2003). Scree covers the high slopes of the southeast-facing cirque headwall and rock slope failure deposits merge with the rock glacier complex beneath Vlasi.

From 1800 m a.s.l. the gradient of the valley floor increases to the mouth of the Laccos Megalon Litharion at 1700 m a.s.l. Here, terminal and lateral moraines, between 1750 and 1700 m a.s.l., make up the next morphostratigraphical set of glacial deposits (Fig. 6). They are located 2.5 km from the southeast-facing cirque headwall, in the transition between Vlasian stage (MIS 6) and Tymphian stage (MIS 5d–2) deposits (Hughes et al., 2006a). A broad outer moraine ridge, 15 m high, and c. 80 m in length, marks the terminal extent of the Laccos Megalon Litharion glacier at this point (Fig. 7a). Terminal moraine ridges 100 m inside of this deposit are also broad crested and rise c. 5 m above the valley floor. Sub-rounded limestone boulders, >1 m diameter, are found on the terminal moraine ridges. To the west a cobble and boulder-rich, sharp crested right lateral moraine ridge rises 45 m above the valley floor between 1750 and 1710 m a.s.l. (Fig. 7a). This moraine dips sharply towards the outer terminal moraine ridge and traces the steep gradient of the palaeo-glacier snout.

4.1.2. Laccos Tselon

The Krevati arête separates the Laccos Megalon Litharion from the Laccos Tselon to the west (Fig. 3). The Laccos Tselon trends SSW from Megali Litharia (2467 m a.s.l.) until it meets the Laccos Megalon Litharion at 1700 m a.s.l., where the valley mouth is orientated to the SSE. Between 2100 and 2000 m a.s.l., boulder-covered lateral moraines mark the upper limit of glaciation in the Laccos Tselon. Irregular hummocky moraines are found on the valley floor within the upper lateral moraines and were probably formed during glacier recession. Below these deposits, streamlined fluted moraines, 200–400 m long, extend down to elevations below 1900 m a.s.l. (Hughes, 2004). Boulder-strewn hummocky moraines also occupy the valley floor towards the mouth of the valley. Moraines in the Laccos Tselon are correlated with those within the Laccos Megalon Litharion on the basis of elevation and soil profile development (Hughes et al., 2006a).

4.1.3. Laccorponti

Immediately down valley from the confluence of the Laccos Megalon Litharion and Laccos Tselon, a series of limestone pavements exhibit well-developed clint and grike morphology with a scatter of glacially-transported boulders (Fig. 3). The limestone pavements dip towards mid-valley terminal and recessional moraines (Hughes, 2004), located between 1700 and 1550 m a.s.l. on the eastern side of the valley (Fig. 3). They correlate with MIS 6 moraines in the Vourtapa valley on the basis of elevation,

Table 5
^{36}Cl exposure ages calculated with varying scaling schemes, production rates and age calculators.

Sample ID	Surface exposure ages		
	Ca spallation (56.0 ± 4.1 atoms ^{36}Cl (g Ca)$^{-1}$ yr^{-1}) (Marrero et al., 2016b) LSDn (Sa) scaling (Lifton et al., 2014)	Ca spallation (48.8 ± 3.4 atoms ^{36}Cl (g Ca)$^{-1}$ yr^{-1}) Stone et al. (1996) Lm scaling (Lal, 1991; Stone, 2000)	Ca spallation (42.2 ± 4.8 atoms ^{36}Cl (g Ca)$^{-1}$ yr^{-1}) Schimmelpfennig et al. (2011) Lm scaling (Lal, 1991; Stone, 2000)
	CRONUS calculator v2.0 erosion corrected (0.6 mm ka^{-1})	Schimmelpfennig spreadsheet erosion corrected (0.6 mm ka^{-1})	Schimmelpfennig spreadsheet erosion corrected (0.6 mm ka^{-1})
	ka	ka	ka
MLL-01	**25.7 ± 2.6**	28.2 ± 4.0	31.7 ± 5.0
MLL-02	15.6 ± 1.6	15.6 ± 2.2	17.7 ± 2.9
MLL-03	10.6 ± 1.1	10.4 ± 1.4	11.9 ± 1.9
MLL-04	16.0 ± 1.6	16.2 ± 2.2	18.3 ± 2.8
MLL-05	15.9 ± 2.2	15.8 ± 2.6	17.9 ± 3.3
MLL-06	15.7 ± 1.9	15.9 ± 2.5	17.8 ± 3.0
MLL-07	17.0 ± 1.7	17.7 ± 2.4	19.9 ± 2.7
MLL-08	18.8 ± 1.9	19.3 ± 2.7	21.8 ± 3.5
MLL-09	**24.5 ± 2.4**	26.6 ± 3.6	29.8 ± 4.6
MLL-10	14.0 ± 1.4	14.5 ± 2.0	16.4 ± 2.6
MLL-11	15.8 ± 1.5	16.6 ± 2.2	18.6 ± 2.8
MLL-12	16.0 ± 1.7	16.7 ± 2.3	18.8 ± 3.0
MLL-13	18.2 ± 2.0	19.0 ± 2.8	21.3 ± 3.4
MLL-14	16.0 ± 1.7	16.2 ± 2.3	18.3 ± 2.9
MLL-15	12.1 ± 1.2	12.1 ± 1.7	13.7 ± 2.1
TMK-01	**29.0 ± 3.0**	31.9 ± 4.6	36.1 ± 5.9
TMK-02	15.5 ± 1.7	15.3 ± 2.2	17.4 ± 2.8
TMK-03	18.9 ± 1.9	19.1 ± 2.8	21.5 ± 3.5
TS-01	8.3 ± 1.3	7.9 ± 1.4	9.0 ± 1.7
TS-02	3.9 ± 0.6	3.6 ± 0.7	4.1 ± 0.8
TS-03	10.3 ± 1.2	9.8 ± 1.4	11.1 ± 1.8
LAC-01	9.2 ± 1.3	10.0 ± 1.5	10.8 ± 1.7
LAC-02	10.8 ± 1.4	11.3 ± 1.6	12.3 ± 1.8
LAC-03	7.6 ± 1.0	8.6 ± 1.4	9.3 ± 1.5
LAC-04	7.1 ± 1.1	8.4 ± 1.4	9.0 ± 1.5
LAC-05	18.0 ± 1.9	17.9 ± 2.5	20.3 ± 3.2
LAC-06	6.7 ± 0.9	7.5 ± 1.1	8.2 ± 1.3

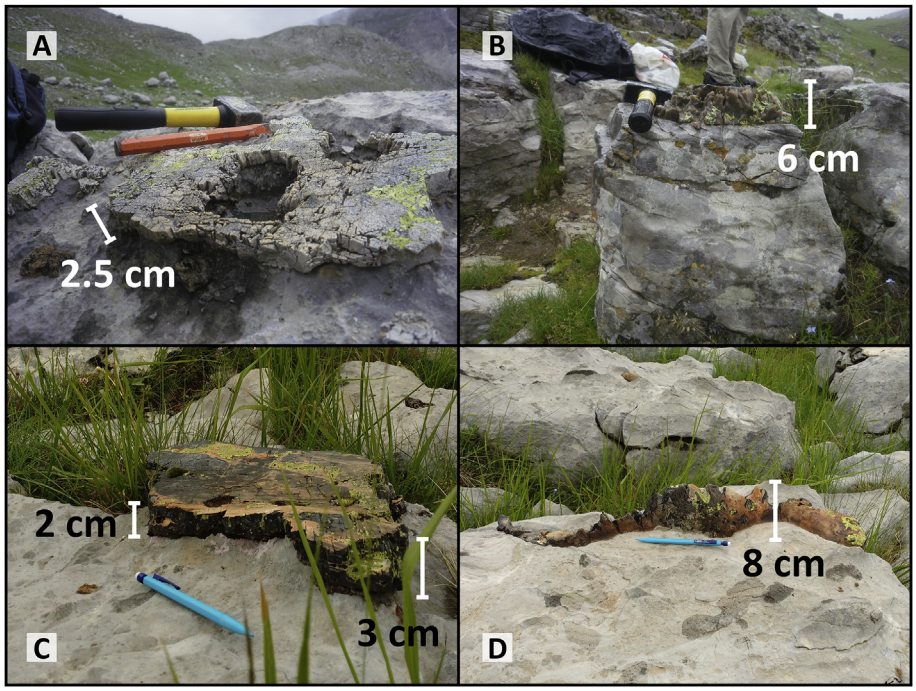

Fig. 5. Up-standing chert veins on limestone clints show evidence of differential erosion in the Vourtapa valley. a) Vlasi-Goura col (2025 m a.s.l. 39.95517°N, 20.85611°E), b) Vourtapa valley (1985 m a.s.l. 39.94855°N, 20.85769°E), c) Vourtapa valley (1985 m a.s.l. 39.94826°N, 20.85709°E), d) Vourtapa valley (1985 m a.s.l. 39.94826°N, 20.85709°E).

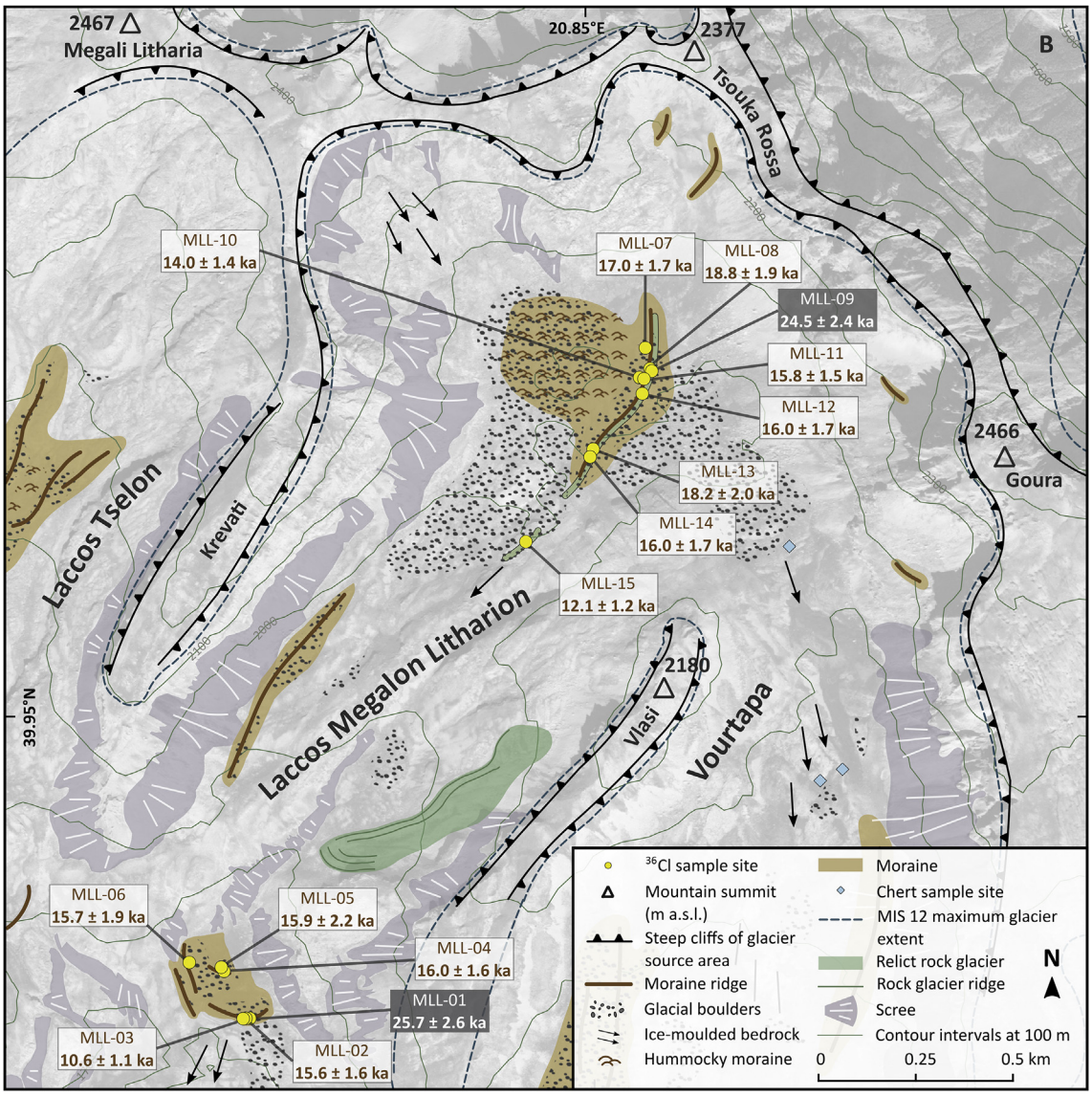

Fig. 6. Glacial geomorphology of the Laccos Megalon Litharion valley showing ^{36}Cl sampling sites and exposure ages. This is map tile B in Fig. 2.

geomorphological context and soil profile development index (after Harden, 1982) as discussed in Hughes et al. (2006a).

From 850 to 1600 m a.s.l., long lateral moraine ridges, with thick and well-developed soils, extend down the Laccorponti valley to the east of Tsepelovo village (Fig. 3). These lateral moraines comprise the Skamnellian stage (MIS 12) (Hughes et al. (2006a)) deposits and include weathered tills and sub-rounded glacial boulders (>2 m diameter). To the east of Tsepelovo, quarry workings expose a deep section in a lateral moraine containing diamicton, including limestone rock flour, sands, striated clasts and sub-rounded boulders (Woodward et al., 1995; Hughes, 2004). The right lateral moraine, immediately to the east of Tsepelovo, extends c. 2 km from 900 to 1200 m a.s.l. Large (>2.5 m diameter) and well-preserved limestone boulders sit on the relatively flat and broad moraine crest (c. 10 m wide) (Fig. 8a). These boulders exhibit rillenkarren channels up to 20 cm deep on their vertical axes from solution weathering. To the east of the main Laccorponti valley, lateral moraine ridges, 10–20 m high, trace the margin of a separate palaeo-glacier lobe (Hughes, 2004).

4.1.4. Vourtapa

The Vourtapa valley is located immediately to the east of the Laccos Megalon Litharion, separated by the Vlasi (2180 m a.s.l.) arête (Fig. 3). The Vourtapa does not have a headwall. Glacial ice was sourced from the Laccos Megalon Litharion cirque and overrode the col between Goura (2466 m a.s.l.) and Vlasi, at c. 2025 m a.s.l., to form the Vourtapa glacier (Hughes, 2004). During the local maximum (Middle Pleistocene) ice extent, the Vourtapa glacier joined with ice from the Vrichos and Tsioumako valleys and extended to 850 m a.s.l., in the Kato Radza valley (Fig. 3). No clear evidence of Tymphian stage (MIS 5d–2) deposits are observed in the upper reaches of the Vourtapa. Nonetheless, small boulder ridges are observed at 2100–2200 m a.s.l. in west-facing hollows beneath Goura (2466 m a.s.l.) and in a small south-facing cirque beneath Tsouka Rossa (2377 m a.s.l.). They are the terminal deposits of niche glaciers. Two moraines in the south-facing Tsouka Rossa cirque suggest ice was restricted on these slopes because they are more exposed to solar radiation and they lack the deep shading of the east face of the Krevati ridge (Fig. 6). There is no geomorphological evidence to suggest that ice filled the eastern cirque basin of

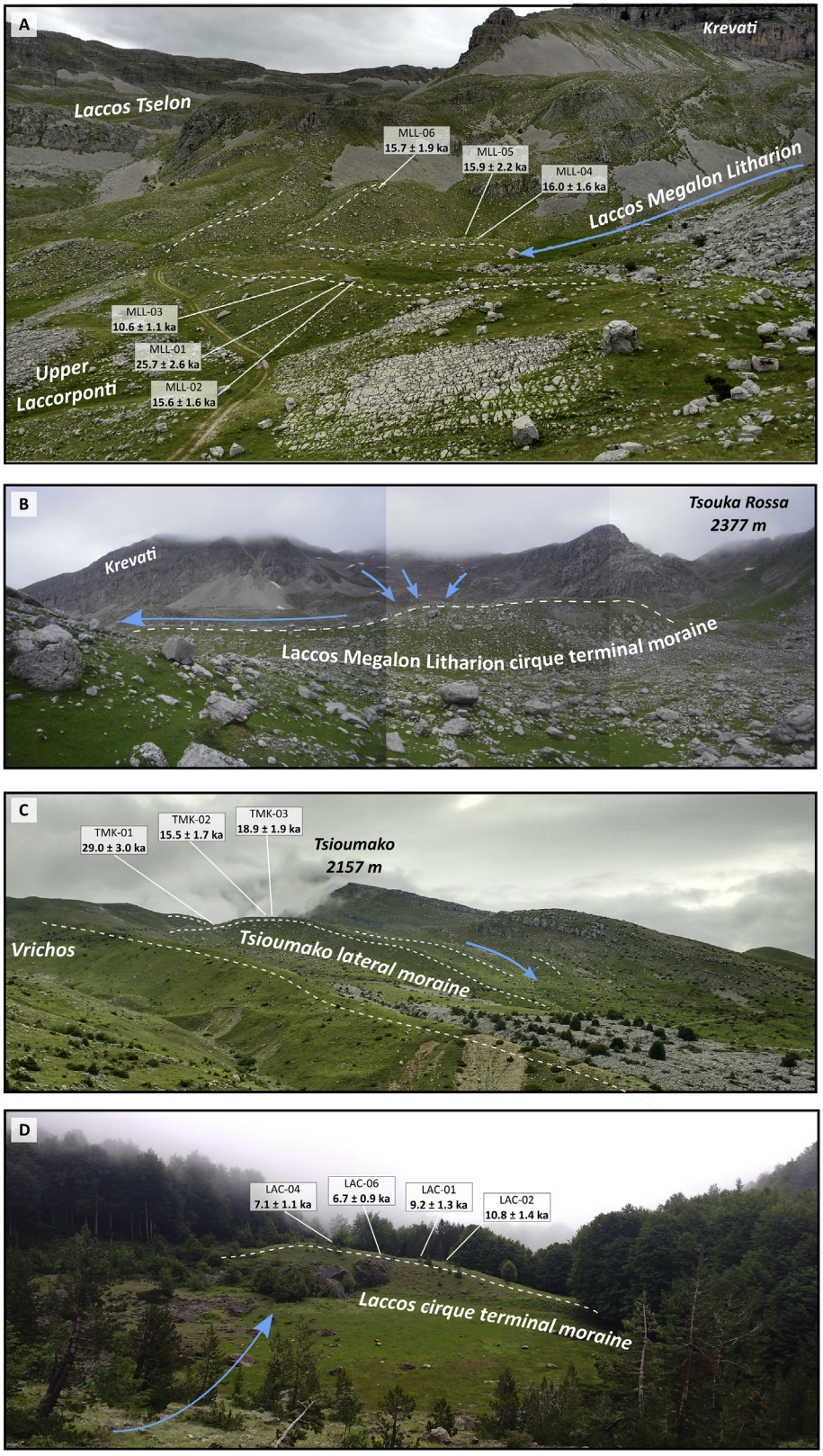

Fig. 7. Glacial geomorphology at key locations on Mount Tymphi **a)** Looking northwest towards the Laccos Megalon Litharion lower valley terminal moraine. **b)** Looking northwest towards the Laccos Megalon Litharion cirque terminal moraine and lateral moraine. **c)** Looking northeast towards the Tsioumako lateral moraine. **d)** Looking northeast within the Laccos cirque at the inner terminal moraine.

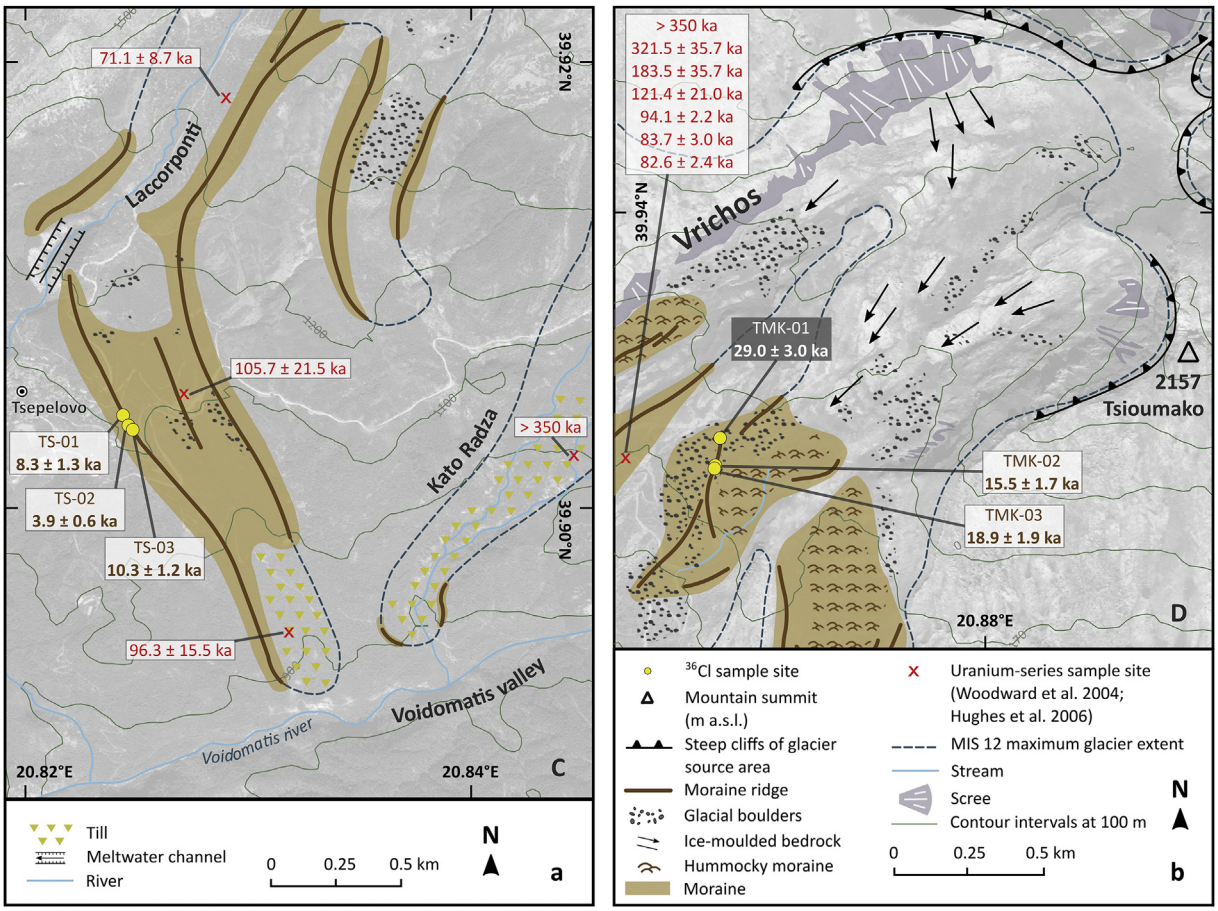

Fig. 8. a) Glacial geomorphology of the Laccorponti valley showing ^{36}Cl sampling sites and exposure ages. This is map tile C in Fig. 2 **b)** Glacial geomorphology of the west cirque of Tsioumako showing ^{36}Cl sampling sites and exposure ages. This is map tile D in Fig. 2.

the Laccos Megalon Litharion during the Tymphian stage. In fact, the east basin contains tills that are well cemented and includes extensive areas of frost-shattered bedrock – in marked contrast to the area within the Late Pleistocene limits in the west cirque basin.

A series of ice-moulded bedrock pavements extend south from the Goura-Vlasi col, between 1900 and 2025 m a.s.l. (Fig. 3). Up-standing chert veins are present on the limestone clints and demonstrate preferential weathering of the bedrock (Fig. 5). Perched boulders and meltwater channels are also evident in the upper Vourtapa. Pronival ramparts and rock slope failure deposits line the east side of the valley, beneath the Tsoukoula cliffs. Well-preserved latero-terminal moraines, up to 30 m high, occupy the mouth of the Vourtapa, between 1650 and 1800 m a.s.l. (Fig. 3). These moraines are part of the Vlasian stage deposits (MIS 6), with U-series ages ranging from 81.7 ± 12.9–131.25 ± 19.25 ka from secondary carbonates within these deposits (Woodward et al., 2004; Hughes et al. (2006a)). Large sub-angular and sub-rounded limestone boulders are strewn across the moraines and valley floor of the lower Vourtapa. Hummocky moraine ridges are present on the valley floor within the terminal limits of MIS 6.

4.1.5. Vrichos

Lateral moraine ridges extend out from the Vrichos valley, between 1600 and 1750 m a.s.l., to the east of the Vourtapa valley (Fig. 3). Boulder-rich hummocky moraine ridges are again evident on the valley floor. A minimum limiting U-series age of 80.45 ± 15.1 ka has been obtained from secondary carbonates within these deposits (Woodward et al., 2004; Hughes et al., 2006a). Soil profile development and geomorphological context correlates these lateral and hummocky moraines to MIS 6. To the east of the long left lateral moraine, a large limestone pavement (c. 0.5 km × 0.2 km), displays deep fissures and well developed grikes, indicative of a long weathering history. Hummocky moraines and fluted moraines occupy the valley floor between 1700 and 1800 m a.s.l. (Hughes, 2004). Glacially-transported boulders and ice-moulded bedrock are also present between 1900 and 2000 m a.s.l. in the upper Vrichos and within the south-facing cirque.

4.1.6. Tsioumako valley

At the eastern extent of the Tymphi massif, the south and west-facing cirques of Tsioumako (also known as Corifula) (2157 m a.s.l.) contain ice-moulded bedrock pavements between 1750 and 2000 m a.s.l. (Fig. 8b). Glacier ice from these cirques fed the Tsioumako palaeo-glacier, which also contributed to the Skamnelli palaeo-glacier during MIS 12 (Fig. 3) (Hughes et al., 2006a). Prominent arcuate lateral moraines are well preserved between 1600 and 1800 m a.s.l. at the mouth of the upper valley and form the Tsioumako member deposits which are correlated with MIS 6 deposits in the Vourtapa valley (Hughes et al., 2006). They host large (>1.5 m diameter) sub-rounded limestone boulders that are partly embedded, with deep (10–15 cm) solution channels and well-developed weathering pits. In some cases, the boulders are completely fractured along their y-axes. U-series ages from secondary carbonates in tills, immediately to the west of the stratigraphic limit of these moraines, range from 82.6 ± 2.4–>350 ka (Fig. 3) (Woodward et al., 2004; Hughes et al., 2006a). A bedrock

knoll separates these lateral moraines from latero-terminal moraines, deposited between 1600 and 1700 m a.s.l., to the east in the Tsioumako valley. A sharp crested right lateral moraine is closely nested just inside of the Tsioumako member deposits (Fig. 7c) and above the division between the Tsioumako and Skamnelli palaeoglacier lobes. It is well preserved, rising c. 50 m above the valley floor. Hummocky moraines are present up-valley of both sets of moraines between 1650 and 1750 m a.s.l. Ice-moulded bedrock, tills and glacially-transported boulders extend to the southwest, to c. 1150 m a.s.l., towards the upper Voidomatis River valley (Hughes, 2004).

4.1.7. Kato Radza

During MIS 12, glacial ice from the Tsioumako cirque merged with ice from the Vrichos and Vourtapa valleys to form the Kato Radza valley glacier which extended beyond the village of Skamnelli (Hughes et al., 2006a, 2007; Woodward and Hughes, 2011). This formed long (1–2.5 km) medial and lateral moraines that extend from 1300 to 1800 m a.s.l. (Fig. 3). These moraines are cemented and well preserved, exhibiting sharp crests. U-series ages from exposures within these deposits are >350 ka (Woodward et al., 2004; Hughes et al., 2006a). Till and glacially-transported boulders extend below Skamnelli village to a glacial limit at 850 m a.s.l. in the Voidomatis River valley (Lewin et al., 1991; Woodward et al., 1995; Hughes, 2004).

4.1.8. Maghoula and Kriopotamos valleys

Three separate units of glacial deposits also occur in the northeast-facing valleys of Mount Tymphi, beneath the summit of Goura (2466 m a.s.l.) (Fig. 3). They correspond with the same chronological sequence observed on the south-facing valleys, although no dating control exists from this side of the massif. Lateral moraines extend down both the Maghoula and Kriopotamos valleys, where the maximum ice extent reached c. 800 m a.s.l. in the Maghoula valley, and c. 1000 m a.s.l. in the Kriopotamos valley respectively (Hughes, 2004). During the maximum glacier advance, ice from the Dimitrios, Laccos and Plaghia cirques coalesced in the Kriopotamos valley. In contrast to glacial deposits on the south-facing valleys of Mount Tymphi, the Vlasian (MIS 6) and Tymphian stage (MIS 5d–2) terminal moraines (Hughes et al., 2006a) are found within 300 m of each other, between 1350 and 1450 m a.s.l. and within the cirques (Fig. 3). The cirques face to the northeast and are located beneath the steep Goura cliffs (600–1000 m tall). Lateral moraines and a medial moraine are also found in the Plaghia cirque at this altitude. Sub-rounded boulders (1–3 m diameter) are present on these moraines, although thick tree cover shrouds most of the deposits in the Maghoula and Kriopotamos valleys.

The stratigraphically youngest deposits occur <0.5 km from the headwalls in the Laccos and Dimitrios cirques. In the Laccos cirque (Fig. 9), a pair of terminal moraine ridges, 100–150 m long, rise 15 m above a seasonal lake that occupies the cirque floor (Fig. 7d). Sub-rounded and partly embedded limestone boulders, (0.5–1.7 m diameter), are found on the terminal moraine crests. Rock slope failure deposits and pronival ramparts containing sub-angular boulders are also apparent within 200 m of the Goura cliffs.

4.1.9. Stani Katsanou

The north-facing valleys of Mount Tymphi form part of the Aoös River basin. Here, sub-rounded glacial boulders have been deposited down to almost 1100 m a.s.l. (Hughes, 2004). Arcuate, boulder-covered terminal moraines occupy mid-valley positions in the Stani Katsanou at c. 1700–1850 m a.s.l. (Fig. 3). The Stani Katsanou valley glacier was fed by ice from the Tsouka Rossa (2377 m a.s.l.) and

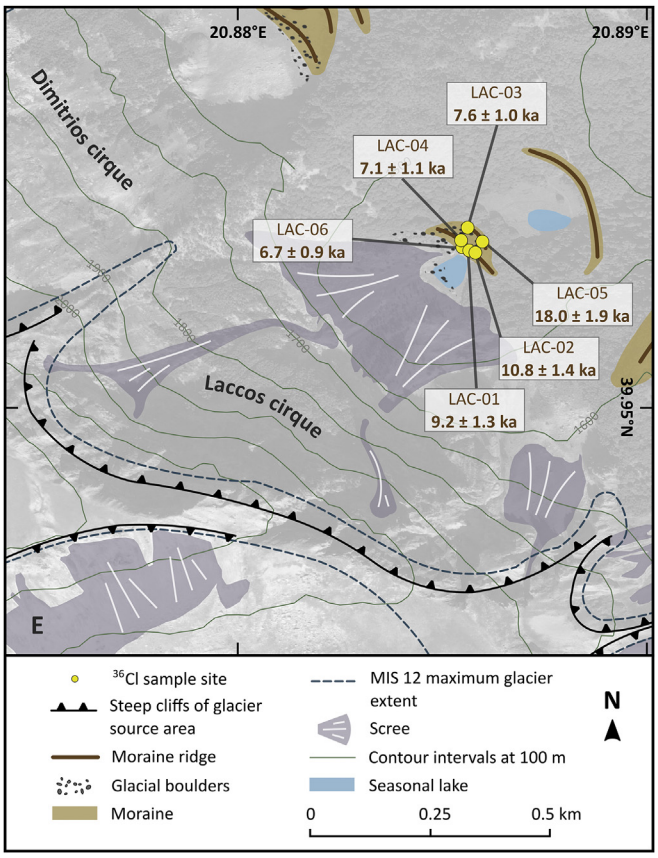

Fig. 9. Glacial geomorphology of the Laccos cirque, showing ^{36}Cl sampling sites and exposure ages. This is map tile E in Fig. 2.

Karteros (2478 m a.s.l.) cirques at the head of valley. Relict debris rock glaciers and multiple lobate boulder ridges are found in the Tsouka Rossa cirques between 2000 and 2100 m a.s.l. (Fig. 3). This was fed by small cirque glaciers, from four inset cirques, which deposited terminal moraines at c. 2150 m a.s.l. (Hughes, 2004). In the Karteros cirque, a relict talus rock glacier was sourced from rockfall deposits from the cirque headwall (Hughes, 2004).

4.2. Geochemistry

The carbonate samples consist of impure limestones and dolomites which are typical of metamorphosed carbonates close to a former active plate margin (Jones and Robertson, 1991). The geochemistry of most samples is typical of limestone with CaO contents ranging from 21.4 to 56.4% (see Table 3). However, three limestone samples had relatively low CaO contents (22–28%) (MLL-01, MLL-09, TMK-03), although values as low as 15–20% CaO are reported for limestone samples in other ^{36}Cl TCN dating studies in the Mediterranean region (e.g. Sarıkaya et al., 2014; Domènech et al., 2018). Six samples from the north side of Mount Tymphi in the Laccos cirque (samples LAC-01 to –06) have a dolomitic geochemical signature with 5–20% MgO content which equates to 17–70% dolomite. Dolomite is marked on geological maps on the northern slopes of the massif (IGME, 1970, 1983) and it is also likely to be present in the steep glacially-eroded headwall cliffs on the southern slopes. Samples containing >1.5% MgO (>5% dolomite) are also present from the moraine samples on the southern slopes and this indicates that dolomitic limestone rocks outcrop here too. The limestone and dolomite samples varied in purity with non-soluble residues after dissolution ranging from 0.3 to 8.6% of sample mass.

Much of this non-soluble residue is likely to be diagenetic silicate (chert), which is common as a secondary mineral in limestone rocks (Zerathe et al., 2013) and widely observed as veins and nodules in the limestones and dolomites of Mount Tymphi (Telbisz et al., 2019). Silicates are not accounted for in the geochemical analyses because samples were prepared as carbonates for ICP analysis. However, chert is almost entirely composed of SiO_2 and contains no major target elements for ^{36}Cl, such as K or Ca. Given this, as well as the fact that diagenetic silicates represent only a minor component of the rocks, the residual chert content is unlikely to affect ^{36}Cl production in the limestone and dolomite samples.

4.3. ^{36}Cl exposure ages

We collected 26 samples from moraine boulders and one sample from an isolated glacially transported boulder for ^{36}Cl exposure age dating. Sampling was focussed in the upper valleys and cirques of the Tymphi massif, to the north of Tsepelovo and Skamnelli (Fig. 3). In some valleys, suspected Late Pleistocene moraines were identified just inside previously identified MIS 6 moraines. The sampled moraines, located in the upper and middle Laccos Megalon Litharion and the cirques of Tsioumako and Laccos, mark the upper limits of glaciation and are therefore the stratigraphically youngest sets of glacial deposits on Mount Tymphi.

4.3.1. Laccos Megalon Litharion glacial chronology

In the Laccos Megalon Litharion cirque, six samples (MLL-07–MLL-12) were collected from boulders on the crest of the terminal moraine ridge between 2029 and 2035m a.s.l. (Fig. 6). The oldest age 24.5 ± 2.4 ka (MLL-09) was attained from a sub-angular boulder on the highest point of the moraine ridge (2035 m a.s.l). Five other boulders yielded ^{36}Cl exposure ages of 17.0 ± 1.7 ka (MLL-07), 18.8 ± 1.9 ka (MLL-08), 14.0 ± 1.4 ka (MLL-10), 15.8 ± 1.5 ka (MLL-11) and 16.0 ± 1.7 ka (MLL-12). The youngest age 14.0 ± 1.4 ka from sample MLL-10 was located on the inside of the moraine ridge, c. 5 m lower than the true crest. The terminal moraine ridge is connected to a left lateral moraine that extends for 300 m to the southwest through the Laccos Megalon Litharion. Here two large (2.3–5.2 m diameter) sub-angular limestone boulders sampled at 2001 m a.s.l. on the moraine crest yielded ages of 18.2 ± 2.0 ka (MLL-13) and 16.0 ± 1.7 ka (MLL-14) (Fig. 6). Further down valley, a large (3.9 m diameter) sub-angular glacially-transported boulder perched on a roche moutonnée at 1996 m a.s.l. gave a ^{36}Cl exposure age of 12.1 ± 1.2 ka (MLL-15). This boulder may have fractured and rotated since deposition as two boulder fragments (1–3 m diameter) are found next to MLL-15. Hence, this age is likely to be an unreliable retreat age for the Laccos Megalon Litharion glacier.

At the mouth of the Laccos Megalon Litharion, six limestone boulders were sampled for ^{36}Cl TCN dating from the next morphostratigraphical set of moraines (Fig. 6). Three ^{36}Cl ages obtained from the outermost terminal moraine ridge between 1710 and 1714 m a.s.l. produced exposure ages of 25.7 ± 2.6 ka (MLL-01), 15.6 ± 1.6 ka (MLL-02) and 10.6 ± 1.1 ka (MLL-03). The largest of these three boulders (2.2 m diameter) produced the oldest age of 25.7 ± 2.6 ka. Two samples from the more subdued terminal moraine deposits, 100 m inside of MLL-01–MLL-03, yielded ages of 16.0 ± 1.6 ka (MLL-04) and 15.9 ± 2.2 ka (MLL-05). A large (2.9 m diameter) sub-angular boulder (MLL-06), positioned on the inside of the right lateral moraine crest gave a ^{36}Cl age of 15.7 ± 1.9 ka.

We argue that the oldest age from the upper and lower elevation moraines (25.7 ± 2.6 ka and 24.5 ± 2.4 ka) is likely to most closely represent the true age of the moraine. The spread of younger ages (or the mean of these younger ages) on each moraine may represent a period of moraine degradation and boulder exhumation. Moraine degradation has been documented in glacio-karst landscapes and can yield boulder ages that are 50% younger than the true landform age (Zreda et al., 1994; Hallet and Putkonen, 1994; Putkonen and Swanson, 2003). Processes of boulder exhumation are more prevalent than inheritance in alpine glacial settings (e.g. Heyman et al., 2011), particularly in younger moraines such as those sampled here (Applegate et al., 2012). Moraines in the Laccos Megalon Litharion are not sharp crested, which provides some evidence for degradation and hence boulder exhumation. In contrast to the moraines at lower elevations in adjacent valleys, the Laccos Megalon Litharion moraines are not cemented which increases their susceptibility to mass wasting and other hillslope processes. Moraine degradation will have been especially prevalent under periglacial conditions during the Late Pleistocene. This supports the interpretation of the oldest boulder age being the most reliable indicator of the timing of landform deposition. Sample MLL-09 (24.5 ± 2.4 ka) is also located at the highest point of the moraine ridge (2035 m a.s.l) and is therefore more likely to have experienced a minimal period of exhumation. The position of the moraine in the centre of the cirque and 1 km from the headwall also removes any potential for inheritance in sample MLL-09. The oldest age from the Laccos Megalon Litharion 25.7 ± 2.6 ka (MLL-01), 300 m lower in elevation than MLL-09, provides evidence for a glacier extending 3.1 km, from above 2000 m a.s.l. in the high cirque, and down to 1700 m a.s.l. at the mouth of the Laccos Megalon Litharion during MIS 2. The oldest age from the Laccos Megalon Litharion cirque terminal moraine 24.5 ± 2.4 ka (MLL-09) indicates the Litharion glacier extended 1 km from the southeast-facing cirque.

4.3.2. Tsioumako valley glacial chronology

Further east, the Tsioumako valley emanates from the south and west-facing cirques of Tsioumako (2157 m). Three moraine boulders embedded on a prominent right lateral moraine at ~1770 m a.s.l. were sampled for ^{36}Cl TCN dating (Fig. 8b). This landform is located slightly up-valley of MIS 6 moraines (Woodward et al., 2004; Hughes et al., 2006a). Large (>2 m diameter) sub-rounded limestone boulders are present along the crest of this moraine and exhibit deep fractures and dissolution channels. ^{36}Cl exposure dating reported ages of 29.0 ± 3.0 ka (TMK-01), 15.5 ± 1.7 ka (TMK-02) and 18.9 ± 1.9 (TMK-03). Sample TMK-01 was obtained from the tallest of the three sampled boulders and is likely to be closest to the true age of this moraine. The younger ages are again likely to be a result of moraine degradation and boulder exhumation, which is consistent with our interpretation of samples MLL-01–MLL-15. An age of 29.0 ± 3.0 ka implies that the Tsioumako glacier reached its last local glacier maximum at the transition from MIS 3 to MIS 2. At this time, the glacier extended approximately 2.4 km from its source area (at 1950–2000 m a.s.l) to its front at ~1700 m a.s.l. Although reaching its maximum extent slightly earlier, the Tsioumako glacier was comparable in area to the Laccos Megalon Litharion glacier during the Late Pleistocene (Table 6).

4.3.3. Laccorponti valley glacial chronology

Long lateral moraine ridges extend from 850 to 1600 m a.s.l. through the Laccorponti valley below the confluence of the Laccos Megalon Litharion and Laccos Tselon. These moraines are typically cemented and capped with well-developed soils. Uranium-series dating of this set of glacial deposits suggests emplacement during MIS 12 (Fig. 8a). Three moraine boulder samples were obtained to determine whether ^{36}Cl TCN dating of limestones could identify ages from older glacier cycles in this region. These very large (>2.9 m diameter) and sub-rounded boulders are well preserved, although sample TS-01 has a 15–20 cm deep dissolution groove

Table 6
Late Pleistocene glacier area (km^2), volume (km^3) and ELA (m) on Mount Tymphi.

Glacier	Length	Area	Maximum thickness	Volume	ELA AABR	Maximum elevation	Minimum elevation	ELA - corrected for uplift and sea-level
	(km)	(km^2)	(m)	(km^3)	(m)	(m)	(m)	(m)
Tselon	2.9	1.4	94	0.061	2057	2322	1790	2161–2169
Litharion	3.1	1.5	238	0.094	1995	2274	1719	2099–2107
Tsioumako	2.4	1.6	133	0.115	1930	2038	1725	2034–2042
Goura 1	0.2	<0.1	30	0.001	2214	2330	2139	2318–2326
Goura 2	0.1	<0.1	40	0.001	2331	2337	2256	2435–2443
Goura 3	0.4	<0.1	56	0.002	2231	2297	2157	2335–2343
Laccos	0.7	0.3	108	0.011	1566	1846	1431	1670–1678
Dimitrios	0.8	0.4	78	0.011	1667	1888	1502	1771–1779
Maghoula	1.2	0.6	91	0.024	1556	1870	1391	1660–1668
Tsouka Rossa	2.1	1.5	172	0.086	2155	2327	1840	2259–2267
Karteros	0.8	0.4	104	0.022	2103	2233	1995	2207–2215
Kopanes	0.9	0.5	107	0.022	2006	2282	1891	2110–2118
Gamila	0.4	0.1	67	0.004	2047	2214	1942	2151–2159
Amarandos	0.5	0.2	64	0.006	1880	1954	1805	1984–1992

along its y-axis. ^{36}Cl TCN dating produced ages of 8.3 ± 1.3 ka (TS-01), 3.9 ± 0.6 ka (TS-02) and 10.3 ± 1.2 (TS-03). Extensive Holocene glaciation is not consistent with the geomorphological evidence at this location on Mount Tymphi and the substantial body of U-series dates for this set of moraines points to deposition in MIS 12 (Woodward et al., 2004; Hughes et al., 2006a). Instead, the ^{36}Cl ages are more likely the product of boulder exhumation following the removal of sediment from the moraine crest. An extended period of moraine degradation at this location has left behind a flat topped moraine crest, ~10 m wide, on which the boulders can be found. These data highlight the challenges of ^{36}Cl TCN dating of limestones on glacial deposits from much older glacial cycles.

4.3.4. Laccos cirque glacial chronology

In the Laccos cirque, six ^{36}Cl samples are the first ages reported from the northeast side of Mount Tymphi. A pair of terminal moraine ridges, approximately 20 m apart, between 1420 and 1435 m a.s.l. were sampled (Fig. 9). Stratigraphically, they are the youngest set of glacial deposits above the Kriopotamos valley. Two moraine boulders sampled on the outer crest yielded exposure ages of 7.6 ± 1.0 ka (LAC-03) and 18.0 ± 1.9 ka (LAC-05). On the inner ridge, four moraine boulders provided ^{36}Cl ages 9.2 ± 1.3 ka (LAC-01), 10.8 ± 1.4 ka (LAC-02), 7.1 ± 1.1 (LAC-04) and 6.7 ± 0.9 ka (LAC-06). The oldest age of 18.0 ± 1.9 ka (LAC-05) was obtained from an embedded limestone boulder on the outer ridge. This could suggest a younger Late Pleistocene glacier maxima on the northeast side of the Tymphi massif. Here, the Laccos cirque glacier extended 0.7 km from the headwall. Avalanching snow accumulation and topographic shading from the steep Goura cliffs may have combined to allow cirque glaciers to persist for longer and at lower elevations than the Late Pleistocene glaciers on the south-facing slopes. Northeast-facing cirques receive less insolation, thus minimising ablation losses. We must be cautious in the interpretation of these ages in view of the paucity of chronological data on this side of the massif.

4.4. Glacier reconstructions

Geomorphological field evidence shows that Late Pleistocene glaciers were restricted to the upper valleys and cirques of Mount Tymphi. Fourteen palaeoglaciers covered an area of ~8.8 km^2 during this period (Fig. 10), with a total glacier volume at their maximum extent of 0.5 km^3 (Table 6). This constitutes just 14.9% of the area covered by glaciers during the maximum ice extent of the Skamnellian stage (MIS 12) (Hughes, 2004). Late Pleistocene glaciers extended up to 3.1 km down-valley from their source areas. The southern slopes hosted the most extensive glaciers, 2.4–3.1 km in length, which covered a total area of 4.5 km^2 (Table 7). This was probably facilitated by accumulation from south-west to north-east storm tracks and topographic shading from a number of very steep arêtes that radiate from the centre of the massif (Fig. 3) (Florineth and Schlüchter, 2000; Hughes, 2004). These glaciers formed above 2000 m a.s.l. in the high cirques and terminated between 1700 and 1800 m a.s.l. (Fig. 10). In contrast, northeast-facing glaciers were confined to their cirques and extended 0.7–1.2 km (Table 6). They were able to develop at much lower elevations due to aspect, topographic shading and the build-up of avalanching snow. These cirque glaciers covered an area of 1.3 km^2 in total. Late Pleistocene glaciers in the northern cirques were typically <1 km in length, although the Tsouka Rossa glacier may have extended up to 2.1 km, fed by the Tsouka Rossa cirques. Glaciers in the north cirques potentially covered 2.7 km^2 and although dating is still lacking from these northern cirques, comparison with the southern cirques would support a larger extent of ice than previously suggested. For example, the last cold stage (MIS 5d–2) glaciers for the Tsouka Rossa cirques were much smaller in Hughes (2004) and Hughes et al. (2006a) who had no geochronological control for any of the Late Pleistocene moraines on Mount Tymphi and focused their geochronology on the older lower moraines of Middle Pleistocene age. The new geochronological data presented here support extending the maximum limits of Tymphian stage (MIS 5d–2) glaciers on the massif and increase the total extent of glacier coverage from 3.9 km^2 (see Hughes, 2004) to 8.8 km^2. The presence of stratigraphically younger moraines within the Tselon, Litharion and Tsouka Rossa cirques (Fig. 10), is evidence of a later and more restricted phase of Late Pleistocene glacial activity. In total, 7 glaciers persisted in this later phase, covering an area of ~1.6 km^2 (Table 8).

4.5. ELA reconstructions

Equilibrium line altitudes for Late Pleistocene glaciers on Mount Tymphi are presented in Tables 6–8. An average ELA of 1994 m from palaeoglaciers on the south slopes ($n = 3$) is comparable to an average ELA of 2038 m for the north cirques ($n = 5$) (Table 7). On the south slopes, the Tsioumako glacier ELA was at 1930 m at 29.0 ± 3.0 ka. This is lower than that of the Laccos Megalon Litharion (1995 m), although this was ~3–4 ka later at 25.7 ± 2.6 ka. In contrast, an average ELA of 1596 m was calculated for the north-east cirques ($n = 3$) (Table 7), although these cirque glaciers formed under

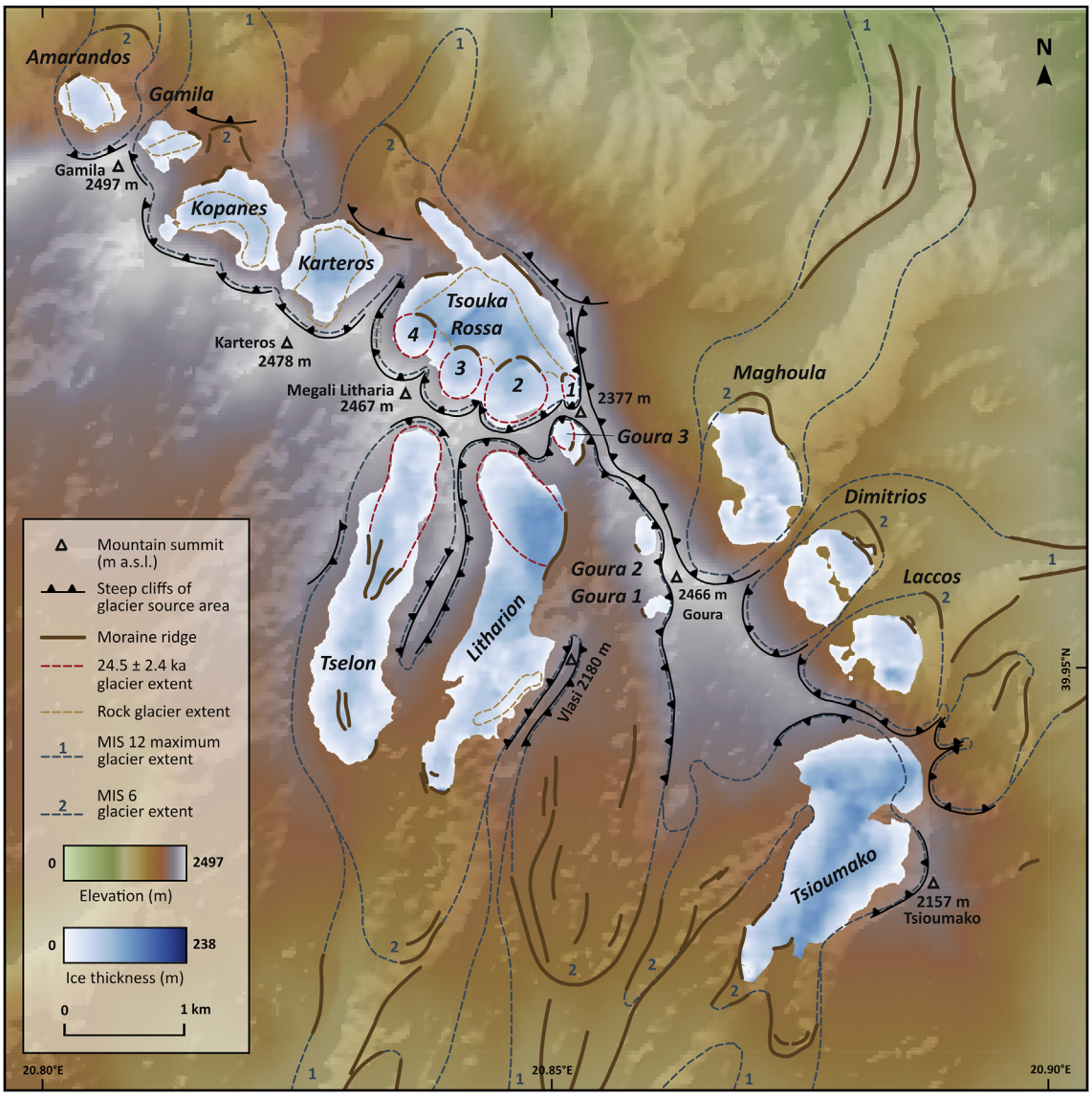

Fig. 10. Reconstruction of the maximum extent of Late Pleistocene Tymphian Stage glaciers (25.7 ± 2.6–29 ± 3.0 ka) on Mount Tymphi (Table 6) using the GlaRe GIS tool developed by Pellitero et al. (2016). Dotted red lines show Late Pleistocene glacier extents at 24.5 ± 2.4 ka, after glacier retreat (Table 8). Dotted brown lines show rock glaciers that developed during glacier retreat (Hughes et al., 2003). The extent of previous glaciations during MIS 12 (Skamnellian Stage) and MIS 6 (Vlasian Stage) are denoted by stratigraphical units 1 and 2 respectively (Woodward et al., 2004; Hughes et al., 2006a). (For interpretation of the references to colour in this figure legend, the reader is referred to the Web version of this article.)

Table 7
Summary of Late Pleistocene glaciers by area on Mount Tymphi.

Area	No. of glaciers	Average length	Total area	Total volume	Average ELA	Average ELA - corrected for uplift and sea-level
		(km)	(km^2)	(km^3)	(m)	(m)
South slopes (excluding niche cirque glaciers)	3	2.8	4.5	0.27	1994	2098–2106
North-east cirques	3	0.9	1.3	0.05	1596	1700–1708
North cirques	5	0.9	2.7	0.14	2038	2142–2150

different micro-climatic conditions. Lower ELAs on the northeast-facing slopes were controlled by slope angle, aspect, topographic shielding and avalanching snow accumulation. Extensive snow patches remain today on this side of the massif during the summer months, fed by avalanching snow and shaded by the Goura cliffs. An average glacier ELA of 2016 m (excluding the northeast cirque), during the maximum extent of Late Pleistocene glaciation, is ~160 m lower than previously calculated (2174 m; Hughes, 2004). However, a later phase of predominantly cirque glaciation at 24.5 ± 2.4 ka (MLL-09) (Fig. 10), saw the average ELA at 2231 m (Table 8).

To account for tectonic uplift and sea-level change since the Late Pleistocene, corrected ELAs are also presented in Tables 6–8. Uplift in the Epirus region has been estimated to be between 40 and 80 m

Table 8
Late Pleistocene glacier ELAs (m) during the glacier retreat phase at 24.5 ± 2.4 ka.

Glacier	Length	Area	Volume	ELA AABR	Maximum elevation	Minimum elevation	ELA - corrected for uplift and sea-level
	(km)	(km^2)	(km^3)	(m)	(m)	(m)	(m)
Tselon	1.5	0.5	0.024	2217	2335	2042	2321–2329
Litharion	1.0	0.5	0.020	2088	2257	2013	2192–2200
Goura 3	0.2	<0.1	<0.001	2227	2271	2202	2331–2339
Tsouka Rossa 1	0.1	<0.1	<0.001	2249	2262	2192	2353–2361
Tsouka Rossa 2	0.4	0.2	0.005	2229	2292	2154	2333–2341
Tsouka Rossa 3	0.4	0.1	0.003	2209	2313	2134	2313–2321
Tsouka Rossa 4	0.3	0.1	0.002	2124	2220	2049	2228–2236

ka^{-1} (King and Bailey, 1985). This is partly countered by sea-level change since global sea level was ~120 m lower during MIS 2 (Lambeck, 1995). Reconstructed ELAs thus underestimate the true ELAs by 104–112 m (Hughes, 2004). As such, a corrected mean ELA of 2120–2128 m above palaeo sea-level is likely to be more accurate for the maximum extent of Late Pleistocene glaciers on Mount Tymphi.

5. Discussion

5.1. ^{36}Cl exposure age uncertainties

Some of the spread in the boulder ages reflects analytical uncertainties inherent in ^{36}Cl TCN dating (Zreda et al., 1994; Kirkbride and Winkler, 2012). However, they account for only a small proportion in the total spread of absolute ^{36}Cl ages. Processes of moraine deposition, degradation and boulder surface erosion, which for the case of limestone is enhanced by carbonate dissolution, affects the duration of boulder surface exposure (Hallet and Putkonen, 1994; Zreda et al., 1994). The spread of ^{36}Cl boulder ages obtained here (Fig. 4) is typical where processes of incomplete exposure and erosion are prevalent in ^{10}Be studies (Heyman et al., 2011; Stroeven et al., 2011; Applegate et al., 2012; D'Arcy et al., 2019). Variability in post-depositional shielding can yield ages that are 50% younger than the true moraine age (Zreda et al., 1994; Zech et al., 2005; Hallet and Putkonen, 1994; Putkonen and Swanson, 2003; Heyman et al., 2011).

5.1.1. Moraine degradation and boulder exhumation

Glacial deposits can be well preserved in glacio-karst landscapes due to effective percolation of rainfall, minimal fluvial reworking and cementation of landforms (Hughes, 2004; Hughes et al., 2006a; Woodward et al., 2008). Nevertheless, in comparison to granitic or siliceous lithologies, moraine degradation and limestone surface erosion is prevalent in glacio-karst landscapes due to the presence of karst depressions and the solubility of limestone (Putkonen and Swanson, 2003; Applegate et al., 2012). The presence of rounded or flattened moraine crests, particularly in the upper valleys and cirques of Mount Tymphi, is consistent with erosion of the moraine surfaces (Hallet and Putkonen, 1994; Putkonen and Swanson, 2003). As the supporting sediment matrix of a moraine erodes and then is removed, boulders can topple, re-position, and over time as moraine degradation continues prior to stabilisation, become exhumed. This is reflected in our dataset by the age spread on each moraine (Table 4). Moraine degradation is understood to be most significant on younger moraines, such as those sampled here and provides the largest uncertainty in the timing of moraine stabilisation following ice retreat (Briner et al., 2005; Applegate et al., 2012). This is especially the case when moraines are subjected to climatic conditions that encourage periglacial processes after their formation, which would have been the case in the Late Pleistocene. The moraines sampled here are not cemented which increases their susceptibility to mass wasting and processes of degradation. Comparable ^{36}Cl age ranges have been reported elsewhere in the Mediterranean mountains (e.g. Pallàs et al., 2010; Çiner and Sarıkaya, 2017; Çiner et al., 2019; Köse et al., 2019; Žebre et al., 2019).

The spread of boulder ages commonly increases with landform age, as they are exposed to erosion processes for longer periods (Zreda et al., 1994; D'Arcy et al., 2019, Palacios et al., 2019). U-series dating and the soil development profiles on mid-valley lateral moraines (1200–1700 m) in the Laccorponti valley constrain them to the Middle Pleistocene (MIS 12) (Woodward et al., 2004; Hughes et al., 2006a). However, three samples (TS-01–TS-03) obtained from the Laccorponti right lateral moraine near the village of Tsepelovo yielded ages of 3.9 ± 0.6–10.3 ± 1.2 ka (Fig. 8a). These anomalously young ages support evidence for an extended period of slow and gradual moraine degradation and boulder exhumation (Hallet and Putkonen, 1994). The moraine degradation must be slow because these surfaces sustain deeply weathered soil profiles (Hughes et al., 2006a), with soil development keeping pace with denudation. The crest of the Laccorponti right lateral moraine is flat and ~10 m wide, suggesting the lowering of the moraine surface and exhumation of the sampled boulders (Hallet and Putkonen, 1994; Zreda et al., 1994). Well-developed red soils are common across Middle Pleistocene moraines on Mount Tymphi – especially those dating to MIS 12 (Hughes, 2004; Hughes et al., 2006a). Sample TS-01 also has a 15–20 cm deep solution groove which suggests a complex exposure history influenced by both boulder exhumation and prolonged surface weathering. The largest boulders on the moraine crest may be gradually lowered as the underlying moraine matrix is removed. Thus, it is quite possible that boulder surface loss by solution is a bigger problem here than boulder exhumation. It is difficult to capture these complex erosion histories in a single erosion rate. This highlights the significant challenges involved in ^{36}Cl TCN dating of limestones from glacial deposits older than one glacial cycle (i.e. >MIS 5e).

5.1.2. Inheritance

Boulders containing inherited ^{36}Cl nuclides from previous exposure can yield boulder ages older than the landform itself (Applegate et al., 2012). If a dataset contains an older outlier and stratigraphic reasons suggest the influence of inheritance, then younger boulder ages may prove to be more accurate (Zech et al., 2005). The probability of such inheritance in moraine boulders is very low <3% (Putkonen and Swanson, 2003). This assertion is consistent with more recent analyses in limestone boulders across Turkey, of which 3.3% from a total of 183 contained inherited ^{36}Cl nuclides (Çiner et al., 2017). Inheritance can be more common in arid regions such as the Central Andes, where 7.9% of 794 moraine boulders contained inherited nuclides (D'Arcy et al., 2019). If we assume the oldest ages (24.5 ± 2.4 ka, 25.7 ± 2.6 ka and 29.0 ± 3.0

ka) contain inheritance, these samples are 11% of our total dataset, which is a distinctly higher proportion than observed elsewhere.

It has been demonstrated that incomplete boulder exposure is more important than prior exposure (Heyman et al., 2011). In short, there is no evidence to suggest that inheritance is a contributor to the older ages obtained from each landform sampled here (i.e. 24.5 ± 2.4 ka (MLL-09), 25.7 ± 2.6 ka (MLL-01), 29.0 ± 3.0 ka (TMK-01). Boulder age scatter is typical of all the sampled moraines reported here. Moraines were sampled >0.5 km away from cirque headwalls, cliffs and rock-fall deposits. While inheritance can be important for cirque moraines close to headwalls (Briner et al., 2005), the local climate is humid and limestone is susceptible to solution weathering – this would remove some of the rock surface and with it the accumulated ^{36}Cl. The argument against inheritance is supported by the absence of micro-erosional features on the sampled boulders and the presence of striations on some recently exhumed boulders. There is widespread evidence of karren features on limestone boulders and bedrock in the study area.

5.1.3. Limestone erosion rate

The erosion of boulder surfaces is common in areas of high precipitation (Levenson et al., 2017; Žebre et al., 2019). Karst denudation rates can vary significantly (0–60 mm ka^{-1}), due to a range of chemical and physical factors including annual precipitation, elevation, mean temperature, rock type and freeze-thaw intensity (e.g. Ford and Williams, 1989; Stone et al., 1994; Fiol et al., 1996; Goldie, 2005; Plan, 2005; Ivy-Ochs et al., 2009; Matsushi et al., 2010; Ryb et al., 2014a, 2014b; Levenson et al., 2017; Krklec et al., 2018; Thomas et al., 2018; Žebre et al., 2019). The loss of ^{36}Cl-enriched boulder surfaces can reduce the apparent exposure age of the boulder and its host deposit (Hallet and Putkonen, 1994; Zech et al., 2005; Applegate et al., 2010). Exposure ages can be corrected by applying a constant erosion rate (Briner et al., 2005). However, limestone is particularly susceptible to solution weathering and uncertainties in erosion rates in glacio-karst landscapes pose particular challenges for the correction of exposure ages (Krklec et al., 2018).

An erosion rate correction of 0.6 mm ka^{-1} was applied to the Mount Tymphi ^{36}Cl exposure ages. This is constrained by observed evidence of differential weathering between very resistant upstanding chert veins (8 cm) that are present on limestone clints at an ice-scoured col within the glacier limits ascribed to MIS 6, in the upper Vourtapa valley (Fig, 5) (see methods). This erosion rate is applicable for all our samples, including the dolomitic limestones, which typically have a substantially lower erosion rate than pure limestones (Cucchi et al., 1995; Furlani et al., 2009). A low erosion rate for the limestone of Mount Tymphi is supported by the preservation of chatter marks (c. 10 cm wide) on moraine boulders in the Laccos Megalon Litharion cirque, which implies minimal surface erosion on some surfaces since deposition (Krklec et al., 2013). Nevertheless, the development of karren features on limestone boulders and bedrock demonstrate the efficacy of erosion by solution (Krklec et al., 2018). However, solutional weathering, whilst active is clearly localised and some bedrock surfaces display minimal erosion. This issue of spatially-variable bedrock erosion can be partly controlled by careful sampling. In all cases in this study, sampling took place away from obvious weathering features on the top surface of each boulder, on areas likely to have undergone significantly less surface erosion.

Most boulders exhibit weathering pits and shallow dish-shaped depressions, whilst rillenkarren grooves up to 30 cm deep on the y-axis of a boulder on the Laccos Megalon Litharion cirque moraine suggests locally-high rates of concentrated weathering by solution. Clint and grike morphology is also well developed on limestone pavements although some of the solution may have occurred beneath the glacier. The rate of karren development varies for each feature and is influenced by rainfall intensity, water temperature, droplet size, viscosity, microtopography and vegetation cover (Fiol et al., 1996; Krklec et al., 2018; Goldie, 2005). As such, an erosion rate derived from the depth of solution grooves would not represent the rate of development of other karren features. These are features developed from selective weathering and are therefore not representative of a uniform denudation rate. For instance, weathering is more concentrated along the vertical axis in solution pits and laterally in kamenitza (Krklec et al., 2018). It is likely that the local erosion rate varies significantly.

A minimum erosion rate of 0.6 mm ka^{-1} is consistent with erosion rate corrections of 0–5 mm ka^{-1} applied to limestone moraine boulders elsewhere in Greece and the wider Balkans (Pope et al., 2017; Gromig et al., 2018; Styllas et al., 2018). Field observations at these sites showed minimal evidence of erosion. Erosion rates are unlikely to ever be truly zero. However, in cases where there is no obvious evidence of erosion, arbitrary erosion correction is more likely to be a cause of error in cosmogenic exposure dating. An erosion rate correction of 40 mm ka^{-1} was applied for limestone moraine boulders sampled in the Velež and Crvanj mountains, and in the Blidinje Polje, Bosnia and Herzegovina (Žebre et al., 2019; Çiner et al., 2019). This erosion rate was based on the presence of solution grooves several centimetres deep and denudation rates of ~20–60 mm ka^{-1} observed elsewhere in the Mediterranean (Levenson et al., 2017; Thomas et al., 2018; Žebre et al., 2019). An erosion rate correction of 20 mm ka^{-1} was also applied to limestone moraine boulders sampled in the Southern Velebit Mountains, Croatia, due to locally high precipitation rates (Sarıkaya et al., 2020). Such a high erosion rate is possible locally on Mount Tymphi, since we have observed deep grooves on some boulders. However, our samples were taken away from deeply weathered surfaces and it is unnecessary to make this “maximum” erosion rate correction.

5.1.4. Landform age interpretation

Previous studies suggest the oldest boulder age as the best estimate for the timing of moraine deposition where post-depositional processes of exhumation and/or erosion are significant and boulder ages are dispersed (Putkonen and Swanson, 2003; Briner et al., 2005; Zech et al., 2005; Hall et al., 2009; May et al., 2011; Heyman et al., 2011; Stroeven et al., 2011; Applegate et al., 2012; Ivy-Ochs and Briner, 2014; D'Arcy et al., 2019). This assumption is supported by the moraine surface degradation diffusion model of Putkonen and Swanson (2003) who concluded that the oldest obtained age is ≥90% of the moraine age (95% probability). For the Mount Tymphi data, we favour the oldest age as the minimum limiting age for each moraine given the widespread evidence for moraine degradation, boulder exhumation, and the uncertainties in erosion rates (Briner et al., 2005; Heyman et al., 2011). This approach has recently been employed in Bosnia and Herzegovina and Croatia in a very similar setting where exhumation and high precipitation rates contributed to the spread of ages (Çiner et al., 2019; Žebre et al., 2019; Sarıkaya et al., 2020). Other methods of landform age interpretation – such as the mean age – can lead to significant inaccuracy where incomplete exposure and erosion are the main geological uncertainties (Applegate et al., 2010; D'Arcy et al., 2019). In the case of Mount Tymphi, the oldest ages on the Late Pleistocene moraines are also consistent with the independently-dated fluvial record immediately downstream (Lewin et al., 1991; Woodward et al., 2008) and with the regional vegetation record (Tzedakis et al., 2002) as discussed below.

5.2. Interpretation of ^{36}Cl ages from Mount Tymphi

The ^{36}Cl exposure ages from Mount Tymphi indicate a history of moraine deposition, moraine stabilisation, boulder exhumation and erosion. For the reasons outlined above, the most accurate minimum ages for moraine deposition are 29.0 ± 3.0 ka (TMK-01) for the Tsioumako right lateral moraine; 25.7 ± 2.6 ka (MLL-01) for the Laccos Megalon Litharion terminal moraine; and 24.5 ± 2.4 ka (MLL-09) for the Laccos Megalon Litharion cirque moraine (Fig. 4). The oldest limiting age in the Laccos cirque on the northeast side of the Tymphi massif is 18.0 ± 1.9 ka (LAC-05) on the outer terminal moraine ridge, although more data are needed from this side of the massif given the widespread evidence for moraine degradation and boulder exhumation. So, moraine crest boulders either stabilised or were exhumed some 5–13.5 ka after moraine deposition. The data indicate that boulder exhumation was particularly prevalent between 7 and 10 ka after ice retreat.

All of this new evidence shows that Late Pleistocene glaciers covered an area of 8.8 km^2 on Mount Tymphi, with a total volume of 0.5 km^3 (Table 6). The largest glaciers, 2.4–3.1 km long, covered an area of 4.5 km^2 on the southern slopes of Mount Tymphi with maximum thicknesses of >200 m, and reached their last terminal positions no later than 25.7 ± 2.6–29.0 ± 3.0 ka (Fig. 10). Cirque glaciers persisted at 24.5 ± 2.4 ka, after glacier retreat, and covered an area of ~1.6 km^2 (Table 8). Initial results suggest that small glaciers (<0.6 km^2) persisted in the northeast cirques at 18.0 ± 1.9 ka, perhaps sustained by avalanching snow and topographic shading from the Goura cliffs. During the cold stages of the last glacial cycle (MIS 5e–2), the glaciers of Mount Tymphi were restricted to the cirques and upper valleys between 1700 and 2350 m. This is in good agreement with previous mapping and the existing set of U-series ages which indicate much more extensive Middle Pleistocene glaciations (MIS 6 and MIS 12) that extended down to elevations of 1500–1700 m and ~900 m a.s.l. respectively (Woodward et al., 2004; Hughes et al., 2006a). Exposure ages from the Laccos Megalon Litharion suggest that this palaeoglacier reached its last maxima 3–4 ka after the Tsioumako palaeoglacier. Both valleys are oriented to the south/southwest exposing them to the afternoon sun which would promote ablation. However, the Laccos Megalon Litharion is bounded by the Krevati cliffs to the west and the Vlasi arête to the east. This setting would provide both shading and a source of wind-blown snow from the west which may explain the younger age observed in this valley (Hughes, 2004).

A last glacier maximum on Mount Tymphi no later than 25.7–29 ka is consistent with welldated outwash sediments in the downstream river record (~24–28 ka) (Lewin et al., 1991; Macklin and Woodward, 2009) and the Ioannina basin pollen record (35 km to the south) which indicates cool and wet conditions, most favourable for glacier growth between 25 and 30 ka (Tzedakis et al., 2002) (Fig. 11). Moraine deposition by 29.0 ± 3.0 ka (TMK-01) in the Tsioumako valley follows a reduced peak in summer solar insolation at ~32 ka (Berger and Loutre, 1991), that resulted in cooler summer temperatures favouring glacier growth across the Mediterranean mountains (Fig. 11d). Heinrich stadial (HS) 3 (31.3–32.7 ka) (Sanchez Goñi and Harrison, 2010) is poorly expressed in the Ioannina pollen record (Tzedakis et al., 2004), suggesting that moisture availability in the Pindus Mountains was higher during this period than during HS 2 (24.3–26.5 ka) and HS 4 (38.3–40.2 ka) (Sanchez Goñi and Harrison, 2010). Cool and wet conditions would have favoured glacier growth at these elevations at this time (Ohmura et al., 1992; Hughes et al., 2006b). Intermediate levels of forest cover also persisted in the region between 26 and 59 ka (Fig. 11c), suggesting moisture availability that would have supported both tree populations and glacier accumulation (Tzedakis et al., 2002). The wider landscape of Epirus at intermediate elevations is believed to have been an important refugia for vegetation during Pleistocene glacials (Tzedakis et al., 2002).

Minimum limiting ages from the Laccos Megalon Litharion imply moraine deposition at the terminus no later than 25.7 ± 2.6 ka (MLL-01) and at 24.5 ± 2.4 ka (MLL-09) in the cirque. This coincided with climatic deterioration during HS 2 (26.5–24.3 ka) (Macklin et al., 1997; Sanchez Goñi and Harrison, 2010) and a marked regional temperature depression between 25.6 and 23.2 ka (Galanidou et al., 2000; Hughes, 2004) when cold and drier conditions prevailed, reducing regional moisture supply. In response, tree populations contracted (Fig. 11c) and glaciers retreated. The Litharion glacier retreated by approximately 2 km from its Late Pleistocene terminus to a position occupying just the highest cirque basin. A talus rock glacier formed after 25.7 ± 2.6 ka (MLL-01) on the west slopes of Vlasi in the lower part of the valley previously occupied by the Litharion glacier. Heinrich Stadial 2 was a period of glacier retreat across Mount Tymphi that also saw debris rock glaciers form in the Tsouka Rossa cirques below small cirque glaciers (Hughes et al., 2003). These rock glaciers are stratigraphically younger than moraines marking the maximum extent of Late Pleistocene glaciers and therefore occupied the high cirques after 25.7 ± 2.6 ka (MLL-01). This is consistent with the development of open vegetation communities at 26.0–11.5 ka (Tzedakis et al., 2002) and more arid pollen taxa dominating the Ioannina pollen record between 25.1 and 15.6 ka (Lawson et al., 2004) (Fig. 11c).

The glaciated slopes on the south side of Mount Tymphi form part of the upper catchment of the Voidomatis River (Lewin et al., 1991). A last local glacier maxima at 25.7–29 ka is consistent with the downstream fluvial record, where coarse grained outwash-dominated river sediments dating to 24.3 ± 2.6–28.2 ± 7.0 ka dominate the Aristi unit at Old Klithonia Bridge (Lewin et al., 1991; Woodward et al., 1994; Macklin et al., 1997; Hamlin et al., 2000; Macklin and Woodward, 2009) (Fig. 11b). This glaciofluvial outwash is dominated by limestone clasts (95%) and has an abundant fine sediment component matching the lithology of the glacial tills above Tsepelovo (Woodward et al., 1992). The Aristi unit contains at least 2 separate fills each from different glacial episodes (Woodward et al., 1994, 2008). Fine sediments dated to 28.2 ± 7.0 ka (Lewin et al., 1991; Macklin et al., 1997) may correspond with an earlier advance (such as at 29 ± 3.0 ka), whilst 3 dates from a red deer jaw bone within the Aristi unit (24.3 ± 2.6, 25.0 ± 0.5 and 26.0 ± 1.9; Macklin et al., 1997) correlate with a later maxima of the Laccos Megalon Litharion palaeoglacier at 25.7 ± 2.6 ka and smaller-scale cirque glaciation at 24.5 ± 2.4 ka.

From 24.3 ± 2.6 to 19.6 ± 3.0 ka, glacially-sourced limestone rock flour is still present in the fluvial deposits in the Vikos unit, but less so than in the Aristi unit, suggesting increased flysch erosion of the lower valley slopes and decreased glacier size (Lewin et al., 1991; Woodward et al., 1992; Macklin et al., 1997). A decline in limestone-derived fine sediment input implies smaller glaciers than previously (Macklin et al., 1997) (Fig. 10). Cold and drier conditions at this time reduced moisture availability for both trees and glaciers. Contracting tree populations reduced vegetation cover on flysch slopes, thus promoting a greater flysch sediment component in the Voidomatis River (Lewin et al., 1991; Macklin et al., 1997). This corresponded with retreat of the Laccos Megalon Litharion glacier by 24.5 ± 2.4 ka and glacier retreat in the Tselon and Tsouka Rossa cirques. Renewed fluvial aggradation is also notable at 25 ± 2.4 ka ka due to an increase in sediment supply under a colder climate (Hamlin et al., 2000; Hughes, 2004). Limestone sediments in the Vikos unit during this period are not necessarily from glaciation,

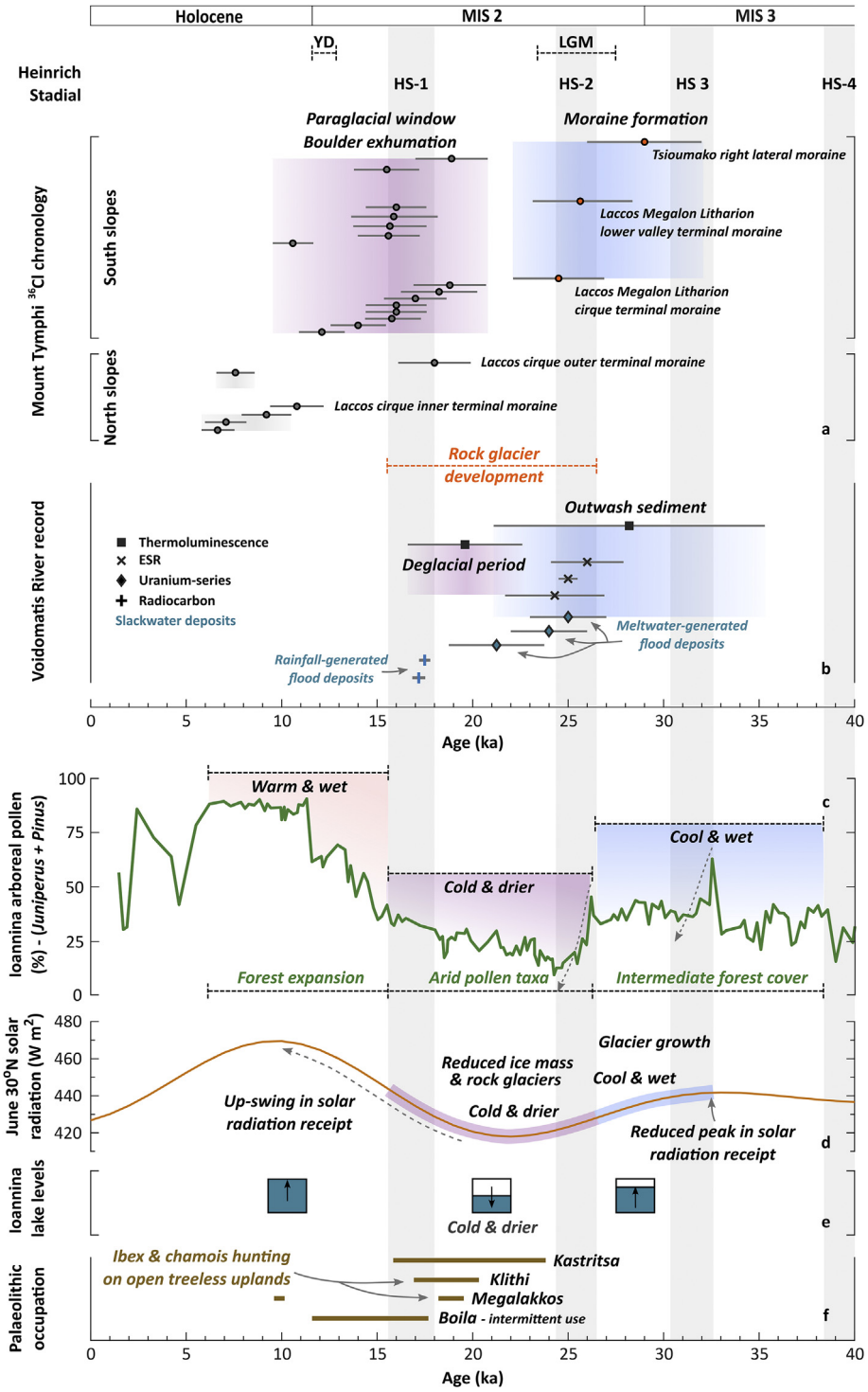

Fig. 11. Palaeoenvironmental and geochronological data for Mount Tymphi, the Voidomatis River basin and Lake Ioannina for the last 40 ka. a) Moraine boulder ages from ^{36}Cl terrestrial cosmogenic nuclide exposure dating (this paper), showing the timing of moraine deposition and the timing of boulder exhumation on Mount Tymphi. b) Age control on the downstream fluvial record of the Voidomatis River including thermoluminescence dates on fine grained sediments (Lewin et al., 1991), ESR dates from a deer tooth (Lewin et al., 1991), Uranium-series dates from cemented alluvium (Hamlin et al., 2000; Woodward et al., 2008) and calibrated radiocarbon dates from slackwater flood deposits (Woodward et al., 2001). c) Arboreal pollen frequency (%) from Ioannina I-284 *(excluding Juniperus and Pinus)*, adapted from Tzedakis et al. (2002) and Lawson et al. (2004). d) June solar radiation at 30°N in the Northern Hemisphere (Berger and Loutre, 1991). e) Ioannina lake level data (Frogley, 1998). f) Timing of Palaeolithic occupation of rockshelters from calibrated radiocarbon dates at Klithi (Bailey and Woodward, 1997), Megalakkos (Woodward, 1997) and Boila (Woodward et al., 2001) in the Lower Vikos Gorge, of the Voidomatis River, and at Kastritsa rockshelter, Ioannina (Galanidou et al., 2000). Heinrich Stadials 1, 2, 3 and 4 are based on Sanchez Goñi and Harrison (2010). Last Glacial Maximum (LGM) 27.5–23.3 ka, based on Hughes and Gibbard (2015).

but likely in part due to the reworking of glacial and earlier outwash sediments by periglacial and paraglacial processes (Hughes, 2004). A locally cold and drier climate persisted during 20–22 ka, as indicated by low lake levels at Ioannina (Frogley, 1998) (Fig. 11e). At ~21 ka, temperatures dropped by 10 °C during January and 6.8 °C during July, with annual rainfall estimated to be around 600 mm (Tzedakis et al., 2002). These conditions inhibited glacier readvances.

The first dates obtained from the northeast-facing Laccos cirque, tentatively suggest that small cirque glaciers, <0.6 km^2, persisted in the Kriopotamos cirques at 18 ± 1.9 ka (LAC-05), possibly facilitated by avalanching snow accumulation and shading beneath the Goura cliffs. The Laccos valley drains into the Aoös basin. However, the Vikos unit of the Voidomatis River dates to 19.6 ± 3.0–24.3 ± 2.6 ka and includes limestone clasts and glacial material input in the fine fraction suggesting either the reworking of glacial or outwash sediments or the presence of smaller glaciers at this time (Macklin et al., 1997). The young limiting age of the Vikos unit overlaps within uncertainty with possible moraine deposition in the Laccos cirque and gives some support to this initial evidence for small cirque glaciers on Mount Tymphi at 18 ka. Nonetheless, more data are needed from the northeast valleys to build a more robust age model.

In the south-facing valleys, 12 ^{36}Cl exposure ages date to 15.5 ± 1.7–18.9 ± 1.9 ka. These ages very likely represent the timing of boulder exhumation as opposed to the age of moraine deposition (Fig. 11a). Critically, there is no glacially-derived outwash sediment detected in the slackwater flood deposits dating to 17.5 ± 0.3 and 17.2 ± 0.4 ka at Boila rockshelter (located in Fig. 2.) (Woodward et al., 2001, 2008) (Fig. 11b), implying the absence of glaciers in the Voidomatis headwaters above Tsepelovo at the time of boulder exhumation. The Boila deposits record a shift from meltwater-generated flood deposits to rainfall-generated flood deposits (Woodward et al., 2008). This period follows increased river incision which, along with an improving climate, facilitated access for Upper Palaeolithic humans into the Lower Vikos gorge (Bailey et al., 1990; Macklin et al., 1997; Bailey and Woodward, 1997). The most intensive human use of Klithi rockshelter occurred between 17.0 and 20.2 ka cal BP (Bailey and Woodward, 1997) (Fig. 11f). Klithi was as a base for ibex and chamois hunting in the wider upland landscape. A comparable faunal assemblage is also evident at nearby Megalakkos rockshelter (Fig. 2), where there is evidence of human activity between 18.1 and 19.6 ka cal BP (Woodward, 1997) (Fig. 11f). Upper Palaeolithic occupation of the Lower Vikos gorge overlaps with the main period of moraine boulder exhumation. Ibex and chamois prefer open treeless upland habitats, which is consistent with cold and drier conditions and reduced tree populations at this time (Tzedakis et al., 2002). Limited moisture availability would have impeded glacier accumulation, particularly on the south-facing slopes of Mount Tymphi.

Heinrich Stadial 1 (15.6–18.0 ka) reinforced the cold and drier conditions (Tzedakis et al., 2002; Sanchez Goñi and Harrison, 2010) so that glacier advances akin to those at 25.7–29 ka were unlikely. Instead, moraines eroded and boulders were exhumed during this paraglacial window (Woodward et al., 2014). Eight of the ^{36}Cl ages date to the very end of HS 1. This may be the result of moraines at this elevation being subjected to periglacial slope processes during the period of intense cold and drying climate (Oliva et al., 2018). This precedes forest expansion from 15.6 ka (Tzedakis et al., 2002) (Fig. 11c). The return of trees to the mountain slopes aided moraine stabilisation (Woodward et al., 2008), after which we see fewer exhumed boulders (Fig. 11a). This coincides with the end of Upper Palaeolithic occupation at Klithi (Fig. 11f). Upper Palaeolithic human activity shifted to the mouth of the Lower Vikos gorge, with intermittent occupation of Boila rockshelter between 17.8 and 11.7 ka cal BP (Woodward et al., 2001). A more diverse fauna at this time indicates exploitation of both the gorge and the Konitsa plain, as hunter-gatherers responded to these environmental changes (Kotjabopoulou et al., 1999). Forested mountain slopes were not favourable for ibex and chamois exploitation.

Climate shifted to warmer and moist interglacial conditions from 15.6 to 9.9 ka (Tzedakis, 1993; et al., 2002; Woodward, 1997; Lawson et al., 2004). Forest cover expanded with birch dominating the Ioannina pollen record between 14.5 and 10 ka. (Lawson et al., 2004). There is little evidence of the Younger Dryas in the glacial record on Tymphi (confirming suggestions by Hughes et al., 2006c), or in the Ioannina pollen record where there is only a minor oscillation recorded in deciduous taxa (Lawson et al., 2004; Tzedakis et al., 1993; et al., 2002).

Well-dated fluvial units in the Lower Vikos gorge and on the Konitsa basin, downstream of the glaciated upper catchment, have identified periods of peak glacial sediment input during the Late Pleistocene (Lewin et al., 1991; Woodward et al., 1992, 1994; Macklin and Woodward, 2009). Coarse grained limestone-rich, till-derived alluvium dominates at c. 78 ka; 55 ± 4 ka; and between 28.2 ± 7–24.3 ± 2.6 ka (Lewin et al., 1991; Woodward et al., 1994; Macklin et al., 1997; Hamlin et al., 2000). We found no evidence of ^{36}Cl ages from moraine boulders that correspond with earlier phases of glaciation during the Late Pleistocene, i.e. at 78 ka and 55 ± 4 ka. Glaciers at these times were probably much smaller than those dated to 25.7–29 ka. Any older moraines, deposited inside of these limits, were very likely reworked by later and more extensive glacier advances. These fluvial units could suggest that glaciers oscillated within the upper valleys and cirques of Mount Tymphi throughout the Late Pleistocene. They could also represent fluvial reworking of the limestone-rich outwash that was deposited during the Middle Pleistocene (Woodward et al., 2008).

5.3. Late Pleistocene glacial chronologies in the Balkans and the Mediterranean

Away from Mount Tymphi, chronological control for the last glaciation in Greece and wider Balkans is still rather limited. These ^{36}Cl ages presented here constrain the timing of glacier maxima in northwest Greece at 25.7–29 ka during the Late Pleistocene. The Tymphi record overlaps with two recalculated ^{36}Cl ages from Mount Chelmos, southern Greece, where a last local glacier maxima is recorded during MIS 3 (28.6 ± 0.6–36.5 ± 0.9 ka) at ~2120 m a.s.l. in the Kato Kambos (Pope et al., 2017) (Fig. 12). Late Pleistocene glaciers were confined to the high valleys and cirques on both Mount Tymphi and Mount Chelmos, with mean ELAs of 2016 m (AABR method) and 2046 m (area altitude ratio (AAR) method) respectively (Pope et al., 2017). Similarly, ~125 km to the east of Tymphi, geomorphological evidence suggests terminal moraine deposition during the Late Pleistocene at 2155 m a.s.l. in the Megala Kazania cirque on Mount Olympus (Styllas et al., 2018).

Elsewhere in the Mediterranean, recalculated TCN ages (with production rates applied in this work) indicate a last local glacier maximum at ~25–31 ka in the south-central Pyrenees and the Iberian Central System (e.g. Pallàs et al., 2006; Domínguez-Villar et al., 2013). In fact, glaciers were at or close to their last local maxima across the Mediterranean from 32 ka (recalculated ages), in southern Spain (e.g. Gómez-Ortiz et al., 2012; Palacios et al., 2016), Corsica (Kuhlemann et al., 2008), and Turkey (e.g. Akçar et al., 2007; et al., 2008; Zahno et al., 2009; Sarıkaya et al., 2009; et al., 2014; Sarıkaya and Çiner, 2017; Köse et al., 2019). This pattern is consistent with calibrated radiocarbon ages of 33–27 ka from glaciofluvial sediments in the central Apennines, Italy (Giraudi,

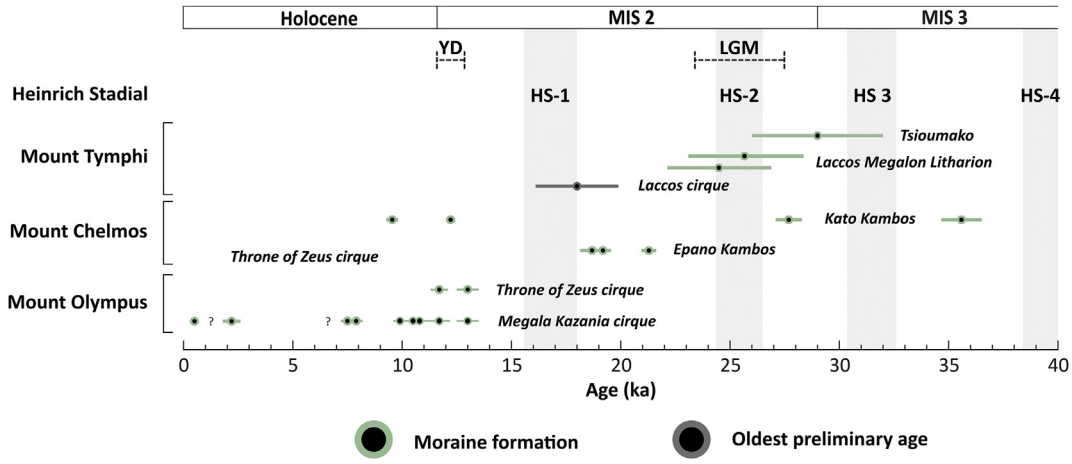

Fig. 12. The ^{36}Cl glacial chronology of Greece, including ages from Mount Tymphi (this paper), recalculated ages from Mount Chelmos (Pope et al., 2017), and recalculated ages from Mount Olympus (Styllas et al., 2018). Heinrich Stadials 1, 2, 3 and 4 are based on Sanchez Goñi and Harrison (2010). Last Glacial Maximum (LGM) 27.5–23.3 ka, based on Hughes and Gibbard (2015).

2012). In most areas, glaciers advanced in MIS 3/early MIS 2 during optimal cool and wet conditions (Oliva et al., 2019), and at a time of reduced solar radiation receipt in the Northern Hemisphere (Berger and Loutre, 1991).

Glacier retreat on Mount Tymphi was very likely driven by cold and drier conditions that limited glacier accumulation after 25.7 ± 2.6 ka (Fig. 11). On Mount Chelmos, retreating glacier margins at 22.2 ± 0.3–19.6 ± 0.5 ka (recalculated ages) were constrained by three ^{36}Cl ages from a recessional moraine in the Epano Kambos (Pope et al., 2017). This period is represented by the widespread evidence of rock glacier development on Mount Tymphi (Hughes et al., 2003). Rock glaciers formed during HS 2 as debris supply exceeded snow accumulation partly due to the drier conditions, but also with increased sediment supply from periglacial weathering of cirque headwalls and valley side instability following glacier retreat (Ballantyne, 2002; Hughes et al., 2003; Ballantyne et al., 2014). We see scree accumulation in Klithi rockshelter at this time (Bailey and Woodward, 1997). Elsewhere in the Pindus Mountains, undated rock glaciers on the Peristeri and Tzoumerka massifs (Fig. 1) likely date to this period (Palmentola and Stamatopoulos, 2006). In contrast, ^{10}Be ages that range from 16.3 ± 1.0–22.5 ± 1.8 ka in the Rila Mountains, western Bulgaria, suggest a later phase of last glacier maxima much further north in the Balkans (Kuhlemann et al., 2013). A ^{10}Be age of 17.8 ± 1.3 ka in the Sara Range, northern Macedonia (Kuhlemann et al., 2009) also highlights the apparent diachronous nature of glacier maxima in the Balkans during the Late Pleistocene. Small glaciers (up to 3.2 km^2) developed on Mount Orjen on the coast of Montenegro during the Late Pleistocene (Hughes et al., 2010). Uranium-series dating of secondary carbonates within a terminal moraine in the Reovci valley provides a *minimum* age for these glaciers of 17.3 ± 0.6 ka (Hughes et al., 2010). A later phase of last glacier maxima is also evident across the Mediterranean, in Turkey (e.g. Akçar et al., 2017; Sarıkaya et al., 2008; Çiner and Sarıkaya, 2017), Italy (e.g. Federici et al., 2012; Baroni et al., 2018) and in some catchments in the Pyrenees (Aránser, Duran and La Llosa; Palacios et al., 2015).

Fifteen ^{36}Cl ages from the southern valleys of Mount Tymphi record an exposure history of 18.9 ± 1.9–10.6 ± 1.1 ka. We interpret these ages as representing the timing of moraine boulder *exhumation* under active periglacial conditions rather than later glacier stabilisation. Evidence of cirque glacier stabilisations towards the end of MIS 2 have been recorded elsewhere in Greece, for example in the recalculated ^{36}Cl exposure age records on Mount Olympus (13.0 ± 0.5–11.7 ± 0.5 ka) (Styllas et al., 2018) and Mount Chelmos (13.1 ± 0.2–10.5 ± 0.3 ka) (Pope et al., 2017) (Fig. 12). In fact, there is evidence of cirque glaciation in the Megala Kazania at Mount Olympus during the early Holocene (11.7 ± 0.5–7.5 ± 0.3 ka) and even the late Holocene (2.4 ± 0.1–0.5 ± 0.0 ka) (Styllas et al., 2018). Further north in the Balkans, cirque glaciation has been dated to the Late-glacial at Mount Pelister (14.7 ± 0.4–14.1 ± 0.4 ka) (Ribolini et al., 2018), and to the Younger Dryas (12.9–11.7 ka) at Magaro Mountain (12.8 ± 2.1–11.0 ± 2.0 ka) in southwest Macedonia. In northern Macedonia, rock glaciers developed within cirques at 12.4 ± 1.0–11.7 ± 0.6 ka, consistent with increasing seasonal aridity (Kuhlemann et al., 2009). Uranium-series dating of secondary calcites within moraines in Montenegro also attests to moraine formation prior to 13.4 ± 0.4 ka, 10.6 ± 0.2 ka and 9.6 ± 0.8 ka in the Kalica valley around the Durmitor Massif (Hughes et al., 2011), and before 9.6 ± 0.8 ka in the Reovci valley at Mount Orjen (Hughes et al., 2010). Conversely, ^{36}Cl ages (14.0 ± 2.6–11.3 ± 2.5 ka) from lateral moraines on Crvanj Mountain and Velež Mountain in Bosnia and Herzegovina suggest glacier extents of 24–28 km^2, with much lower ELAs at 1541 m and 1388 m respectively (Žebre et al., 2019). Similar palaeo-piedmont glaciers have been constrained to 13.2 ± 1.8 ka at Svinjača and 13.5 ± 1.8 ka at Glavice in the Blidinje Polje, Bosnia and Herzegovina (Çiner et al., 2019). It is important to appreciate, however, that the moraine boulders sampled in Bosnia and Herzegovina have undergone complex exhumation and weathering histories which creates challenges for interpreting the ^{36}Cl ages (Žebre et al., 2019; Çiner et al., 2019). There is no substantive evidence of Late-glacial, Younger Dryas or Holocene glaciation in our dataset at Mount Tymphi. It is very likely that the ^{36}Cl ages of 6.7 ± 0.9–18.9 ± 1.9 ka represent the timing of moraine boulder exhumation, as opposed to later glacier stabilisations.

6. Conclusions

Late Pleistocene glaciers were restricted to the upper valleys and cirques of Mount Tymphi covering an area of ~8.8 km^2 at their maximum extent. Terminal and lateral moraines between 1700 m and 2050 m a.s.l. mark the extent of Late Pleistocene glaciers on the southern side of Mount Tymphi. These moraines date to 29.0 ± 3.0 ka, 25.7 ± 2.6 ka and 24.5 ± 2.4 ka, taking the oldest age as the most representative of moraine emplacement. A last local glacier maxima at 25.7–29 ka is in good agreement with outwash sediments dating to ~24–28 ka in the Voidomatis river record downstream

and is consistent with the Ioaninna basin pollen record, indicating cool and wet conditions, most favourable for glacier growth between 25 and 30 ka. Glaciers had retreated to the high cirques by 24.5 ± 2.4 ka during Heinrich Stadial 2. Rock glaciers formed under cold and drier conditions during this period of glacier retreat as debris supply exceeded snow accumulation. This TCN dataset complements existing U-series ages obtained from secondary calcites in glacial sediments at elevations below 1700 m a.s.l. on Mount Tymphi, which demonstrate more extensive Middle Pleistocene glaciations during MIS 6 and MIS 12. The younger outliers on each Late Pleistocene moraine indicate the exhumation of moraine boulders, well after moraine deposition and deglaciation. Three TCN dates from a Middle Pleistocene (MIS 12) moraine highlight the challenges involved in ^{36}Cl TCN dating of limestones from glacial deposits older than one glacial cycle (i.e. >MIS 5e). Preliminary results from the northeast cirques on Mount Tymphi suggest a later phase of moraine stabilisation, although more data are needed from that side of the massif to fully test this theory, given the widespread evidence of moraine degradation and boulder exhumation. This paper presents 27 ^{36}Cl exposure ages, from 5 sets of moraines, which address a significant geographical gap in Mediterranean glacial chronologies and provide a valuable insight into the extent and timing of Late Pleistocene glaciation in the Pindus Mountains.

CRediT authorship contribution statement

James L. Allard: Conceptualization, Methodology, Formal analysis, Investigation, Data curation, Writing - original draft, Writing - review & editing, Visualization, Funding acquisition. **Philip D. Hughes:** Conceptualization, Methodology, Formal analysis, Investigation, Writing - original draft, Writing - review & editing, Supervision, Funding acquisition. **Jamie C. Woodward:** Conceptualization, Methodology, Formal analysis, Investigation, Writing - original draft, Writing - review & editing, Supervision. **David Fink:** Methodology, Investigation, Formal analysis, Resources, Writing - original draft, Writing - review & editing, Supervision. **Krista Simon:** Formal analysis, Investigation, Resources, Writing - original draft, Writing - review & editing. **Klaus M. Wilcken:** Formal analysis, Investigation, Resources, Writing - original draft, Writing - review & editing.

Declaration of competing interest

The authors declare that they have no known competing financial interests or personal relationships that could have appeared to influence the work reported in this paper.

Acknowledgements

We thank Jonathan Yarwood and John Moore from the Department of Geography Laboratories, The University of Manchester, for their help with the laboratory work. We also thank Alex Woodward for his assistance during fieldwork in June 2018. We thank the Institute of Geology and Mineral Exploration (IGME), Greece, for issuing fieldwork permits. We thank the Royal Geographical Society with IBG for awarding J.A. the Dudley Stamp Memorial Award, which supported the fieldwork. We also thank the Quaternary Research Association for awarding J.A. the New Research Workers' Award, which facilitated ^{36}Cl sample processing and training at the Australian Nuclear Science and Technology Organisation (ANSTO Research Portal Number: 11382), Sydney, Australia. J.A. was funded by a School of Environment Education and Development (SEED) PhD Studentship in the Department of Geography at The University of Manchester. We thank Marc Oliva and David Palacios for their constructive reviews of this paper.

References

Adamson, K.R., Woodward, J.C., Hughes, P.D., 2014. Glaciers and rivers: Pleistocene uncoupling in a Mediterranean mountain karst. Quat. Sci. Rev. 94, 28–43. https://doi.org/10.1016/j.quascirev.2014.04.016.

Adamson, K.R., Woodward, J.C., Hughes, P.D., 2016. Middle Pleistocene glacial outwash in poljes of the Dinaric karst. In: Feinberg, J., Gao, Y., Alexander Jr., E.C. (Eds.), Caves and Karst across Time, vol. 516. Geological Society of America Special Paper, pp. 247–262. https://doi.org/10.1130/2015.2516(20).

Akçar, N., Yavuz, V., Ivy-Ochs, S., Kubik, P.W., Vardar, M., Schlüchter, C., 2007. Paleoglacial records from Kavron Valley, NE Turkey: field and cosmogenic exposure dating evidence. Quaternary International, From the Swiss Alps to the Crimean Mountains - Alpine Quaternary stratigraphy in a European context 164– 165, 170–183. https://doi.org/10.1016/j.quaint.2006.12.020.

Akçar, N., Yavuz, V., Ivy-Ochs, S., Kubik, P.W., Vardar, M., Schlüchter, C., 2008. A case for a downwasting mountain glacier during Termination I, Verçenik valley, northeastern Turkey. J. Quat. Sci. 23, 273–285. https://doi.org/10.1002/jqs.1144.

Akçar, N., Yavuz, V., Yeşilyurt, S., Ivy-Ochs, S., Reber, R., Bayrakdar, C., Kubik, P.W., Zahno, C., Schlunegger, F., Schlüchter, C., 2017. Synchronous Last Glacial Maximum across the Anatolian peninsula. In: Hughes, P.D., Woodward, J.C. (Eds.), Quaternary Glaciation in the Mediterranean Mountains. Quaternary Glaciation in the Mediterranean Mountains. Geological Society, London, Special Publications, pp. 251–269. https://doi.org/10.1144/SP433.7.

Anavasi, 2018. Zagori - Epirus [3.1]. Topo 50. 1:50 000. Anavasi Maps & Guides, Athens, Greece.

Andrés, N., Gómez-Ortiz, A., Fernández-Fernández, J.M., Tanarro, L.M., Salvador-Franch, F., Oliva, M., Palacios, D., 2018. Timing of deglaciation and rock glacier origin in the southeastern Pyrenees: a review and new data. Boreas 47, 1050–1071. https://doi.org/10.1111/bor.12324.

Applegate, P.J., Urban, N.M., Laabs, B.J.C., Keller, K., Alley, R.B., 2010. Modeling the statistical distributions of cosmogenic exposure dates from moraines. Geosci. Model Dev. (GMD) 3, 293–307. https://doi.org/10.5194/gmd-3-293-2010.

Applegate, P.J., Urban, N.M., Keller, K., Lowell, T.V., Laabs, B.J.C., Kelly, M.A., Alley, R.B., 2012. Improved moraine age interpretations through explicit matching of geomorphic process models to cosmogenic nuclide measurements from single landforms. Quat. Res. 77, 293–304. https://doi.org/10.1016/j.yqres.2011.12.002.

Bailey, G.N., Lewin, J., Macklin, M.G., Woodward, J.C., 1990. The "Older Fill" of the Voidomatis valley, North-west Greece and its relationship to the Palaeolithic archaeology and glacial history of the region. J. Archaeol. Sci. 17, 145–150. https://doi.org/10.1016/0305-4403(90)90055-A.

Bailey, G.N., Woodward, J.C., 1997. The Klithi deposits: sedimentology, stratigraphy and chronology. In: Bailey, G.N. (Ed.), Klithi: Palaeolithic Settlement and Quaternary Landscapes in Northwest Greece, Volume 1: the Klithi Deposits: Sedimentology, Stratigraphy and Chronology. McDonald Institute, Cambridge, pp. 61–94. https://doi.org/10.13140/RG.2.1.1671.1128.

Balco, G., 2018. Topographic Shielding Calculator. http://stoneage.ice-d.org/math/skyline/skyline_in.html.

Balco, G., 2011. Contributions and unrealized potential contributions of cosmogenic-nuclide exposure dating to glacier chronology, 1990–2010. Quat. Sci. Rev. 30, 3–27. https://doi.org/10.1016/j.quascirev.2010.11.003.

Ballantyne, C.K., 2002. Paraglacial geomorphology. Quat. Sci. Rev. 21, 1935–2017. https://doi.org/10.1016/S0277-3791(02)00005-7.

Ballantyne, C.K., Wilson, P., Gheorghiu, D., Rodés, À., 2014. Enhanced rock-slope failure following ice-sheet deglaciation: timing and causes. Earth Surf. Process. Landforms 39, 900–913. https://doi.org/10.1002/esp.3495.

Baroni, C., Guidobaldi, G., Salvatore, M.C., Christl, M., Ivy-Ochs, S., 2018. Last glacial maximum glaciers in the Northern Apennines reflect primarily the influence of southerly storm-tracks in the western Mediterranean. Quat. Sci. Rev. 197, 352–367. https://doi.org/10.1016/j.quascirev.2018.07.003.

Ben Israel, M., Matmon, A., Hidy, A., Avni, Y., Balco, G., 2020. Early-to-mid Miocene erosion rates inferred from pre-Dead Sea rift Hazeva River fluvial chert pebbles using cosmogenic ^{21}Ne. Earth Surface Dynamics 8, 289–301. https://doi.org/10.5194/esurf-8-289-2020.

Berger, A., Loutre, M.F., 1991. Insolation values for the climate of the last 10 million years. Quat. Sci. Rev. 10, 297–317. https://doi.org/10.1016/0277-3791(91)90033-Q.

Borchers, B., Marrero, S., Balco, G., Caffee, M., Goehring, B., Lifton, N., Nishiizumi, K., Phillips, F., Schaefer, J., Stone, J., 2016. Geological calibration of spallation production rates in the CRONUS-Earth project. Quat. Geochronol. 31, 188–198. https://doi.org/10.1016/j.quageo.2015.01.009.

Briner, J.P., Kaufman, D.S., Manley, W.F., Finkel, R.C., Caffee, M.W., 2005. Cosmogenic exposure dating of Late Pleistocene moraine stabilization in Alaska. GSA Bulletin 117, 1108–1120. https://doi.org/10.1130/B25649.1.

Brückner, E., 1890. Eisziet-Studien in den südöstlichen Alpen. Jahresbericht der Geographisher Geselschaft von Bern 10, 156–164.

Çiner, A., Sarıkaya, M.A., 2017. Cosmogenic ^{36}Cl geochronology of late Quaternary glaciers in the Bolkar Mountains, south central Turkey. In: Hughes, P.D., Woodward, J.C. (Eds.), Quaternary Glaciation in the Mediterranean Mountains. Geological Society, London, Special Publications, pp. 271–287. https://doi.org/10.1144/SP433.3.

Çiner, A., Sarıkaya, M.A., Yıldırım, C., 2017. Misleading old age on a young landform?

The dilemma of cosmogenic inheritance in surface exposure dating: moraines vs. rock glaciers. Quat. Geochronol. 42, 76–88. https://doi.org/10.1016/j.quageo.2017.07.003.
Çiner, A., Stepišnik, U., Sarıkaya, M.A., Žebre, M., Yıldırım, C., 2019. Last Glacial Maximum and Younger Dryas piedmont glaciations in Blidinje, the Dinaric Mountains (Bosnia and Herzegovina): insights from ^{36}Cl cosmogenic dating. Med. Geosc. Rev. 1, 25–43. https://doi.org/10.1007/s42990-019-0003-4.
Cucchi, F., Forti, F., Marinetti, E., 1995. Surface degradation of carbonate rocks in the Karst of Trieste (Classical Karst, Italy). In: Formos, J.J., Ginés, A. (Eds.), Karren Landforms. Universitat de les Illes Balears, Palma, pp. 41–51.
Cvijić, J., 1889. Glacijalne I Morfološke Studije O Planinama Bosne. Hercegovine i Crne Gore. Glas SKA 57–21. Beograd.
D'Arcy, M., Schildgen, T.F., Strecker, M.R., Wittmann, H., Duesing, W., Mey, J., Tofelde, S., Weissmann, P., Alonso, R.N., 2019. Timing of past glaciation at the Sierra de Aconquija, northwestern Argentina, and throughout the Central Andes. Quat. Sci. Rev. 204, 37–57. https://doi.org/10.1016/j.quascirev.2018.11.022.
Darvill, C.M., 2013. Cosmogenic nuclide analysis. In: Geomorphological Techniques. British Society for Geomorphology, London, UK, pp. 1–25. http://geomorphology.org.uk/sites/default/files/geom_tech_chapters/4.2.10_CosmogenicNuclideAnalysis.pdf.
Delmas, M., Calvet, M., Gunnell, Y., Braucher, R., Bourlès, D., 2011. Palaeogeography and ^{10}Be exposure-age chronology of Middle and Late Pleistocene glacier systems in the northern Pyrenees: implications for reconstructing regional palaeoclimates. Palaeogeogr. Palaeoclimatol. Palaeoecol. 305, 109–122. https://doi.org/10.1016/j.palaeo.2011.02.025.
Dirks, P.H.G.M., Placzek, C.J., Fink, D., Dosseto, A., Roberts, E., 2016. Using ^{10}Be cosmogenic isotopes to estimate erosion rates and landscape changes during the Plio-Pleistocene in the Cradle of Humankind, South Africa. J. Hum. Evol. 96, 19–34. https://doi.org/10.1016/j.jhevol.2016.03.002.
Domènech, G., Corominas, J., Mavrouli, O., Merchel, S., Abellán, A., Pavetich, S., Rugel, G., 2018. Calculation of the rockwall recession rate of a limestone cliff, affected by rockfalls, using cosmogenic chlorine-36. Case study of the Montsec Range (Eastern Pyrenees, Spain). Geomorphology 306, 325–335. https://doi.org/10.1016/j.geomorph.2017.04.005.
Domínguez-Villar, D., Carrasco, R., Pedraza, J., Cheng, H., Edwards, R.L., Willenbring, J.K., 2013. Early maximum extent of paleoglaciers from Mediterranean mountains during the last glaciation. Sci. Rep. 3, 2034. https://doi.org/10.1038/srep02034.
Farber, D.L., Mériaux, A.-S., Finkel, R.C., 2008. Attenuation length for fast nucleon production of ^{10}Be derived from near-surface production profiles. Earth Planet Sci. Lett. 274, 295–300. https://doi.org/10.1016/j.epsl.2008.07.015.
Federici, P.R., Granger, D.E., Ribolini, A., Spagnolo, M., Pappalardo, M., Cyr, A.J., 2012. Last Glacial Maximum and the Gschnitz stadial in the Maritime Alps according to ^{10}Be cosmogenic dating. Boreas 41, 277–291. https://doi.org/10.1111/j.1502-3885.2011.00233.x.
Fiol, L., Fornós, J.J., Ginés, A., 1996. Effects of biokarstic processes on the development of solutional rillenkarren in limestone rocks. Earth Surf. Process. Landforms 21, 447–452. https://doi.org/10.1002/(SICI)1096-9837(199605)21:5<447::AID-ESP607>3.0.CO;2-X.
Florineth, D., Schlüchter, C., 2000. Alpine evidence for atmospheric circulation patterns in Europe during the Last Glacial Maximum. Quat. Res. 54, 295–308. https://doi.org/10.1006/qres.2000.2169.
Ford, D.C., Williams, P.W., 1989. Karst Geomorphology and Hydrology. Unwin Hyman, London, p. 601.
Fotiadi, A.K., Metaxas, D.A., Bartzokas, A., 1999. A statistical study of precipitation in northwest Greece. Int. J. Climatol. 19, 1221–1232. https://doi.org/10.1002/(SICI)1097-0088(199909)19:11<1221::AID-JOC436>3.0.CO;2-H.
Frogley, M.R., 1998. The Biostratigraphy, Palaeoecology and Geochemistry of a Long Lacustrine Sequence from NW Greece (Thesis). University of Cambridge. https://doi.org/10.17863/CAM.16400.
Furbish, D.J., Andrews, J.T., 1984. The use of hypsometry to indicate long-term stability and response of valley glaciers to changes in mass transfer. J. Glaciol. 30, 199–211. https://doi.org/10.3189/S0022143000005931.
Furlan, D., 1977. The Climate of Southeast Europe. In: Wallen, C.C. (Ed.), Climates of Central and Southern Europe. Elsevier, Amsterdam, pp. 185–223.
Furlani, S., Cucchi, F., Forti, F., Rossi, A., 2009. Comparison between coastal and inland Karst limestone lowering rates in the northeastern Adriatic Region (Italy and Croatia). Geomorphology, Coastal Geomorphology 104, 73–81. https://doi.org/10.1016/j.geomorph.2008.05.015.
Galanidou, N., Tzedakis, P.C., Lawson, I.T., Frogley, M.R., 2000. A revised chronological and paleoenvironmental framework for the Kastritsa rockshelter, northwest Greece. Antiquity 74, 349–355. https://doi.org/10.1017/S0003598X00059421.
Giraudi, C., 2012. The Campo Felice Late Pleistocene glaciation (Apennines, central Italy). J. Quat. Sci. 27, 432–440. https://doi.org/10.1002/jqs.1569.
Goldie, H.S., 2005. Erratic judgements: Re-evaluating solutional erosion rates of limestones using erratic-pedestal sites, including Norber, Yorkshire. Area 37, 433–442. https://doi.org/10.1111/j.1475-4762.2005.00653.x.
Gómez-Ortiz, A., Palacios, D., Palade, B., Vázquez-Selem, L., Salvador-Franch, F., 2012. The deglaciation of the Sierra Nevada (Southern Spain). Geomorphology 159–160, 93–105. https://doi.org/10.1016/j.geomorph.2012.03.008.
Gosse, J.C., Phillips, F.M., 2001. Terrestrial in situ cosmogenic nuclides: theory and application. Quat. Sci. Rev. 20, 1475–1560. https://doi.org/10.1016/S0277-3791(00)00171-2.
Granger, D.E., Lifton, N.A., Willenbring, J.K., 2013. A cosmic trip: 25 years of cosmogenic nuclides in geology. GSA bulletin 125 (9–10), 1379–1402. https://doi.org/10.1130/B30774.180.
Gromig, R., Mechernich, S., Ribolini, A., Wagner, B., Zanchetta, G., Isola, I., Bini, M., Dunai, T.J., 2018. Evidence for a Younger Dryas deglaciation in the Galicica Mountains (FYROM) from cosmogenic ^{36}Cl. Quat. Int. 464, 352–363. https://doi.org/10.1016/j.quaint.2017.07.013.
Hagedorn, J., 1969. Beiträge zur Quartärmorphologie griechischer Hochgebirge. Gottinger Geogr. Abh. 50, 135.
Hall, S.R., Farber, D.L., Ramage, J.M., Rodbell, D.T., Finkel, R.C., Smith, J.A., Mark, B.G., Kassel, C., 2009. Geochronology of Quaternary glaciations from the tropical Cordillera Huayhuash, Peru. Quat. Sci. Rev. 28, 2991–3009. https://doi.org/10.1016/j.quascirev.2009.08.004.
Hallet, B., Putkonen, J., 1994. Surface dating of dynamic landforms: young boulders on aging moraines. Science 265, 937–940. https://doi.org/10.1126/science.265.5174.937.
Hamlin, R.H.B., Woodward, J.C., Black, S., Macklin, M.G., 2000. Sediment fingerprinting as a tool for interpreting long-term river activity: the Voidomatis basin, Northwest Greece. In: Foster, I.D.L. (Ed.), Tracers in Geomorphology. Sediment Fingerprinting as a Tool for Interpreting Long-Term River Activity: the Voidomatis Basin, Northwest Greece. John Wiley and Sons, pp. 473–501.
Harden, J.W., 1982. A quantitative index of soil development from field descriptions: examples from a chronosequence in central California. Geoderma 28, 1–28.
Heyman, J., Stroeven, A.P., Harbor, J.M., Caffee, M.W., 2011. Too young or too old: evaluating cosmogenic exposure dating based on an analysis of compiled boulder exposure ages. Earth Planet Sci. Lett. 302, 71–80. https://doi.org/10.1016/j.epsl.2010.11.040.
Hughes, P.D., 2004. Quaternary Glaciation in the Pindus Mountains, Northwest Greece (Thesis). University of Cambridge. https://doi.org/10.17863/CAM.20476.
Hughes, P.D., Gibbard, P.L., Woodward, J.C., 2003. Relict rock glaciers as indicators of Mediterranean palaeoclimate during the Last Glacial Maximum (Late Würmian) in northwest Greece. J. Quat. Sci. 18, 431–440. https://doi.org/10.1002/jqs.764.
Hughes, P.D., Woodward, J.C., 2017. Quaternary glaciation in the Mediterranean mountains: a new synthesis. In: Quaternary Glaciation in the Mediterranean Mountains, 433. Geological Society, London, Special Publications, pp. 1–23. https://doi.org/10.1144/SP433.14.
Hughes, P.D., Woodward, J.C., Gibbard, P.L., Macklin, M.G., Gilmour, M.A., Smith, G.R., 2006a. The glacial history of the Pindus Mountains, Greece. J. Geol. 114, 413–434. https://doi.org/10.1086/504177.
Hughes, P.D., Woodward, J.C., Gibbard, P.L., 2006b. Late Pleistocene glaciers and climate in the Mediterranean. Global Planet. Change 50, 83–98. https://doi.org/10.1016/j.gloplacha.2005.07.005.
Hughes, P.D., Woodward, J.C., Gibbard, P.L., 2006c. The last glaciers of Greece. Zeitschrift für Geomorphologie 50, 37–61.
Hughes, P.D., Woodward, J.C., Gibbard, P.L., 2007. Middle Pleistocene cold stage climates in the Mediterranean: new evidence from the glacial record. Earth Planet Sci. Lett. 253, 50–56.
Hughes, P.D., Woodward, J.C., 2008. Timing of glaciation in the Mediterranean mountains during the last cold stage. J. Quat. Sci. 23, 575–588. https://doi.org/10.1002/jqs.1212.
Hughes, P.D., Woodward, J.C., van Calsteren, P.C., Thomas, L.E., Adamson, K.R., 2010. Pleistocene ice caps on the coastal mountains of the Adriatic Sea. Quat. Sci. Rev. 29, 3690–3708. https://doi.org/10.1016/j.quascirev.2010.06.032.
Hughes, P.D., Woodward, J.C., van Calsteren, P.C., Thomas, L.E., 2011. The glacial history of the Dinaric Alps, Montenegro. Quat. Sci. Rev. 30, 3393–3412. https://doi.org/10.1016/j.quascirev.2011.08.016.
Hughes, P.D., 2013. Morphostratigraphy/allostratigraphy. In: Elias, S. (Ed.), Encyclopedia of Quaternary Sciences, second ed. Elsevier, Amsterdam, pp. 2841–2847.
Hughes, P.D., Fink, D., Rodés, Á., Fenton, C.R., Fujioka, T., 2018. Timing of Pleistocene glaciations in the High Atlas, Morocco: New ^{10}Be and ^{36}Cl exposure ages. Quat. Sci. Rev. 180, 193–213. https://doi.org/10.1016/j.quascirev.2017.11.015.
IGME, 1970. 1:50,000 Geological Map of Greece. Tsepelovon Sheet. Institute of Geological and Mineral Exploration, Athens.
IGME, 1983. Geological Map of Greece, Northern Part, second ed. Institute of Geological and Mineral Exploration, Athens.
Ivy-Ochs, S., Kober, F., 2008. Surface exposure dating with cosmogenic nuclides. Quaternary Science Journal (Eiszeitalter und Gegenwart) 57, 179–209. https://doi.org/10.3285/eg.57.1-2.7.
Ivy-Ochs, S., Poschinger, A.v., Synal, H.-A., Maisch, M., 2009. Surface exposure dating of the Flims landslide, Graubünden, Switzerland. Geomorphology, Dating, triggering, modelling, and hazard assessment of large landslides 103, 104–112. https://doi.org/10.1016/j.geomorph.2007.10.024.
Ivy-Ochs, S., Briner, J.P., 2014. Dating disappearing ice with cosmogenic nuclides. Elements 10, 351–356. https://doi.org/10.2113/gselements.10.5.351.
Jones, G., Robertson, A.H.F., 1991. Tectono-stratigraphy and evolution of the Mesozoic Pindos ophiolite and related units, northwestern Greece. J. Geol. Soc. 148, 267–288. https://doi.org/10.1144/gsjgs.148.2.0267.
King, G.C.P., Bailey, G.N., 1985. The palaeoenvironment of some archaeological sites in Greece: the influence of accumulated uplift in a seismically active region. Proc. Prehist. Soc. 51, 273–282. https://doi.org/10.1017/S0079497X0000712X.
Kirkbride, M.P., Winkler, S., 2012. Correlation of Late Quaternary moraines: impact of climate variability, glacier response, and chronological resolution. Quat. Sci. Rev. 46, 1–29. https://doi.org/10.1016/j.quascirev.2012.04.002.
Köse, O., Sarıkaya, M.A., Çİner, A., Candaş, A., 2019. Late Quaternary glaciations and

cosmogenic ^{36}Cl geochronology of Mount Dedegöl, south-west Turkey. J. Quat. Sci. 34, 51–63. https://doi.org/10.1002/jqs.3080.
Kotjabopoulou, E., Panagopoulou, E., Adam, E., 1999. The Boila rockshelter: further evidence of human activity in the Voidomatis Gorge. In: Bailey, G.N., Adam, E., Panagopoulou, E., Perle`s, C., Zachos, K. (Eds.), The Palaeolithic Archaeology of Greece and Adjacent Areas. British School at Athens Studies 3. British School at Athens, London, pp. 197–210. https://www.jstor.org/stable/40960228.
Krklec, K., Domínguez-Villar, D., Perica, D., 2013. Preservation of Microscale Erosive Glacial Features in Carbonate Rocks of Croatia.
Krklec, K., Domínguez-Villar, D., Braucher, R., Perica, D., Mrak, I., 2018. Morphometric comparison of weathering features on side by side carbonate rock surfaces with different exposure ages — A case from the Croatian coast. Quaternary International, Quaternary of Croatia 494, 275–285. https://doi.org/10.1016/j.quaint.2017.04.012.
Kuhlemann, J., Rohling, E.J., Krumrei, I., Kubik, P., Ivy-Ochs, S., Kucera, M., 2008. Regional synthesis of Mediterranean atmospheric circulation during the Last Glacial Maximum. Science 321, 1338–1340. https://doi.org/10.1126/science.1157638.
Kuhlemann, J., Milivojević, M., Krumrei, I., Kubik, P.W., 2009. Last glaciation of the Šara Range (Balkan Peninsula): increasing dryness from the LGM to the Holocene. Austrian Journal of Earth Sciences 102, 146–158.
Kuhlemann, J., Gachev, E., Gikov, A., Nedkov, S., Krumrei, I., Kubik, P., 2013. Glaciation in the Rila Mountains (Bulgaria) during the Last Glacial Maximum. Quaternary International, Advancing Pleistocene and Holocene Climate Change Research in the Carpathian-Balkan Region 293, pp. 51–62. https://doi.org/10.1016/j.quaint.2012.06.027.
Lal, D., 1991. Cosmic ray labeling of erosion surfaces: in situ nuclide production rates and erosion models. Earth Planet Sci. Lett. 104, 424–439. https://doi.org/10.1016/0012-821X(91)90220-C.
Lambeck, K., 1995. Late Pleistocene and Holocene sea-level change in Greece and south-western Turkey: a separation of eustatic, isostatic and tectonic contributions. Geophys. J. Int. 122, 1022–1044. https://doi.org/10.1111/j.1365-246X.1995.tb06853.x.
Lawson, I.T., Frogley, M.R., Bryant, C., Preece, R.C., Tzedakis, P.C., 2004. The Lateglacial and Holocene environmental history of the Ioannina basin, north-west Greece. Quat. Sci. Rev. 23, 1599–1625. https://doi.org/10.1016/j.quascirev.2004.02.003.
Leontaritis, A.D., Kouli, K., Pavlopoulos, K., 2020. The glacial history of Greece: a comprehensive review. Mediterranean Geoscience Reviews 2, 65–90. https://doi.org/10.1007/s42990-020-00021-w.
Levenson, Y., Ryb, U., Emmanuel, S., 2017. Comparison of field and laboratory weathering rates in carbonate rocks from an Eastern Mediterranean drainage basin. Earth Planet Sci. Lett. 465, 176–183. https://doi.org/10.1016/j.epsl.2017.02.031.
Lewin, J., Macklin, M.G., Woodward, J.C., 1991. Late Quaternary fluvial sedimentation in the Voidomatis Basin, Epirus, Northwest Greece. Quat. Res. 35, 103–115. https://doi.org/10.1016/0033-5894(91)90098-P.
Lewin, J., Woodward, J.C., 2009. Karst geomorphology and environmental change. In: Woodward, J.C. (Ed.), The Physical Geography of the Mediterranean. Oxford University Press, Oxford, pp. 287–317.
Lewis, C.J., McDonald, E.V., Sancho, C., Peña, J.L., Rhodes, E.J., 2009. Climatic implications of correlated Upper Pleistocene glacial and fluvial deposits on the Cinca and Gállego Rivers (NE Spain) based on OSL dating and soil stratigraphy. Global Planet. Change 67, 141–152. https://doi.org/10.1016/j.gloplacha.2009.01.001.
Lifton, N., Sato, T., Dunai, T.J., 2014. Scaling in situ cosmogenic nuclide production rates using analytical approximations to atmospheric cosmic-ray fluxes. Earth Planet Sci. Lett. 386, 149–160. https://doi.org/10.1016/j.epsl.2013.10.052.
Macklin, M.G., Lewin, J., Woodward, J.C., 1997. Quaternary river sedimentary sequences of the Voidomatis basin. In: Bailey, G.N. (Ed.), Klithi: Palaeolithic Settlement and Quaternary Landscapes in Northwest Greece. McDonald Institute, Cambridge, pp. 347–359.
Macklin, M.G., Woodward, J.C., 2009. Rivers and environmental change. In: Woodward, J.C. (Ed.), The Physical Geography of the Mediterranean. Oxford University Press, Oxford, pp. 319–352.
Manz, L.A., 1998. Cosmogenic ^{36}Cl Chronology for Deposits of Presumed Pleistocene Age on the Eastern Piedmont of Mount Olympus, Pieria, Greece. Unpublished MSc Thesis, Ohio University.
Marjanac, L., 2012. Pleistocene Glacial and Periglacial Sediments of Kvarner, Northern Dalmatia and Southern Velebit Mt. - Evidence of Dinaric Glaciation. Doctoral Thesis, University of Zagreb.
Marjanac, L., Marjanac, T., Hughes, P.D., 2008. Dinaric glaciation - a formal proposal of a new model. In: Monnier, J.L., Lefort, J.P., Danukalova, G. (Eds.), INQUA-SEQS 2008, Differences and Similarities in Quaternary Stratigraphy between Atlantic and Continental Europe, 22-27 September 2008, Rennes, France, Abstracts, vol. 45. Laboratoire d'anthropologie de Rennes, pp. 29–30. https://www.inqua-seqs.org/wp-content/uploads/SEQS2008AbstractsRennes.pdf.
Marjanac, L., Marjanac, T., 2004. Glacial history of the Croatian Adriatic and Coastal Dinarides. In: Ehlers, J., Gibbard, P.L. (Eds.), Quaternary Glaciations - Extent and Chronology. Part I: Europe. Elsevier, Amsterdam, pp. 19–26.
Marjanac, T., Marjanac, L., 2016. The extent of middle Pleistocene ice cap in the coastal Dinaric Mountains of Croatia. Quat. Res. 85, 445–455. https://doi.org/10.1016/j.yqres.2016.03.006.
Marrero, S.M., Phillips, F.M., Borchers, B., Lifton, N., Aumer, R., Balco, G., 2016a. Cosmogenic nuclide systematics and the CRONUScalc program. Quat. Geochronol. 31, 160–187. https://doi.org/10.1016/j.quageo.2015.09.005.
Marrero, S.M., Phillips, F.M., Caffee, M.W., Gosse, J.C., 2016b. CRONUS-Earth cosmogenic ^{36}Cl calibration. Quat. Geochronol. 31, 199–219. https://doi.org/10.1016/j.quageo.2015.10.002.
Matsushi, Y., Sasa, K., Takahashi, T., Sueki, K., Nagashima, Y., Matsukura, Y., 2010. Denudation rates of carbonate pinnacles in Japanese karst areas: estimates from cosmogenic ^{36}Cl in calcite. Nuclear instruments and methods in physics research section B: beam interactions with materials and atoms. In: Proceedings of the Eleventh International Conference on Accelerator Mass Spectrometry, vol. 268, pp. 1205–1208. https://doi.org/10.1016/j.nimb.2009.10.134.
May, J.-H., Zech, J., Zech, R., Preusser, F., Argollo, J., Kubik, P.W., Veit, H., 2011. Reconstruction of a complex late Quaternary glacial landscape in the Cordillera de Cochabamba (Bolivia) based on a morphostratigraphic and multiple dating approach. Quat. Res. 76, 106–118. https://doi.org/10.1016/j.yqres.2011.05.003.
Nye, J.F., 1952. The mechanics of glacier flow. J. Glaciol. 2, 82–93. https://doi.org/10.3189/S0022143000033967.
Ohmura, A., Kasser, P., Funk, M., 1992. Climate at the equilibrium line of glaciers. J. Glaciol. 38, 15. https://doi.org/10.3189/S0022143000002276.
Oliva, M., Žebre, M., Guglielmin, M., Hughes, P.D., Çiner, A., Vieira, G., Bodin, X., Andrés, N., Colucci, R.R., García-Hernández, C., Mora, C., Nofre, J., Palacios, D., Pérez-Alberti, A., Ribolini, A., Ruiz-Fernández, J., Sarıkaya, M.A., Serrano, E., Urdea, P., Valcárcel, M., Woodward, J.C., Yıldırım, C., 2018. Permafrost conditions in the Mediterranean region since the last glaciation. Earth Sci. Rev. 185, 397–436. https://doi.org/10.1016/j.earscirev.2018.06.018.
Oliva, M., Palacios, D., Fernández-Fernández, J.M., Rodríguez-Rodríguez, L., García-Ruiz, J.M., Andrés, N., Carrasco, R.M., Pedraza, J., Pérez-Alberti, A., Valcárcel, M., Hughes, P.D., 2019. Late Quaternary glacial phases in the Iberian Peninsula. Earth Sci. Rev. 192, 564–600. https://doi.org/10.1016/j.earscirev.2019.03.015.
Osmaston, H., 2005. Estimates of glacier equilibrium line altitudes by the Area×Altitude, the Area×Altitude balance ratio and the Area×Altitude balance index methods and their validation. Quaternary International, Snowlines at the Last Glacial Maximum and tropical cooling 138– 139, 22–31. https://doi.org/10.1016/j.quaint.2005.02.004.
Osmaston, H.A., 1975. Models for the estimation of firnlines of present and Pleistocene glaciers. In: Peel, R.F., Chisholm, M.D.I., Haggett, P. (Eds.), Processes in Physical and Human Geography. Bristol Essays, pp. 218–245.
Palmentola, G., Stamatopoulos, L., 2006. Preliminary data about sporadic permafrost on Peristeri and Tzoumerka massifs (Pindos chain, Northwestern Greece). Revista de geomorlogie 8, 17–23.
Palacios, D., Gómez-Ortiz, A., Andrés, N., Vázquez-Selem, L., Salvador-Franch, F., Oliva, M., 2015. Maximum extent of Late Pleistocene glaciers and last deglaciation of La Cerdanya mountains, Southeastern Pyrenees. Geomorphology 231, 116–129. https://doi.org/10.1016/j.geomorph.2014.10.037.
Palacios, D., Gómez-Ortiz, A., Andrés, N., Salvador, F., Oliva, M., 2016. Timing and new geomorphologic evidence of the last deglaciation stages in Sierra Nevada (southern Spain). Quat. Sci. Rev. 150, 110–129. https://doi.org/10.1016/j.quascirev.2016.08.012.
Palacios, D., Gómez-Ortiz, A., Alcalá-Reygosa, J., Andrés, N., Oliva, M., Tanarro, L.M., Salvador-Franch, F., Schimmelpfennig, I., Fernández-Fernández, J.M., Léanni, L., 2019. The challenging application of cosmogenic dating methods in residual glacial landforms: the case of Sierra Nevada (Spain). Geomorphology 325, 103–118. https://doi.org/10.1016/j.geomorph.2018.10.006.
Pallàs, R., Rodés, Á., Braucher, R., Carcaillet, J., Ortuño, M., Bordonau, J., Bourlès, D., Vilaplana, J.M., Masana, E., Santanach, P., 2006. Late Pleistocene and Holocene glaciation in the Pyrenees: a critical review and new evidence from ^{10}Be exposure ages, south-central Pyrenees. Quat. Sci. Rev. 25, 2937–2963. https://doi.org/10.1016/j.quascirev.2006.04.004.
Pallàs, R., Rodés, Á., Braucher, R., Bourlès, D., Delmas, M., Calvet, M., Gunnell, Y., 2010. Small, isolated glacial catchments as priority targets for cosmogenic surface exposure dating of Pleistocene climate fluctuations, southeastern Pyrenees. Geology 38, 891–894. https://doi.org/10.1130/G31164.1.
Pavlopoulos, K., Leontaritis, A., Athanassas, C., Petrakou, C., Vandarakis, D., Nikolakopoulos, K., Stamatopoulos, L., Theodorakopoulou, K., 2018. Last glacial geomorphologic records in Mt Chelmos, North Peloponnesus, Greece. J. Mt. Sci. 15 https://doi.org/10.1007/s11629-017-4563-0.
Pellitero, R., Rea, B.R., Spagnolo, M., Bakke, J., Hughes, P., Ivy-Ochs, S., Lukas, S., Ribolini, A., 2015. A GIS tool for automatic calculation of glacier equilibrium-line altitudes. Comput. Geosci. 82, 55–62. https://doi.org/10.1016/j.cageo.2015.05.005.
Pellitero, R., Rea, B.R., Spagnolo, M., Bakke, J., Ivy-Ochs, S., Frew, C.R., Hughes, P., Ribolini, A., Lukas, S., Renssen, H., 2016. GlaRe, a GIS tool to reconstruct the 3D surface of palaeoglaciers. Comput. Geosci. 94, 77–85. https://doi.org/10.1016/j.cageo.2016.06.008.
Phillips, F.M., Leavy, B.D., Jannik, N.O., Elmore, D., Kubik, P.W., 1986. The accumulation of cosmogenic chlorine-36 in rocks: a method for surface exposure dating. Science 231, 41–43. https://doi.org/10.1126/science.231.4733.41.
Plan, L., 2005. Factors controlling carbonate dissolution rates quantified in a field test in the Austrian alps. Geomorphology 68, 201–212. https://doi.org/10.1016/j.geomorph.2004.11.014.
Pope, R.J., Hughes, P.D., Skourtsos, E., 2017. Glacial history of Mt Chelmos, Peloponnesus, Greece. In: Hughes, P.D., Woodward, J.C. (Eds.), Quaternary Glaciation in the Mediterranean Mountains, vol. 433. Geological Society, London, Special Publications, pp. 211–236. https://doi.org/10.1144/SP433.11.
Putkonen, J., Swanson, T., 2003. Accuracy of cosmogenic ages for moraines. Quat. Res. 59, 255–261. https://doi.org/10.1016/S0033-5894(03)00006-1.
Rea, B., 2009. Defining modern day Area-Altitude Balance Ratios (AABRs) and their

use in glacier–climate relationships. Quat. Sci. Rev. 28, 237–248. https://doi.org/10.1016/j.quascirev.2008.10.011.
Reber, R., Akçar, N., Yesilyurt, S., Yavuz, V., Tikhomirov, D., Kubik, P.W., Schlüchter, C., 2014. Glacier advances in northeastern Turkey before and during the global Last Glacial Maximum. Quat. Sci. Rev. 101, 177–192. https://doi.org/10.1016/j.quascirev.2014.07.014.
Ribolini, A., Bini, M., Isola, I., Spagnolo, M., Zanchetta, G., Pellitero, R., Mechernich, S., Gromig, R., Dunai, T., Wagner, B., Milevski, I., 2018. An Oldest Dryas glacier expansion on Mount Pelister (Former Yugoslavian Republic of Macedonia) according to ^{10}Be cosmogenic dating. J. Geol. Soc. 175, 100–110. https://doi.org/10.1144/jgs2017-038.
Rodríguez-Rodríguez, L., Jiménez-Sánchez, M., Domínguez-Cuesta, M.J., Aranburu, A., 2015. Research history on glacial geomorphology and geochronology of the Cantabrian Mountains, north Iberia (43–42°N/7–2°W). Quaternary International, Quaternary of the Western Pyrenean region 364, 6–21. https://doi.org/10.1016/j.quaint.2014.06.007.
Ryb, U., Matmon, A., Erel, Y., Haviv, I., Benedetti, L., Hidy, A.J., 2014a. Styles and rates of long-term denudation in carbonate terrains under a Mediterranean to hyperarid climatic gradient. Earth Planet Sci. Lett. 406, 142–152. https://doi.org/10.1016/j.epsl.2014.09.008.
Ryb, U., Matmon, A., Erel, Y., Haviv, I., Katz, A., Starinsky, A., Angert, A., Team, A., 2014b. Controls on denudation rates in tectonically stable Mediterranean carbonate terrain. GSA Bulletin 126, 553–568. https://doi.org/10.1130/B30886.1.
Sanchez Goñi, M.F., Harrison, S.P., 2010. Millennial-scale climate variability and vegetation changes during the Last Glacial: concepts and terminology. Quat. Sci. Rev. 29, 2823–2827. https://doi.org/10.1016/j.quascirev.2009.11.014.
Sarıkaya, M.A., Zreda, M., Çiner, A., Zweck, C., 2008. Cold and wet Last Glacial Maximum on Mount Sandıras, SW Turkey, inferred from cosmogenic dating and glacier modeling. Quat. Sci. Rev. 27, 769–780. https://doi.org/10.1016/j.quascirev.2008.01.002.
Sarıkaya, M.A., Zreda, M., Çiner, A., 2009. Glaciations and paleoclimate of Mount Erciyes, central Turkey, since the Last Glacial Maximum, inferred from ^{36}Cl cosmogenic dating and glacier modeling. Quat. Sci. Rev. 28, 2326–2341. https://doi.org/10.1016/j.quascirev.2009.04.015.
Sarıkaya, M., Çiner, A., Haybat, H., Zreda, M., 2014. An early advance of glaciers on Mount Akdağ, SW Turkey, before the global Last Glacial Maximum; insights from cosmogenic nuclides and glacier modeling. Quat. Sci. Rev. 88, 96–109. https://doi.org/10.1016/j.quascirev.2014.01.016.
Sarıkaya, M.A., Çiner, A., 2017. Late Quaternary glaciations in the eastern Mediterranean. In: Hughes, P.D., Woodward, J.C. (Eds.), Quaternary Glaciation in the Mediterranean Mountains. Geological Society, London, Special Publications, pp. 289–305.
Sarıkaya, M.A., Stepišnik, U., Žebre, M., Çiner, A., Yıldırım, C., Vlahović, I., Tomljenović, B., Matoš, B., Wilcken, K.M., 2020. Last glacial maximum deglaciation of the Southern Velebit Mt. (Croatia): insights from cosmogenic ^{36}Cl dating of Rujanska Kosa. Med. Geosc. Rev. 2, 53–64. https://doi.org/10.1007/s42990-020-00030-9.
Schimmelpfennig, I., Benedetti, L., Garreta, V., Pik, R., Blard, P.-H., Burnard, P., Bourlès, D., Finkel, R., Ammon, K., Dunai, T., 2011. Calibration of cosmogenic ^{36}Cl production rates from Ca and K spallation in lava flows from Mt. Etna (38°N, Italy) and Payun Matru (36°S, Argentina). Geochem. Cosmochim. Acta 75, 2611–2632. https://doi.org/10.1016/j.gca.2011.02.013.
Smith, G.R., Nance, R., Genes, A., 1997. Quaternary glacial history of Mount Olympus, Greece. Geol. Soc. Am. Bull. 109, 809–824. https://doi.org/10.1130/0016-7606(1997)109<0809:QGHOMO>2.3.CO;2.
Stone, J., Allan, G.L., Fifield, L.K., Evans, J.M., Chivas, A.R., 1994. Limestone erosion measurements with cosmogenic chlorine-36 in calcite — preliminary results from Australia. Nucl. Instrum. Methods Phys. Res. B 92, 311–316. https://doi.org/10.1016/0168-583X(94)96025-9.
Stone, J.O., Allan, G.L., Fifield, L.K., Cresswell, R.G., 1996. Cosmogenic chlorine-36 from calcium spallation. Geochem. Cosmochim. Acta 60, 679–692. https://doi.org/10.1016/0016-7037(95)00429-7.
Stroeven, A.P., Fabel, D., Harbor, J.M., Fink, D., Caffee, M.W., Dahlgren, T., 2011. Importance of sampling across an assemblage of glacial landforms for interpreting cosmogenic ages of deglaciation. Quat. Res. 76, 148–156. https://doi.org/10.1016/j.yqres.2011.04.004.
Styllas, M.N., Schimmelpfennig, I., Benedetti, L., Ghilardi, M., Aumaître, G., Bourlès, D., Keddadouche, K., 2018. Late-glacial and Holocene history of the northeast Mediterranean mountain glaciers - new insights from in situ-produced ^{36}Cl-based cosmic ray exposure dating of paleo-glacier deposits on Mount Olympus, Greece. Quat. Sci. Rev. 193, 244–265. https://doi.org/10.1016/j.quascirev.2018.06.020.
Telbisz, T., Stergiou, C.L., Mindszenty, A., Chatzipetros, A., 2019. Karst features and related social processes in the region of the Vikos Gorge and Tymphi Mountain (Northern Pindos National Park, Greece). Acta Carsol. 48 https://doi.org/10.3986/ac.v48i1.6806.
Thomas, F., Godard, V., Bellier, O., Benedetti, L., Ollivier, V., Rizza, M., Guillou, V., Hollender, F., Aumaître, G., Bourlès, D.L., Keddadouche, K., 2018. Limited influence of climatic gradients on the denudation of a Mediterranean carbonate landscape. Geomorphology 316, 44–58. https://doi.org/10.1016/j.geomorph.2018.04.014.
Tzedakis, P.C., 1993. Long-term tree populations in northwest Greece through multiple Quaternary climatic cycles. Nature 364, 437–440. https://doi.org/10.1038/364437a0.
Tzedakis, P.C., Lawson, I.T., Frogley, M.R., Hewitt, G.M., Preece, R.C., 2002. Buffered tree population changes in a Quaternary refugium: evolutionary implications. Science 297, 2044–2047. https://doi.org/10.1126/science.1073083.
Tzedakis, P.C., Frogley, M.R., Lawson, I.T., Preece, R.C., Cacho, I., de Abreu, L., 2004. Ecological thresholds and patterns of millennial-scale climate variability: the response of vegetation in Greece during the last glacial period. Geol. 32, 109. https://doi.org/10.1130/G20118.1.
USGS, 2019. Earth explorer. Available at: https://earthexplorer.usgs.gov/ [Accessed September 2019].
Veress, M., Telbisz, T., Tóth, G., Lóczy, D., Ruban, D.A., Gutak, J.M., 2019. Glaciokarsts. Springer Geography. Springer International Publishing. https://doi.org/10.1007/978-3-319-97292-3.
Waltham, A.C., 1978. The Caves and Karst of Astraka, Greece. Trans. Br. Cave Res. Assoc. 5, 1–12.
Weertman, J., 1971. Shear stress at the base of a rigidly rotating cirque glacier. J. Glaciol. 10, 31–37. https://doi.org/10.3189/S0022143000012971.
Wilcken, K.M., Fujioka, T., Fink, D., Fülöp, R.H., Codilean, A.T., Simon, K., Mifsud, C., Kotevski, S., 2019. SIRIUS Performance: 10Be, 26Al and 36Cl measurements at ANSTO. Nucl. Instrum. Methods Phys. Res. Sect. B Beam Interact. Mater. Atoms 455, 300–304. https://doi.org/10.1016/j.nimb.2019.02.009.
Woodward, J.C., Lewin, J., Macklin, M.G., 1992. Alluvial sediment sources in a glaciated catchment: the Voidomatis basin, Northwest Greece. Earth Surf. Process. Landforms 17, 205–216. https://doi.org/10.1002/esp.3290170302.
Woodward, J.C., Macklin, M.G., Lewin, J., 1994. Pedogenic weathering and relative age dating of Quaternary alluvial sediments in the Pindus Mountains of northwest Greece. In: Robinson, D.A., Williams, R.B.G. (Eds.), Rock Weathering and Landform Evolution. Wiley, Chichester, pp. 259–283.
Woodward, J.C., Lewin, J., Macklin, M.G., 1995. Glaciation, river behaviour and Palaeolithic settlement in upland northwest Greece. In: Lewin, J., Macklin, M.G., Woodward, J.C. (Eds.), Mediterranean Quaternary River Environments. Rotterdam, Balkema, pp. 115–129.
Woodward, J.C., 1997. Late Pleistocene rockshelter sedimentation at Megalakkos. In: Bailey, G.N. (Ed.), Klithi: Palaeolithic Settlement and Quaternary Landscapes in Northwest Greece, Volume 2: Klithi in its Local and Regional Setting. MacDonald Institute for Archaeological Research, Cambridge, pp. 377–393.
Woodward, J.C., Hamlin, R.H.B., Macklin, M.G., Karkanas, P., Kotjabopoulou, E., 2001. Quantitative sourcing of slackwater deposits at Boila rockshelter: a record of lateglacial flooding and Paleolithic settlement in the Pindus Mountains, Northwest Greece. Geoarchaeology 16, 501–536. https://doi.org/10.1002/gea.1003.
Woodward, J.C., Macklin, M.G., Smith, G.R., 2004. Pleistocene glaciation in the mountains of Greece. In: Ehlers, J., Gibbard, P.L. (Eds.), Quaternary Glaciations - Extent and Chronology: Part I: Europe. Developments in Quaternary Science, vol. 2, pp. 155–173. https://doi.org/10.1016/S1571-0866(04)80066-6.
Woodward, J.C., Hamlin, R.H.B., Macklin, M.G., Hughes, P.D., Lewin, J., 2008. Glacial activity and catchment dynamics in northwest Greece: long-term river behaviour and the slackwater sediment record for the last glacial to interglacial transition. Geomorphology 101 (1–2), 44–67. https://doi.org/10.1016/j.geomorph.2008.05.018.
Woodward, J.C., Hughes, P.D., 2011. Glaciation in Greece: a new record of cold stage environments in the Mediterranean. In: Ehlers, J., Gibbard, P.L., Hughes, P.D. (Eds.), Quaternary Glaciations - Extent and Chronology, Part IV - A Closer Look. Elsevier, Amsterdam, pp. 175–198.
Woodward, J.C., Macklin, M., Hughes, P.D., Adamson, K., Lewin, J., 2014. The paraglacial concept revisited: the record from the Mediterranean mountains of Southern Europe. In: EGU General Assembly Conference Abstracts, p. 5517. https://meetingorganizer.copernicus.org/EGU2014/EGU2014-5517.pdf.
Woodward, J.C., Hughes, P.D., 2019. Glaciated limestone landscapes: landforms and processes. Geogr. Rev. 33 (1), 33–37.
Zahno, C., Akçar, N., Yavuz, V., Kubik, P.W., Schlüchter, C., 2009. Surface exposure dating of Late Pleistocene glaciations at the Dedegöl Mountains (Lake Beyşehir, SW Turkey). J. Quat. Sci. 24, 1016–1028. https://doi.org/10.1002/jqs.1280.
Žebre, M., Sarıkaya, M.A., Stepišnik, U., Yıldırım, C., Çiner, A., 2019. First ^{36}Cl cosmogenic moraine geochronology of the Dinaric mountain karst: Velež and Crvanj Mountains of Bosnia and Herzegovina. Quat. Sci. Rev. 208, 54–75. https://doi.org/10.1016/j.quascirev.2019.02.002.
Zech, R., Glaser, B., Sosin, P., Kubik, P.W., Zech, W., 2005. Evidence for long-lasting landform surface instability on hummocky moraines in the Pamir Mountains (Tajikistan) from ^{10}Be surface exposure dating. Earth Planet Sci. Lett. 237, 453–461. https://doi.org/10.1016/j.epsl.2005.06.031.
Zerathe, S., Braucher, R., Lebourg, T., Bourlès, D., Manetti, M., Léanni, L., 2013. Dating chert (diagenetic silica) using in-situ produced ^{10}Be: possible complications revealed through a comparison with ^{36}Cl applied to coexisting limestone. Quat. Geochronol. 17, 81–93. https://doi.org/10.1016/j.quageo.2013.01.003.
Zreda, M.G., Phillips, F.M., Elmore, D., 1994. Cosmogenic ^{36}Cl accumulation in unstable landforms: 2. Simulations and measurements on eroding moraines. Water Resour. Res. 30, 3127–3136. https://doi.org/10.1029/94WR00760.